Electron density change across the pressure-induced iron spin transition

Matthew R. Diamond¹, Guoyin Shen², Dmitry Y. Popov², Changyong Park², Steven D. Jacobsen³, and Raymond Jeanloz¹

¹Department of Earth and Planetary Science, University of California, Berkeley, CA 94720, USA
²HPCAT, X-ray Science Division, Argonne National Laboratory, Lemont, IL 60439, USA
³Department of Earth and Planetary Sciences, Northwestern University, Evanston, IL 60208, USA

High-pressure single-crystal x-ray diffraction is used to experimentally map the electron-density distribution changes in (Fe,Mg)O as ferrous iron undergoes a pressure-induced transition from high to low spin. As the bulk density and elasticity of magnesiowüstite — one of the dominant minerals of Earth's mantle — are affected by this electronic transition, our results have applications to geophysics as well as to validating first-principles calculations. The observed changes in diffraction intensities indicate a spin transition-induced change in orbital occupancies of the Fe ion consistent with crystal-field theory, illustrating the use of electron density measurements for characterizing chemical bonding under pressure.

Ferrous iron undergoes a pressure-induced, *d*-electron spin-pairing magnetic transition, transforming its chemical nature with a 30-45 percent reduction in ionic volume [1–3]. First-principles theory predicts the electron charge distribution of the ferrous ion to change due to the shift of electrons to energetically favored orbitals [4]. Moreover, measurements and theory provide compelling evidence that the spin transition takes place in relevant mineral phases at the pressure-temperature conditions of Earth's lower mantle, affecting physical and chemical properties deep inside our planet [2,5-18]. Building on the legacy of a handful of prior laboratory studies on high-pressure charge density, here we present the first report of experimental electron density images across this high-pressure spin collapse [19–26].

We use high-resolution single-crystal x-ray diffraction to determine the spatial distribution of electrons in (Fe,Mg)O magnesiowüstite as a function of pressure. Our focus on this rock-salt (B1) structured compound, the second most abundant mineral phase in Earth's lower mantle, is motivated by its higher crystal symmetry than the more abundant (Mg,Fe)SiO₃ bridgmanite. However, iron in the perovskite-structured bridgmanite undergoes a similar pressure-induced spin transition [1], so our results are broadly applicable to Earth's interior [27].

In the traditional crystal-field picture of chemical bonding, the 3d electrons of the Fe(II) ion at ambient conditions are split into two sets of orbitals due to the electrostatic influence of the six nearest-neighbor, octahedrally coordinated oxygen ions: a lower-energy t_{2g} set with electron density preferentially oriented in the <100> direction of the second-neighbor cations, and a higher-energy e_g set with electron density oriented in the <111> direction of the nearest oxygen neighbors. Under compression, theory predicts that band broadening combined with the increased energy of the e_g relative to the t_{2g} orbitals overcomes the repulsive energy required to pair opposite-spin electrons into one orbital set; the two electrons in the e_g states then empty into the t_{2g} orbitals, inducing a collapse in ionic radius [1,2,28–30]. Temperature mainly serves to broaden and slightly shift the spin-transition pressure range, without affecting the transition mechanism [1,2,4–6,15,16,30].

Using a diamond-anvil cell with helium pressure-transmitting medium, we used monochromatic (39.41-40.43 keV energy [31]) synchrotron-based x-rays to obtain diffraction patterns from single-crystal samples at room temperature. Two samples, of compositions (Fe_{0.53}Mg_{0.47})O and (Fe_{0.15}Mg_{0.85})O, cut from previously characterized material [32], were studied on compression and decompression in separate experiments up to 58 and 74 GPa, respectively. Data were collected in 1 degree horizontal rotational steps, for respective 54 and 67 degree scattering-angle ranges for the Fe-rich and Fe-poor samples [25]; each image was collected with 1

or 2 second exposures onto an image-plate detector, and data sets were reduced using the XDS software [31]. Well-resolved diffraction peaks show no systematic evidence of non-hydrostaticity (e.g., splitting), such as caused by the sample bridging between the anvils, or other deviation from the B1 structure.

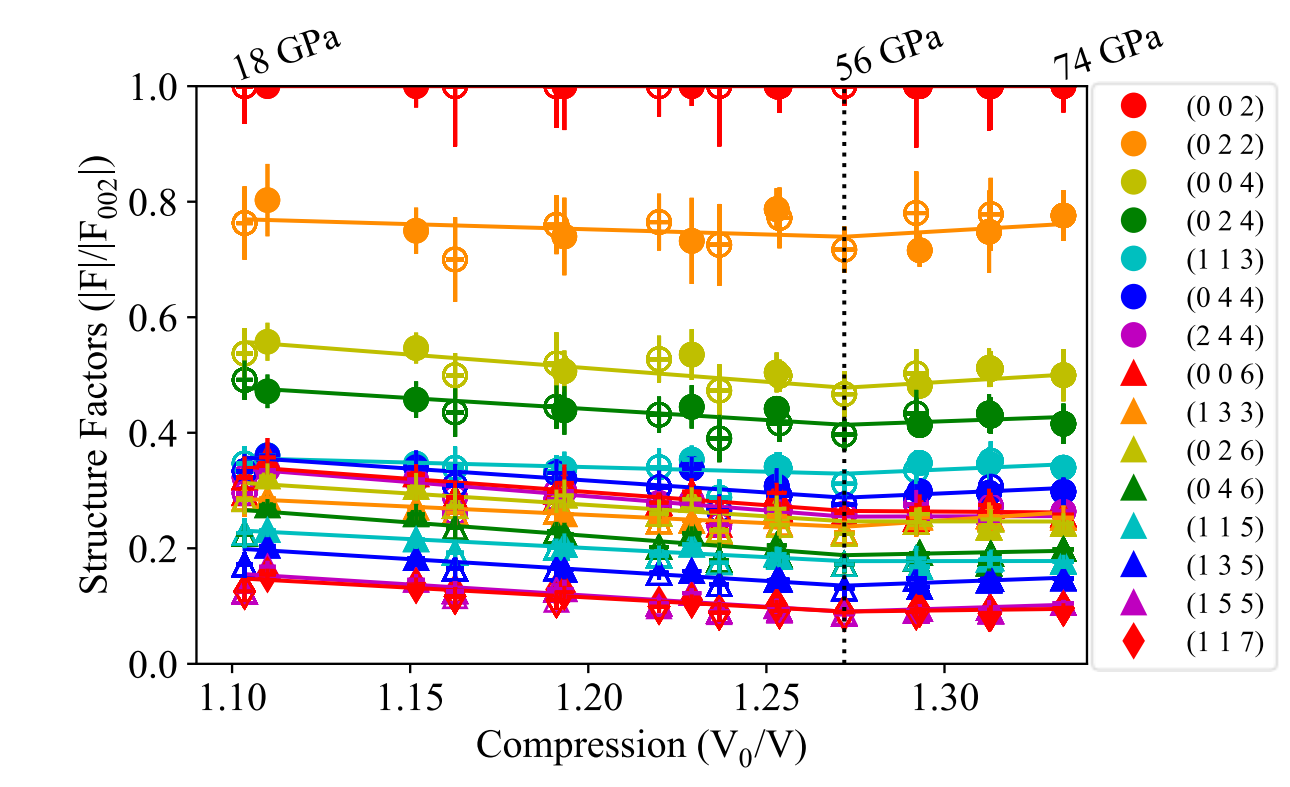


FIG. 1. Structure factors for $(Fe_{0.53}Mg_{0.47})O$ as a function of compression at room temperature. Values are given relative to the structure factor for the brightest peak, F(002) [31], with results for compression and decompression indicated by *closed* and *open symbols*, respectively. The *straight lines* show the result of a least-squares fit to all of the data, assuming two linear trends with a single break in slope: the loss-function minimization documents preference for the break in slope at 56 GPa (Fig. S2). This two-trend fit to the structure factors has statistical significance, after Bonferroni correction of fourteen structure factors [not including $(0\ 0\ 2)$], when compared with a linear fit with no break in slope (Table SI).

The spin transition affects the pressure–volume (P-V) equation of state of magnesiowüstite, with our new measurements documenting the transition at pressures similar to those found in previous studies [Fig. S1(b)]: around 45 GPa for $(Fe_{0.15}Mg_{0.85})O$ and 56 GPa for $(Fe_{0.53}Mg_{0.47})O$ [2,7,9,33–35]. The spin-induced shift in the equation of state – determined by diffraction angles [Fig. S1(b)] – occurs at the same pressures (within our resolution) as the changes in electron densities obtained from diffraction intensities, as next described.

Electron density within the crystal structure determines the intensities I(hkl) of x-ray diffraction peaks through the complex structure factor F(hkl), as the incident x rays scatter off the electron clouds in vector direction hkl: $I(hkl) = F(hkl) * F^*(hkl)$, where F^* is the complex conjugate of F. Diffraction samples the electron density through a discrete Fourier transform over n atoms at positions r_n , $F(hkl) = |F(hkl)| \sum_n e^{-i(hkl*r_n)} = |F(hkl)| * e^{-i\alpha(hkl)}$. Although diffraction does not determine the phase factor α , the centrosymmetric cubic crystal structure in our case allows α to be set to zero for both even and odd hkl [36], leading to a solution for the

structure factor amplitude $|F(hkl)| = \sqrt{I(hkl)}$. We empirically account for absorption by the diamond anvils by comparing a common set of hkl reflections between diffraction patterns obtained under pressure from the same sample in the same cell. For the (Fe_{0.53}Mg_{0.47})O data, we use a Grüneisen model to correct for the effect of compression on the Debye-Waller temperature factor [31].

The structure factors show systematic trends as a function of compression for (Fe_{0.53}Mg_{0.47})O (Fig. 1), with a break in slope at 56 GPa for the Fe-rich sample, in the same pressure range that the pressure–volume measurements indicate the spin-transition (Fig. S1). Our two-component fit is based on finding the break-in-slope compressions that minimize the squared residuals relative to the data (Fig. S2). Not surprisingly, because of lower iron abundance, the structure factors for the Fe-poor sample show less definitive evidence of the spin transition. Still, the structure-factor trends for (Fe_{0.15}Mg_{0.85})O also show an anomaly at about 45 GPa (Fig. S3), near the transition pressure suggested by compression measurements (Fig. S1). Note that these systematic trends in structure factor cause the standard output from the SHELX program to indicate an unphysical increase in temperature factors with compression (Fig. S13) [31].

Recognizing that the spin transition has been shown to take place over a pressure range of 10-20 GPa or more, with hysteresis evident on compression and decompression [2,6,15], we interpret these breaks in the structure-factor trends as representing the end of the spin transition (the spin transition takes place over comparable albeit slightly higher pressures at high relative to room temperatures [1,15,30]). That is, the subsequent treatment of our data assumes that Fe-rich and Fepoor samples contain only low-spin Fe above 56 and 45 GPa, respectively, and have either highspin or a mixture of high- and low-spin iron at lower pressures.

Our measurement uncertainties do not justify a three-trend fit (i.e., for high-, mixed- and low-spin states); we include all points starting from the minimum compression point (18 GPa) as belonging to the mixed region, thereby allowing for a lower transition onset pressure limit than found by other techniques. Note that the spin transition can be kinetically hindered because it involves a volume strain that requires viscous relaxation toward equilibrium, so differences in stress environments can explain variability in reported transitions. Still, our end-transition pressure is within uncertainties of the expected Fe-spin transition pressure range in (Fe,Mg)O based on independent measurements by Mössbauer, x-ray emission, Brillouin spectroscopy or compression [2,5,7–12,15].

Electron density ρ is determined from the inverse discrete Fourier transform of the structure factor, and the general expression can be simplified in the present case of cubic symmetry to

$$\rho(xyz) = \frac{8}{V} \sum_{h,k,l=0}^{hkl_{max}} |F(hkl)| \cos(2\pi hx) \cos(2\pi ky) \cos(2\pi lz)$$
 (1)

(V is the unit-cell volume) [37]. We use the fits to our structure-factor measurements (i.e., the lines shown in Fig. 1) to solve for the relative electron density across the crystallographic unit cell, doing so at minimum compression ($V_0/V = 1.10$, P = 18 GPa), end of transition compression ($V_0/V = 1.27$, P = 56 GPa), and maximum compression ($V_0/V = 1.33$, P = 74 GPa) for our experiments (Fig. S4). Several high-pressure measurements, obtained both on compression and decompression, thus determine each map of electron density. Though limited by resolution and completeness, our method reveals electron density changes in a direct manner, as compared with standard powder-diffraction or maximum-entropy methods [21,24].

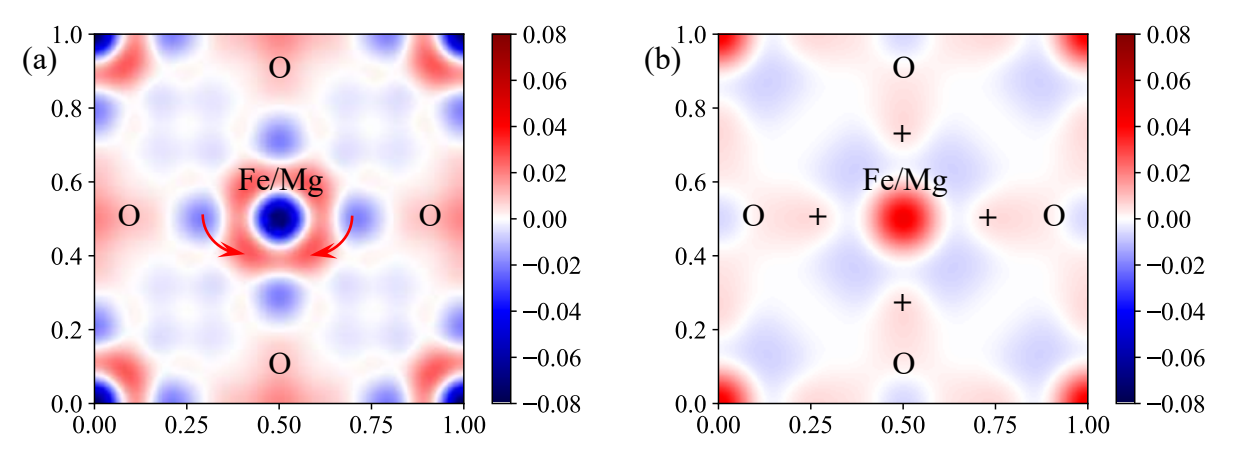


FIG. 2. Electron-density distribution difference maps in the (100) plane for (Fe_{0.53}Mg_{0.47})O at room temperature, with *red* and *blue* respectively indicating increased and decreased electron density. (a) End-transition (56 GPa) minus minimum compression (18 GPa), with *arrows* illustrating transfer of electron density. (b) Maximum (74 GPa) minus end-transition compression (56 GPa): the pressure-induced electron density increase between the iron/magnesium and oxygen (labelled with +) indicates an increase in covalency of the compressed bond. The scale is relative to the maximum electron density at 18 GPa (see Supplementary Material [31] for additional details).

The electron density maps for (Fe_{0.53}Mg_{0.47})O reveal subtle changes under compression, as best seen in difference maps (Fig. 2), shown along the (100) plane to capture the behavior of the Fe 3d orbitals and O 2p orbitals. A comparison of end-transition (fully low-spin) and minimum-compression (fully high-spin) results [Fig. 2(a)] shows -2.0 and +2.6 percent changes across the transition, with electron density redistributed from regions between the Fe/Mg and nearest-neighbor O sites toward regions between Fe/Mg (second-neighbor) sites with increased pressure [red arrows in Fig. 2(a)]. The observed change in electron density is close to the expected change of about 6 percent [31].

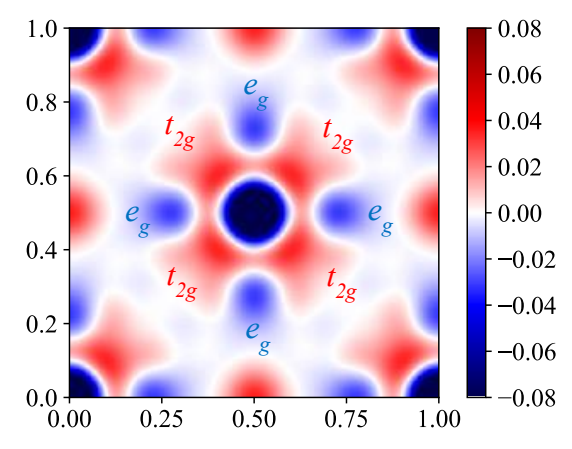


FIG. 3. Electron-density distribution difference map in the (100) plane across the high- to low-spin transition in (Fe_{0.53}Mg_{0.47})O, corrected for pressure-induced covalency changes. The effect of compression increasing electron density between nearest neighbors [Fig. 2(b)] is subtracted from the change in electron density between end-transition (56 GPa) and minimum-compression (18 GPa) [Fig. 2(a)] in order to isolate the change in electron density due to the spin transition alone (see Fig. S10). Orientations of t_{2g} and e_g orbitals are labeled, and the lowest peak intensities (to -0.187) are saturated on the present color scale (see Fig. S11 for more details).

Further compression increases the electron density along the nearest-neighbor bonds, which we interpret as pressure-enhancement of covalency due to increased overlap between O 2p orbitals and the cation valence electrons [+ in Fig. 2(b)]. Removing this change in covalency as a function of compression allows us to isolate the change in electron density due to the spin transition alone (Fig. 3) (see Fig. S10 in the Supplemental Material [31]). The results clearly show increased electron density in the central Fe/Mg ion toward the second-neighbor Fe/Mg sites (i.e., in diagonal directions relative to the unit cell, labelled t_{2g}), as compared with the regions of decreased electron density between nearest neighbors (horizontal and vertical directions, labelled e_g). This result is as expected for 3d electrons being shifted from e_g to t_{2g} orbitals according to crystal-field theory, and it emulates changes predicted from first-principles calculations [4].

Three-dimensional rendering of our results [Fig. 4(a)] clearly shows the effects of the pressure-induced spin transition at the cation site (*left* side of figure) as a decreased electron density in the directions of first- and second-neighbor oxygen ions (*blue* surfaces in the <100> and <111> directions around the cation, respectively), and increased electron density in the <110> directions of the nearest cations; the electron density distribution at the cation site shifts toward a truncated-cube configuration (cf. [4]). Comparing with the 3*d* hydrogenic orbitals [Fig. 4(b)], these changes are in line with destabilization of the e_g [Fig. 4(c)] relative to the t_{2g} orbitals [Fig. 4(d)], in accord with expected crystal-field effects. The influence of second-neighbor anion interactions present in the (Fe,Mg)O crystal (<111> *blue* surfaces around the cation) and enhanced oxygen p—orbital electron density (red extensions in <100> directions at the anion site), neither of which is typically accounted for in crystal-field models, are evident in the data [Fig. 4(a)].

Electron density is a primary output of first-principles quantum mechanical calculations, as density-functional theory (DFT) is based on the energy and derived properties of a crystal being determined by charge density via the Hohenberg–Kohn theorems. As such, agreement between experimental and theoretical determinations of electron density serves as a foundation for understanding the chemical and physical properties of materials.

Here we experimentally document the effect of the high-pressure *d*-electron spin-pairing transition on electron density, previously portrayed only by theory. Our quantitative maps of local electron density changes are consistent with the classical crystal-field model and resemble difference electron density output from DFT calculations [4], despite theory indicating that crystal field splitting is secondary to band broadening [28–30]. The results also improve on the classical use of ionic radii by documenting that the reduced nearest-neighbor Fe–O bond length in the low-spin state is caused by a change in shape of the Fe(II) ion through the spin transition [3].

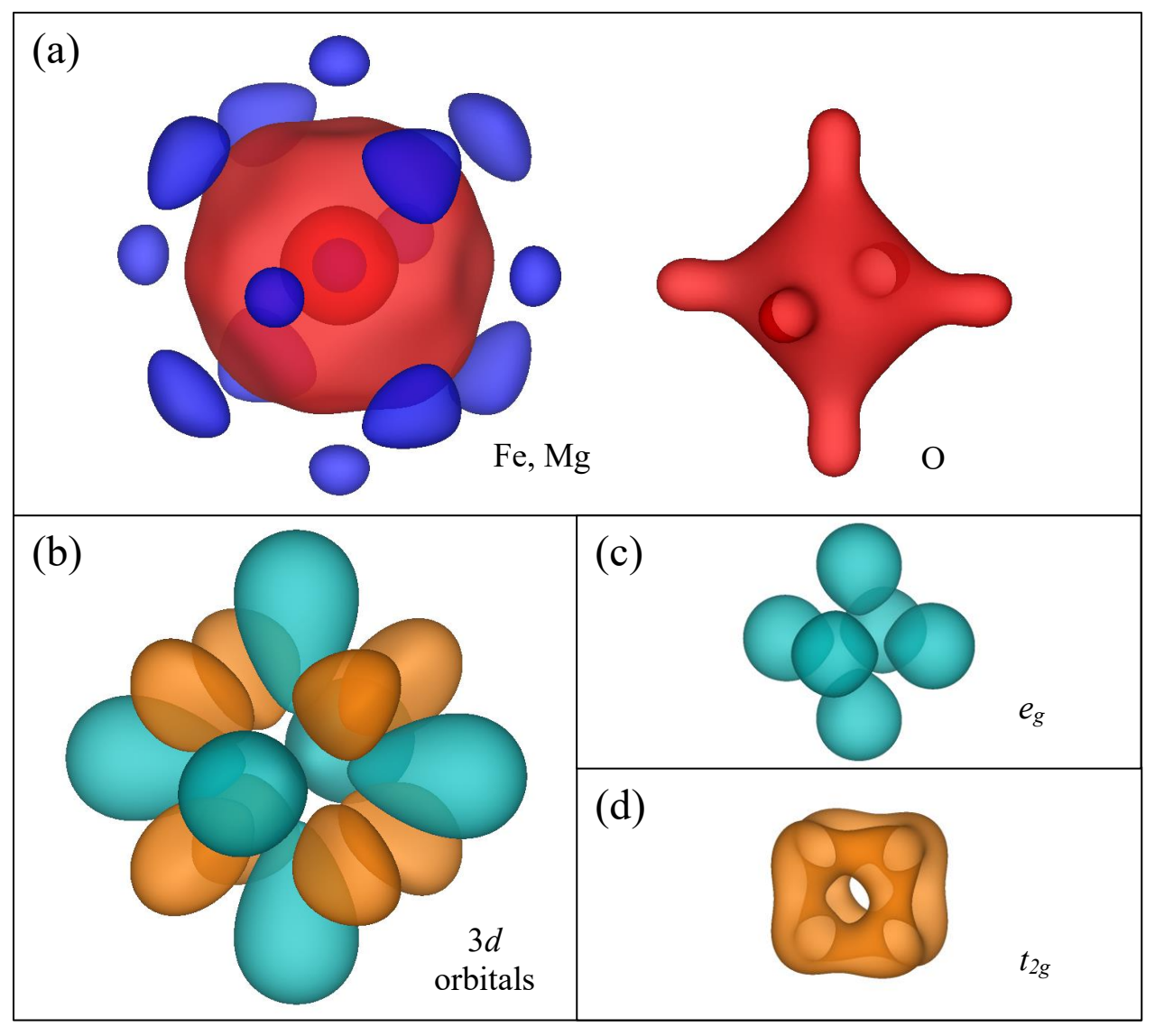


FIG. 4. (a) Three-dimensional contours of increased (red) and decreased (blue) electron density across the spin transition, with the Fe-Mg (cation) site on the left and the O (anion) site on the right, as derived from room temperature unfiltered end-transition (56 GPa) minus minimum compression (18 GPa) results for (Fe_{0.53}Mg_{0.47})O (see Fig. 2: constant-value isosurface maps are for \pm 0.013 relative to 18 GPa data, hence dimensionless, and are plotted using VESTA [50]). (b) Hydrogenic 3d orbitals, distinguishing the $d_{x^2-y^2}$ and d_{z^2} (teal) from the d_{xy} , d_{xz} and d_{yz} (orange) orbitals, which make up the e_g (c) and t_{2g} (d) orbitals respectively (isosurface values at 1.78 e^- /nm³). See Supplementary Materials [32]. The color scheme in (b)-(d) refers to hydrogen orbitals, so is distinct from that in (a) that represents the measured data.

The work was performed at HPCAT (Sector 16), Advanced Photon Source (APS), Argonne National Laboratory. HPCAT operations are supported by DOE-NNSA's Office of Experimental Sciences. The Advanced Photon Source is a U.S. Department of Energy (DOE) Office of Science User Facility operated for the DOE Office of Science by Argonne National Laboratory under Contract No. DE-AC02-06CH11357. We thank Yu-Sheng Chen (ChemMatCARS), James Walsh (UMass Amherst), Kenneth Raymond (UC Berkeley), Jonathan Ma (UC Berkeley), Kenneth Hung (UC Berkeley), H.-R. Wenk (UC Berkeley), M. Manga (UC Berkeley), B. Militzer (UC Berkeley), and M. Kunz (LBNL) for helpful discussion. We also thank Wolfgang Kapsch (Max-Planck-Institut für Medizinische Forschung) for XDS help and Rostislav Hrubriak, Curtis Kenney-Benson, and Eric Rod (HPCAT) for experimental help. G.S. acknowledges the support by DOE-DMSE under Award No. DEFG02-99ER45775. S.D.J. acknowledges support from the US National Science Foundation award EAR-1853521. This project was supported by Carnegie/DOE Alliance Center (CDAC), both for funding and with beamtime access, and by the DOE through CMEC.

- [1] J. F. Lin, S. Speziale, Z. Mao, and H. Marquardt, Effects of the Electronic Spin Transitions of Iron in Lower Mantle Minerals: Implications for Deep Mantle Geophysics and Geochemistry, Rev. Geophys. 51, 244 (2013).
- [2] S. Speziale, A. Milner, V. E. Lee, S. M. Clark, M. P. Pasternak, and R. Jeanloz, *Iron Spin Transition in Earth's Mantle*, Proc. Natl. Acad. Sci. U.S.A. **102**, 17918 (2005).
- [3] R. D. Shannon and C. T. Prewitt, *Effective Ionic Radii in Oxides and Fluorides*, Acta Crystallogr. Sect. B Struct. Sci. Cryst. Eng. Mater. **25**, 925 (1969).
- [4] T. Tsuchiya, R. M. Wentzcovitch, C. R. S. da Silva, and S. de Gironcoli, *Spin Transition in Magnesiowüstite in Earth's Lower Mantle*, Phys. Rev. Lett. **96**, 198501 (2006).
- [5] M. P. Pasternak, R. D. Taylor, R. Jeanloz, X. Li, J. H. Nguyen, and C. A. McCammon, *High Pressure Collapse of Magnetism in Fe_{0.94}O: Mössbauer Spectroscopy beyond 100 GPa*, Phys. Rev. Lett. **79**, 5046 (1997).
- [6] W. Sturhahn, J. M. Jackson, and J. F. Lin, *The Spin State of Iron in Minerals of Earth's Lower Mantle*, Geophys. Res. Lett. **32**, L12307 (2005).
- [7] J.-F. Lin, V. V. Struzhkin, S. D. Jacobsen, M. Y. Hu, P. Chow, J. Kung, H. Liu, H. Mao, and R. J. Hemley, *Spin Transition of Iron in Magnesiowüstite in the Earth's Lower Mantle*, Nature **436**, 377 (2005).
- [8] J.-F. Lin, A. G. Gavriliuk, V. V. Struzhkin, S. D. Jacobsen, W. Sturhahn, M. Y. Hu, P. Chow, and C. S. Yoo, *Pressure-Induced Electronic Spin Transition of Iron in Magnesiowustite-(Mg,Fe)O*, Phys. Rev. B Condens. Matter Mater. Phys. **73**, 73 (2006).
- [9] S. Speziale, V. E. Lee, S. M. Clark, J. F. Lin, M. P. Pasternak, and R. Jeanloz, *Effects of Fe Spin Transition on the Elasticity of (Mg, Fe)O Magnesiowüstites and Implications for the Seismological Properties of the Earth's Lower Mantle*, J. Geophys. Res. Solid Earth 112, B10212 (2007).
- [10] J. C. Crowhurst, J. M. Brown, A. F. Goncharov, and S. D. Jacobsen, *Elasticity of (Mg,Fe)O through the Spin Transition of Iron in the Lower Mantle*, Science. **319**, 451 (2008).
- [11] H. Marquardt, S. Speziale, H. J. Reichmann, D. J. Frost, F. R. Schilling, and E. J. Garnero, *Elastic Shear Anisotropy of Ferropericlase in Earth's Lower Mantle*, Science. **324**, 224 (2009).
- [12] H. Marquardt, S. Speziale, H. J. Reichmann, D. J. Frost, and F. R. Schilling, *Single-Crystal Elasticity of (Mg0.9Fe0.1)O to 81 GPa*, Earth Planet. Sci. Lett. **287**, 345 (2009).
- [13] R. Caracas, D. Mainprice, and C. Thomas, *Is the Spin Transition in Fe*²⁺-*Bearing Perovskite Visible in Seismology?*, Geophys. Res. Lett. **37**, (2010).
- [14] D. Antonangeli, J. Siebert, C. M. Aracne, D. L. Farber, A. Bosak, M. Hoesch, M. Krisch, F. J. Ryerson, G. Fiquet, and J. Badro, *Spin Crossover in Ferropericlase at High Pressure: A Seismologically Transparent Transition?*, Science. **331**, 64 (2011).
- [15] Z. Mao, J.-F. Lin, J. Liu, and V. B. Prakapenka, *Thermal Equation of State of Lower-Mantle Ferropericlase across the Spin Crossover*, Geophys. Res. Lett. **38**, L23308 (2011).
- [16] J. Badro, Spin Transitions in Mantle Minerals, Annu. Rev. Earth Planet. Sci. 42, 231

- (2014).
- [17] J. Deng and K. K. M. Lee, Viscosity Jump in the Lower Mantle Inferred from Melting Curves of Ferropericlase, Nat. Commun. 8, 1997 (2017).
- [18] H. Marquardt, J. Buchen, A. S. J. Mendez, A. Kurnosov, M. Wendt, A. Rothkirch, D. Pennicard, and H. P. Liermann, *Elastic Softening of (Mg_{0.8}Fe_{0.2})O Ferropericlase Across the Iron Spin Crossover Measured at Seismic Frequencies*, Geophys. Res. Lett. **45**, 6862 (2018).
- [19] T. Yamanaka, T. Fukuda, Y. Komatsu, and H. Sumiya, *Charge Density Analysis of SiO*² under Pressures over 50 GPa Using a New Diamond Anvil Cell for Single-Crystal Structure Analysis, J. Phys. Condens. Matter **14**, 10545 (2002).
- [20] T. Yamanaka, Y. Komatsu, and H. Nomori, *Electron Density Distribution of FeTiO3 Ilmenite under High Pressure Analyzed by MEM Using Single Crystal Diffraction Intensities*, Phys. Chem. Miner. **34**, 307 (2007).
- [21] T. Yamanaka, T. Okada, and Y. Nakamoto, *Electron Density Distribution and Static Dipole Moment of KNbO₃ at High Pressure*, Phys. Rev. B **80**, 094108 (2009).
- [22] R. Li, J. Liu, L. Bai, J. S. Tse, and G. Shen, *Pressure-Induced Changes in the Electron Density Distribution in α-Ge near the α-β Transition*, Appl. Phys. Lett. **107**, 072109 (2015).
- [23] N. Casati, A. Kleppe, A. P. Jephcoat, and P. Macchi, *Putting Pressure on Aromaticity along with in Situ Experimental Electron Density of a Molecular Crystal*, Nat. Commun. 7, 10901 (2016).
- [24] T. Yamanaka, Y. Nakamoto, M. Ahart, and H. K. Mao, *Pressure Dependence of Electron Density Distribution and D-p-π Hybridization in Titanate Perovskite Ferroelectrics*, Phys. Rev. B **97**, 144109 (2018).
- [25] R. Li, J. Liu, D. Popov, C. Park, Y. Meng, and G. Shen, *Experimental Observations of Large Changes in Electron Density Distributions in β-Ge*, Phys. Rev. B **100**, 224106 (2019).
- [26] R. Gajda, M. Stachowicz, A. Makal, S. Sutula, J. Parafiniuk, P. Fertey, and K. Wozniak, Experimental Charge Density of Grossular under Pressure – a Feasibility Study, IUCrJ 7, 383 (2020).
- [27] Other forms of iron (e.g., ferric) are expected to be far less abundant than the ferrous ion throughout most of Earth's mantle, so are not addressed here except to note that they can also undergo pressure-induced spin transition.
- [28] R. E. Cohen, I. I. Mazin, and D. G. Isaak, *Magnetic Collapse in Transition Metal Oxides at High Pressure: Implications for the Earth*, Science. **275**, 654 (1997).
- [29] L. Shulenburger, S. Y. Savrasov, and R. E. Cohen, *Relative Importance of Crystal Field versus Bandwidth to the High Pressure Spin Transition in Transition Metal Monoxides*, J. Phys. Conf. Ser. **215**, 012122 (2010).
- [30] E. Holmström and L. Stixrude, *Spin Crossover in Ferropericlase from First-Principles Molecular Dynamics*, Phys. Rev. Lett. **114**, 117202 (2015).

- [31] N. V. Solomatova, J. M. Jackson, W. Sturhahn, J. K. Wicks, J. Zhao, T. S. Toellner, B. Kalkan, and W. M. Steinhardt, *Equation of State and Spin Crossover of (Mg,Fe)O at High Pressure, with Implications for Explaining Topographic Relief at the Core-Mantle Boundary*, Am. Mineral. **101**, 1084 (2016).
- [32] See Supplementary Materials.
- [33] S. D. Jacobsen, H.-J. Reichmann, H. A. Spetzler, S. J. Mackwell, J. R. Smyth, R. J. Angel, and C. A. McCammon, *Structure and Elasticity of Single-Crystal (Mg,Fe)O and a New Method of Generating Shear Waves for Gigahertz Ultrasonic Interferometry*, J. Geophys. Res. **107**, 2037 (2002).
- [34] A. P. Kantor, S. D. Jacobsen, I. Y. Kantor, L. S. Dubrovinsky, C. A. McCammon, H. J. Reichmann, and I. N. Goncharenko, *Pressure-Induced Magnetization in FeO: Evidence from Elasticity and Mössbauer Spectroscopy*, Phys. Rev. Lett. **93**, 19 (2004).
- [35] J. Badro, G. Fiquet, F. Guyot, J. P. Rueff, V. V. Struzhkin, G. Vankó, and G. Monaco, Iron Partitioning in Earth's Mantle: Toward a Deep Lower Mantle Discontinuity, Science. 300, 789 (2003).
- [36] J. Badro, V. V. Struzhkin, J. Shu, R. J. Hemley, H. Mao, C. C. Kao, J. P. Rueff, and G. Shen, *Magnetism in FeO at Megabar Pressures from X-Ray Emission Spectroscopy*, Phys. Rev. Lett. **83**, 4101 (1999).
- [37] B. D. Cullity, *Elements of X-Ray Diffraction*, 3rd ed. (Reading, MA, 1956).
- [38] I.-H. Seo, Structure Factor Electron Density, Korean J. Crystallogr. 11, 241 (2000).
- [39] C. Prescher and V. B. Prakapenka, DIOPTAS: A Program for Reduction of Two-Dimensional X-Ray Diffraction Data and Data Exploration, High Press. Res. 35, 223 (2015).
- [40] G. M. Sheldrick, *Crystal Structure Refinement with SHELXL*, Acta Crystallogr. Sect. C Struct. Chem. **71**, 3 (2015).
- [41] K. K. M. Lee, B. O'Neill, W. R. Panero, S. H. Shim, L. R. Benedetti, and R. Jeanloz, Equations of State of the High-Pressure Phases of a Natural Peridotite and Implications for the Earth's Lower Mantle, Earth Planet. Sci. Lett. 223, 381 (2004).
- [42] I. Jackson, *Elasticity, Composition and Temperature of the Earth's Lower Mantle: A Reappraisal*, Geophys. J. Int. **134**, 291 (1998).
- [43] N. R. Draper and H. Smith, *Applied Regression Analysis*, 3rd ed. (Wiley, New York, NY, 1998).
- [44] G. Vidal-Valat, J. P. Vidal, and K. Kurki-Suonio, *X-ray Study of the Atomic Charge Densities in MgO, CaO, SrO and BaO*, Acta Crystallogr. Sect. A **34**, 594 (1978).
- [45] R. Jeanloz and A. B. Thompson, *Phase Transitions and Mantle Discontinuities*, Rev. Geophys. Sp. Phys. **21**, 51 (1983).
- [46] D. L. Heinz and R. Jeanloz, *The Equation of State of the Gold Calibration Standard*, J. Appl. Phys. **55**, 885 (1984).
- [47] F. Birch, Finite Strain Isotherm and Velocities for Single-Crystal and Polycrystalline NaCl at High Pressures and 300°K, J. Geophys. Res. 83, 1257 (1978).

- [48] H. K. Mao, J. Xu, and P. M. Bell, *Calibration of the Ruby Pressure Gauge to 800 Kbar under Quasi-Hydrostatic Conditions*, J. Geophys. Res. **91**, 4673 (1986).
- [49] Y. Akahama and H. Kawamura, *Diamond Anvil Raman Gauge in Multimegabar Pressure Range*, High Press. Res. **27**, 473 (2007).
- [50] I. Jackson and H. Nielsler, *The Elasticity of Periclase to 3 GPa and Some Geophysical Implications*, Adv. Earth Planet. Sci. **12**, 93 (1982).
- [51] K. Momma and F. Izumi, *VESTA 3 for Three-Dimensional Visualization of Crystal, Volumetric and Morphology Data*, J. Appl. Crystallogr. **44**, 1272 (2011).
- [52] D. Serebrennikov, E. Clementyev, A. Semenov, and A. Snigirev, *Optical Performance of Materials for X-Ray Refractive Optics in the Energy Range 8-100 KeV*, J. Synchrotron Radiat. **23**, 1315 (2016).

Supplementary Material: Electron density change across the pressure- induced iron spin transition

Matthew R. Diamond¹, Guoyin Shen², Dmitry Y. Popov², Changyong Park², Steven D. Jacobsen³, and Raymond Jeanloz¹

¹Department of Earth and Planetary Science, University of California, Berkeley, CA 94720, USA ²HPCAT, X-ray Science Division, Argonne National Laboratory, Lemont, IL 60439, USA ³Department of Earth and Planetary Sciences, Northwestern University, Evanston, IL 60208, USA

Sample

The single-crystal samples, with approximate dimensions 20 μ m by 20 μ m across and 10 μ m thick, were cut from larger synthesized grains described in Ref. [32] applying a hand-held razor to {001} cleavage planes. Wide-angle x-ray diffraction data were collected using a BX90 diamond-anvil cell, with 300 μ m culets for the (Fe_{0.15}Mg_{0.85})O sample and 200 μ m culets for the (Fe_{0.53}Mg_{0.47})O sample. For both sample chambers we used a rhenium gasket and helium as a pressure medium, with ruby spheres for pressure calibration. CeO₂ powder was used for calibration of the detector geometry, and data were processed with the software Dioptas [38].

Experiment

The high-pressure single-crystal diffraction experiments were performed at the 16-BM-D beamline of HPCAT (Sector 16), Advanced Photon Source, Argonne National Laboratory. The incident x-ray energy was chosen by a Si (111) double crystal monochromator in a pseudo channelcut geometry, and the beam was focused to 4 µm x 4 µm at the FWHM with Pt-coated Kirkpatrick-Baez type mirrors. Energy of 40.00 keV was used in all experiments except for the following: for (Fe_{0.53}Mg_{0.47})O an x-ray energy of 39.44 keV was used for the compression data at \leq 58 GPa, and an x-ray energy of 39.52 keV was used for the ambient data set; for (Fe_{0.15}Mg_{0.85})O x-ray energies of 39.62 keV and 39.41 keV were used for the decompression data sets at 38 GPa and 28 GPa, respectively, and an x-ray energy of 40.43 keV was used for the maximum-compression data set. The single-crystal diffraction patterns were collected under a pseudo 3-circle diffractometer geometry; phi and omega angles for sample orientations were degenerate, and 2-theta and chi angles were resolved on a large-area detector located at a fixed distance from the sample rotation center. The sphere of confusion of the sample rotation center was maintained at less than 1 µm during the serial collection of single-crystal diffraction patterns at different omega angles. The resolved omega, chi, and 2-theta angles were used to index the set of single-crystal diffraction peaks. The diffraction intensities were collected using a Mar345 Image Plate detector (processed at 2300 pixels), typically positioned approximately 25 cm from the sample.

Data reduction

In order to separate reflections produced by the samples from those produced by the diamonds, we used the HPCAT grain identification Python code Trommel, written by D. Popov. The area between the regions shadowed by the diamond cell was used as the rotation range (set by counts measured by beamline diode), and background was taken from middle images. Peak profiles were determined iteratively in XDS by XDS-suggested integration parameters. Peak corrections were suppressed in XDS by setting N BATCH to REFLECTIONS/CORRECTIONS factor to 100. Data sets collected at different axial rotations of the diamond cell (orthogonal to the x-ray beam) were combined in data reduction for determination of peak intensities, but only reflections shared among all data sets were considered. These typically included 1-3 rotations, of mainly ~90- and ~45-degree rotational offsets. The intensities are taken from the XSCALE.hkl file, a combined output from all measurements for a given compression. The structure factor (square root of intensities: see main text) for each hkl set is taken as an average of structure factors from measured symmetrically equivalent reflections [shown in Fig. 1 as a fraction of the largest averaged value, (0 0 2)].

For self-consistent treatment of the data, reflections not shared among all compressional measurements were excluded in data reduction. Also, data sets that did not contain all reflections considered were excluded, and the ambient data set is not discussed here because it was collected under different conditions, outside a diamond-anvil cell. Missing reflections are due to the diffraction geometry relative to the orientations of the sample, gasket, and diamond cell. The reflections shown here for the (Fe_{0.53}Mg_{0.47})O sample have a resolution limit up to the (0 4 6) reflection, with fifteen out of twenty-two possible reflections reported (an effective completeness of 0.681 [hkl indices (1 1 1), (2 2 2), (2 2 4), (3 3 3), (3 3 5), (2 2 6), and (4 4 4) are not accounted for]).

Data processing

We found that crystal-structure refinement using the software SHELX [39], based on approximate spherical form factors, produces good *R* factors (Fig. S12) but struggles with the correlation of the Fe and Mg structure-factor contributions. Specifically, SHELX tends to attribute our observed changes in diffraction intensities to an increase in the Debye-Waller thermal scattering factor, which is deemed unphysical because isothermal compression increases vibrational frequencies and therefore decreases vibrational amplitudes (Fig. S13). Also, SHELX gives significantly different – hence unrealistic – results for Mg than for Fe and O.

Therefore, we use a Debye-Grüneisen model to estimate the change in thermal factor over the compression range of our experiments on $(Fe_{0.53}Mg_{0.47})O$, as described next. We correct the intensities by this thermal factor, and use the corrected intensities to derive the electron densities that we report. We find that the thermal correction to the relative structure factors is almost indistinguishable at all of our pressures, and it is therefore applied more out of formality than necessity, but the important point is that we consider the apparent pressure-induced increase suggested by the SHELX output to be wrong both in magnitude and sign. Additional corrections due to changes in effective absorption under compression are found to be negligible (Fig. S14).

Debye-Waller Thermal factor

The thermal scattering factor M is modeled as follows, with subscript zero denoting ambient pressure [36]. The Grüneisen parameter γ varies with compression as $\gamma = \gamma_0 \left(\frac{V}{V_0}\right)^q$, and the Debye temperature is then given by $\theta_M = \theta_{M_0} e^{(\gamma_0 - \gamma)/q}$, as described in Section 5.2 of Ref. [40]. The square of the average thermal scattering distance is $U = \frac{3\hbar^2}{mk_BTx^2} \left(\phi(x) + \frac{x}{4}\right)$, using $x = \frac{\theta_M}{T}$ and $\phi(x) = \frac{1}{x} \int_0^x \frac{\xi}{e^{\xi}-1} d\xi \approx 1 - \frac{x}{4} + \frac{x^2}{36}$. With the Debye-Waller factor given as $B = 8\pi^2 U$, we solve for $M = B\left(\frac{\sin\theta}{\lambda}\right)^2$ and therefore $M = B\left(\frac{1}{2d}\right)^2$ (as $\lambda = 2d\sin\theta$ means $\frac{\sin\theta}{\lambda} = \frac{1}{2d}$), where $d = \frac{\sqrt[3]{V}}{|hkl|}$ for cubic symmetry. Modeled crystal properties were taken from Table 1 of Ref. [41]. The model values are shown in Fig. S14.

Structure factor fits

The relative structure factors are simultaneously fit using a model that has two linear trends:

$$Y_i = a[X_i - X_0] + b + cZ_i[X_i - X_0 - (t - X_0)]$$
 (1)

giving the relative structure factor Y as a function of compression X (starting at initial considered compression X_0), where t is the dividing compression (taken as the end-transition point, to be determined by the fit), Z is a dummy variable equal to 0 for the lower-pressure set of data (preend-transition) and 1 for the higher-pressure set of data (post-end-transition), and c is the change in slope of the trends (Ch. 14 in Ref. [42]). Table SI presents statistics for the (Fe_{0.53}Mg_{0.47})O data, with the fit giving a compression of $V_0/V = 1.27$ for t (corresponding to P = 56 GPa). R^2 values for the fits are typically around 70-80%, with many statistically significant values of c (p < 0.05) and an overall statistically significant observation of a change in c in at least one c with p = 0.0028 [for (1 3 3)] after a Bonferroni correction of $p_B = p * 14$ (14 reflections considered).

The values in Table S1 are output from the Python library 'statsmodels.api', using uncertainty-weighted fits. 'p-val' is the statistical p value; 'SSR' is the sum of squared residuals. 'S' is shorthand for 'Slope'. In reference to supplementary equation (1), Slope_1 refers to the slope a, and Slope_2 refers to the change in slope c after the end-transition point t (56 GPa); Slope_0 refers to the slope from fitting all pressure steps with one line. To answer the question of whether the Slope_2 change is statistically non-zero, we ran statistical two-sample t (not to be confused with t) tests of the two-trend model [supplementary equation (1)] for each hkl. The p values for Slope_2 are in many instances below 0.05 by themselves, and a few are below or near 0.05 when multiplied by 14 (total number of relative structure factors) as a Bonferroni correction, the latter condition indicating that some change occurs over the whole dataset.

Electron density map observations

From Fig. 2(a), we quantify the change in electron density in regions around the central iron/magnesium atom to be approximately -2.00 percent (blue) or +2.61 percent (red) of the cation peak intensity from Fig. S5(a) [-3.08 percent (blue) or +3.43 percent (red) from Fig. 3]. This can be compared with our expectations for the two-electron spin collapse assuming the ionic model of traditional crystal field theory [1]. From our assumed Fe/Mg composition of 0.527/(1-0.527) and ionic electron counts for Fe and Mg of 24 and 10, respectively, we calculate the average number of electrons per cation as (1-0.527)*10+0.527*24 = 17.378. Accounting for composition, the number of electrons per cation undergoing spin transition would be 0.527*2 = 1.054. From this argument we expect a change of intensity of 1.054/17.378 = 6.07 percent in the electron density map, which agrees with our experimental numbers to within nearly a factor of two.

To further explore our result, we look at the ratio of peak electron densities from the cation and oxygen sites (cation/oxygen), about 3.45 in Fig. S5(a). By counting electrons, we expect this ratio to be [(1-0.527)*10+0.527*24]/10 = 1.7378. Dividing these numbers, we find a scaling adjustment of about 1.99: also a factor of two. If this factor were to be accounted for, our valence electron percent changes would then be about –3.98 percent (blue) and +5.19 percent (red) [–6.13 percent (blue) or +6.81 percent (red) from Fig. S3], close to our 6.07 percent expectation (see also [43] regarding the effective valence of oxygen in MgO). If we use the cation/oxygen ratio from Fig. S5(b), which is about 3.01, we get a scaling of about 1.73 and scaled electron density changes of –3.46 percent (blue) and +4.51 percent (red) [–4.45 percent (blue) or +4.94 percent (red) from Fig. S3 when referencing the covalency-adjusted version of Fig. S5(b), which provides a cation/oxygen ratio of about 2.51 and respective scaling of about 1.44].

Looking at Fig. S11, the electron change in regions around the central iron/magnesium atom is approximately –3.11 percent (blue) or +3.75 percent (red) of the cation peak intensity from the unfiltered Fig. S4(a). The associated cation/oxygen peak intensity ratio is about 3.49, corresponding to a scaling of about 2.01; the scaled electron density changes are about –6.24 percent (blue) or +7.53 percent (red). Referencing instead the covalency-adjusted version of Fig. S4(b), the cation/oxygen peak intensity ratio is about 2.47, corresponding to a scaling of about 1.42; the scaled electron density changes are about –4.42 percent (blue) or +5.34 percent (red).

Overall, we find this to be good agreement between expectations from the simple crystal-field ionic model and our observations, despite the limitations of our resolution and reflection completeness.

3d orbital electron density

To provide an expectation for the spin collapse of the two electrons from two e_g orbitals to three t_{2g} orbitals with increasing pressure, the electron densities P of the hydrogen 3d orbitals were summed in the following way, assuming linear independence.

$$P = \frac{2}{3}(|\Psi_{xy}|^2 + |\Psi_{xz}|^2 + |\Psi_{yz}|^2) - (|\Psi_{x^2 - y^2}|^2 + |\Psi_{z^2}|^2)$$
 (2)

TABLE SI. Results from linear regression and two-sample t test for the change in slope of each structure-factor fit.

hkl	Slope0	p-val_S0	SSR_S0	Slope1	p-val_S1	Slope2	p-val_S2	SSR_S1S2
(0 0 2)	-0.0000	0.7775	0.0000	-0.0000	0.2234	0.0000	0.5766	0.0000
(0 2 2)	-0.0700	0.5472	5.5163	-0.1790	0.2773	0.5361	0.3393	5.1557
(0 0 4)	-0.3193	0.0002	5.6173	-0.4708	0.0001	0.8379	0.0436	4.1570
(0 2 4)	-0.2712	0.0004	4.2956	-0.3802	0.0001	0.6012	0.0478	3.2149
(1 1 3)	-0.0632	0.2033	5.9545	-0.1584	0.0343	0.4226	0.0844	4.7769
(0 4 4)	-0.2823	0.0005	9.1580	-0.4133	0.0001	0.6864	0.0285	6.4235
(2 4 4)	-0.3714	0.0000	20.1251	-0.4900	0.0000	0.5063	0.0095	12.2463
(0 0 6)	-0.3430	0.0000	7.1338	-0.4544	0.0000	0.4116	0.0524	5.4011
(1 3 3)	-0.1589	0.0013	4.9578	-0.2858	0.0000	0.6892	0.0002	1.8405
(0 2 6)	-0.3052	0.0001	8.7878	-0.3939	0.0004	0.3876	0.1935	7.7545
(0 4 6)	-0.3646	0.0000	16.7547	-0.4638	0.0000	0.5868	0.0666	13.0640
(1 1 5)	-0.2420	0.0000	4.9290	-0.3128	0.0000	0.3158	0.0317	3.5040
(1 3 5)	-0.2497	0.0000	9.0935	-0.3767	0.0000	0.6003	0.0006	3.8516
(1 5 5)	-0.2351	0.0002	35.3840	-0.3858	0.0000	0.5784	0.0041	19.2674
(1 1 7)	-0.2476	0.0000	11.8041	-0.3389	0.0000	0.4149	0.0055	6.6863

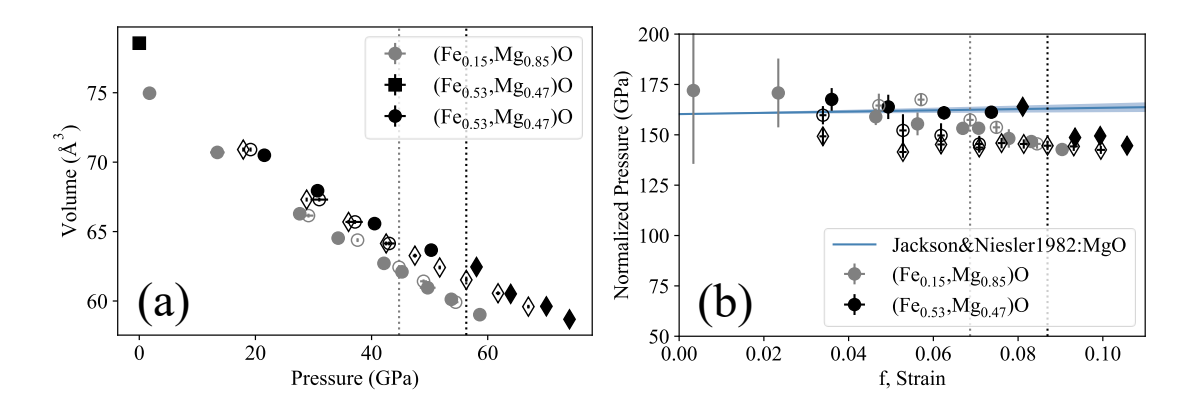


FIG. S1. Measured unit-cell volume V as a function of pressure P(a) and normalized pressure $(P/[3f(1+2f)^{5/2}] = K_0[1$ $+(3/2)(K_0'-4)f+...$ as a function of Eulerian finite strain $(f=[(V/V_0)^{-2/3}-1]/2$ [44–46]) (b) for two compositions of (Fe,Mg)O at room temperature: closed symbols on compression, open symbols on decompression (subscript zero indicates ambient conditions). Circles denote pressures measured by ruby fluorescence [47], and diamonds denote pressures measured by diamond Raman edge [48]; the ambient (0 GPa) measurement, taken outside the diamond cell, is denoted by a square. Pressure values represent an average of multiple measurements, including before and after xray data collection; the uncertainty in pressure was taken as half the total range of measured values (with the exceptions of the two lowest-pressure decompression diamond Raman points, for which each has only one measurement reported, and the value and uncertainty for the second lowest pressure decompression ruby fluorescence point, which was derived from a projection of the ruby fluorescence measurements taken before the diamond cell had relaxed to the measured difference in the diamond Raman values from before and after relaxation). Compressions at which our diffraction-intensity measurements indicate changes in structure factor trends, interpretted as due to electron-density changes, are marked by corresponding gray and black dotted vertical lines at pressures (strains) of P = 45 GPa (f =0.069) and P = 56 GPa (f = 0.087) for (Fe_{0.15}Mg_{0.85})O (gray symbols) and (Fe_{0.53}Mg_{0.47})O (black symbols), respectively. In the volume vs. pressure measurements (a), a phase change is detectable for (Fe_{0.53}Mg_{0.47})O around 60 GPa on compression, with hysteresis on decompression. Normalized pressure as a function of strain (b) effectively shows the slope of the equation of state, so is sensitive to small deviations from the baseline reference, for which we use prior measurements on pure MgO [49]. The value and uncertainty for V_{θ} are taken for both samples from the cube of the unit cell length reported in Table 1 of Ref. [44]: $75.722 \pm 0.027 \text{ Å}^3$ for $(\text{Fe}_{0.15}\text{Mg}_{0.85})\text{O}$ and $78.246 \pm 0.070 \text{ Å}^3$ for (Fe_{0.53}Mg_{0.47})O. The equation of state of MgO (blue line, with uncertainty band) is obtained from high-precision ultrasonic measurements under pressure [49]; it is expected to be close to that of (Mg,Fe)O solid solutions prior to the spin transition [32]. Our results show that, within the uncertainty and scatter of the data, the spin transition appears in the compression data at comparable strains to those indicated by the structure factors (Fig. 1 and Fig. S2). Data collected on compression and on decompression document the effects on the pressure-volume measurements of both nonhydrostatic stresses and hysteresis on the spin transition (even in a quasi-hydrostatic pressure medium such as He, the state of stress inside a single crystal undergoing a volume change is in general expected to be nonhydrostatic). We estimate the uncertainty in lattice parameter as less than 0.2 percent (0.005 Å). Where not shown, error bars are smaller than the symbols. Points (Fe_{0.15}Mg_{0.85})O: 'P2' (13 GPa compression, measured in the diamond cell but not containing all reflections, and (Fe_{0.53}Mg_{0.47})O: 'PO' (0 GPa ambient) are included here but are not included in the structure-factor plots and corresponding analysis.

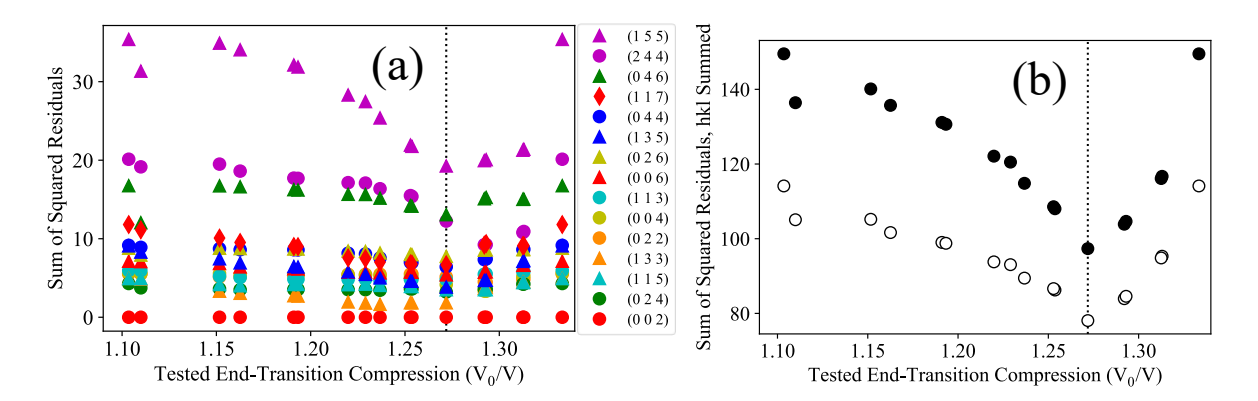


FIG. S2. Sum of squared residuals (SSR) between relative structure factors and a two-trend linear model for (Fe_{0.53}Mg_{0.47})O, shown as a function of compression at which a break in slope is obtained between the two trends. The values are normalized by the square of the uncertainties for each data point per hkl. The SSR values are shown for each hkl (a) and as a sum all hkls (b), where closed symbols are sums over all hkls and open symbols are sums over all but the hkl with largest SSRs. Each break-in-slope compression corresponds to a data set from Fig. 1. The SSR values for most structure factors achieve a minimum value at the compression of 1.27 (SSR_S1S2 values in Table SI) (56 GPa), so we take this to be the end-transition point. The SSR values at the minimum and maximum compression points are the same as those obtained when assuming no break in slope; that these values are global maxima reinforce the suitability of the two-trend model. As in Table SI, the values are output from the Python library 'statsmodels.api', using uncertainty-weighted fits.

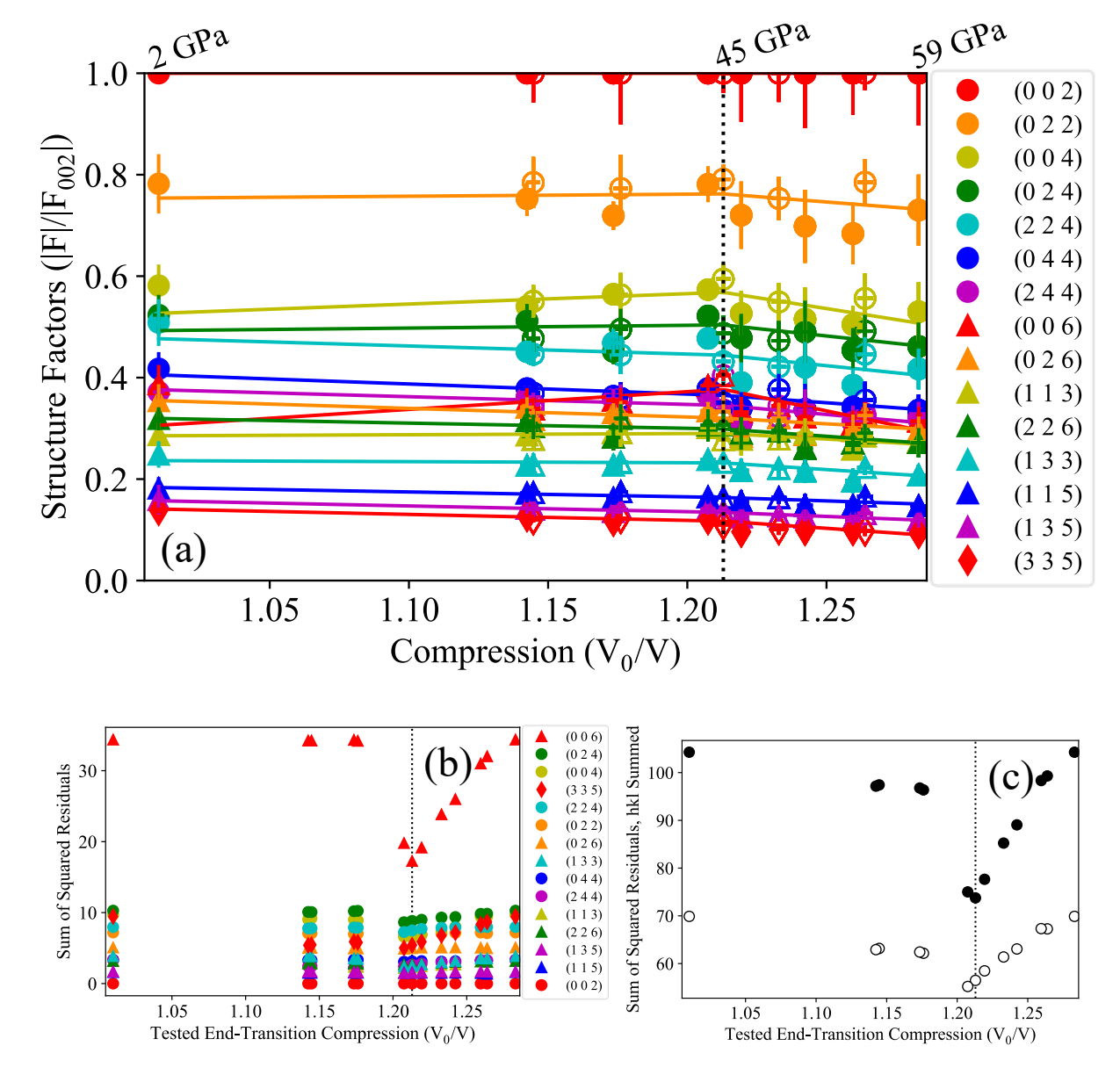


FIG. S3. Structure factors for $(Fe_{0.15}Mg_{0.85})O$. Relative structure factors (a) and sum of squared residual tests [(b) and (c)] (as in Fig. S2) indicate a change in slope around a compression of 1.21 (45 GPa), though less discernably than for the iron-rich composition (cf. Fig. 1 and Fig. S2).

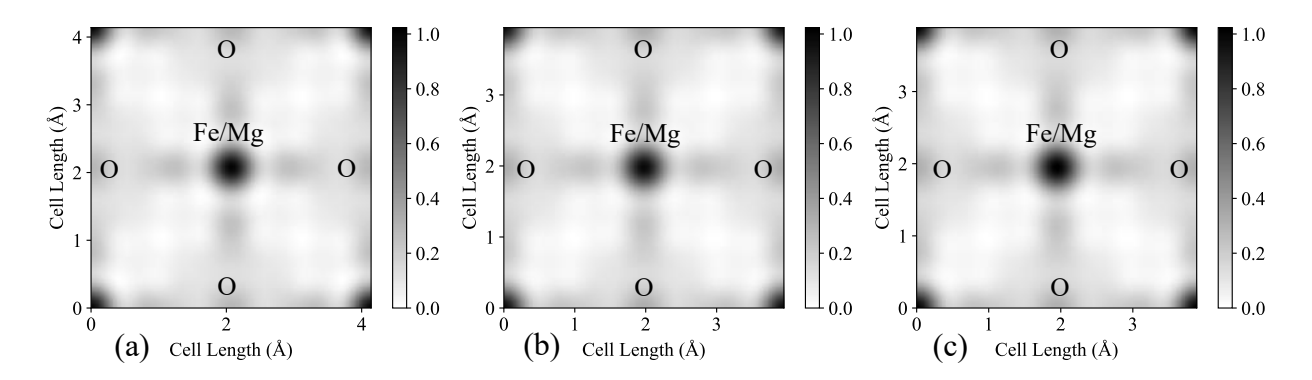


FIG. S4. Electron-density distribution maps (unfiltered) in the (100) plane for (Fe_{0.53}Mg_{0.47})O at three compressions: (a) minimum compression (18 GPa), (b) end-transition compression (56 GPa), and (c) maximum compression (74 GPa). All maps are normalized to positive values and displayed as a percentage of the intensities in the minimum compression map, with the sum of the electron density values in the entire (three-dimensional) unit cell at minimum compression used to scale the values in the end-transition-compression and maximum-compression maps. Maps (a), (b), and (c) have maximum values relative to (a) of 1.00, 0.98, and 1.02, respectively (prior to normalization, the maps have negative intensities of 8.8, 9.3, and 8.9 percent of their range of values). Spatial aliasing (horizontal and vertical texture) seen in the low-intensity regions results from the model being limited to fifteen hkls. Differences between the maps are difficult to see at this intensity scale; they are better revealed in the difference maps (Fig. 2 and Fig. S6).

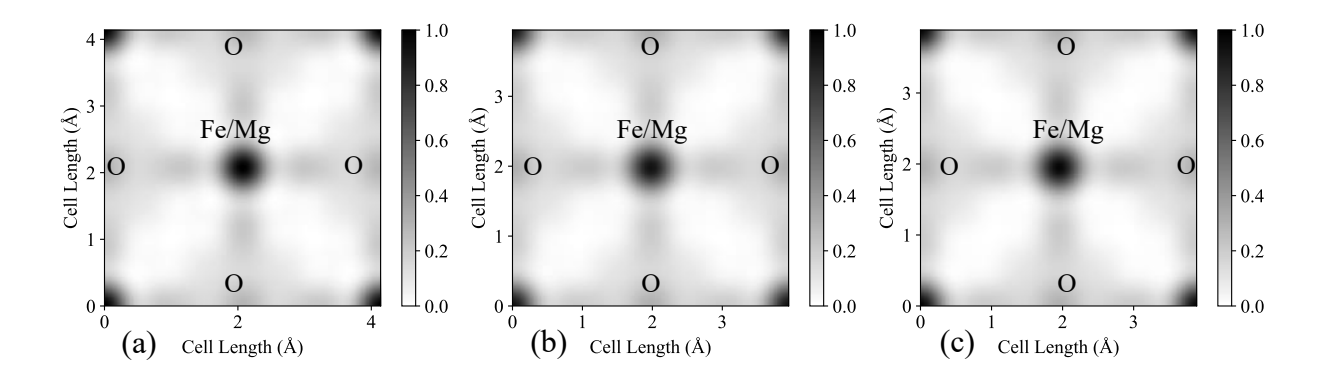


FIG. S5. Butterworth-filtered electron-density distribution maps in the (100) plane for (Fe_{0.53}Mg_{0.47})O at three compressions: (a) minimum compression (18 GPa), (b) end-transition compression (56 GPa), and (c) maximum compression (74 GPa). Butterworth filtering reduces the spatial aliasing evident in Fig. S4 (see Fig. S6 for details). Maps (a), (b), and (c) have maximum values relative to (a) of 1.00, 0.93, and 0.97, respectively (prior to normalization, the maps have negative intensities of 8.2, 8.9, and 8.5 percent of their maximum values). Note the slightly different color scale to that in Fig. S4.

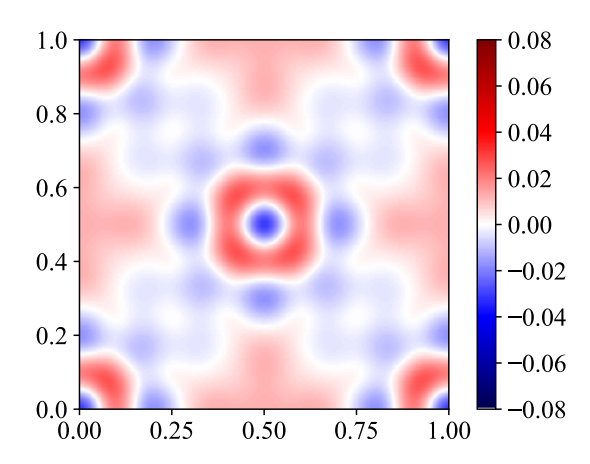


FIG. S6. Electron-density distribution difference map in the (100) plane for $(Fe_{0.53}Mg_{0.47})O$ at room temperature for maximum (74 GPa) minus minimum compression (18 GPa). A Butterworth filter [n = 4 and cut-off frequency = 0.8*highest resolution <math>hkl, (0 4 6)] is applied to the higher resolution structure factors to dampen cut-off aliasing, and the same filter is applied in obtaining Fig. 2 (see Fig. S7(c) for unfiltered plot). This map is equivalent to the summation of Figs. 2(a) and 2(b).

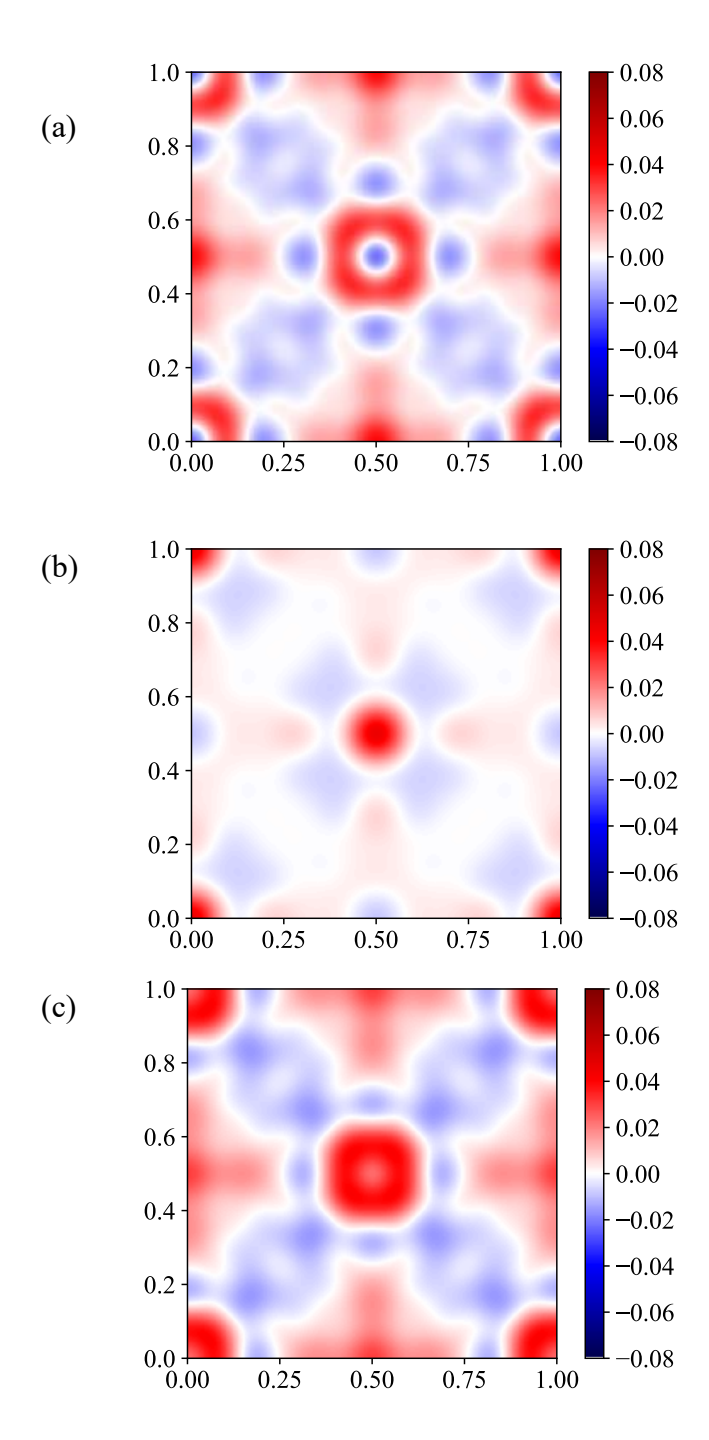


FIG. S7. Electron-density distribution difference maps (unfiltered) in the (100) plane for (Fe_{0.53}Mg_{0.47})O at room temperature for (a) end-transition (56 GPa) minus minimum compression (18 GPa), (b) maximum (74 GPa) minus end-transition compression (56 GPa), and (c) maximum (74 GPa) minus minimum compression (18 GPa). Figs. 2a, 2b and S6 present the Butterworth-filtered versions of these plots.

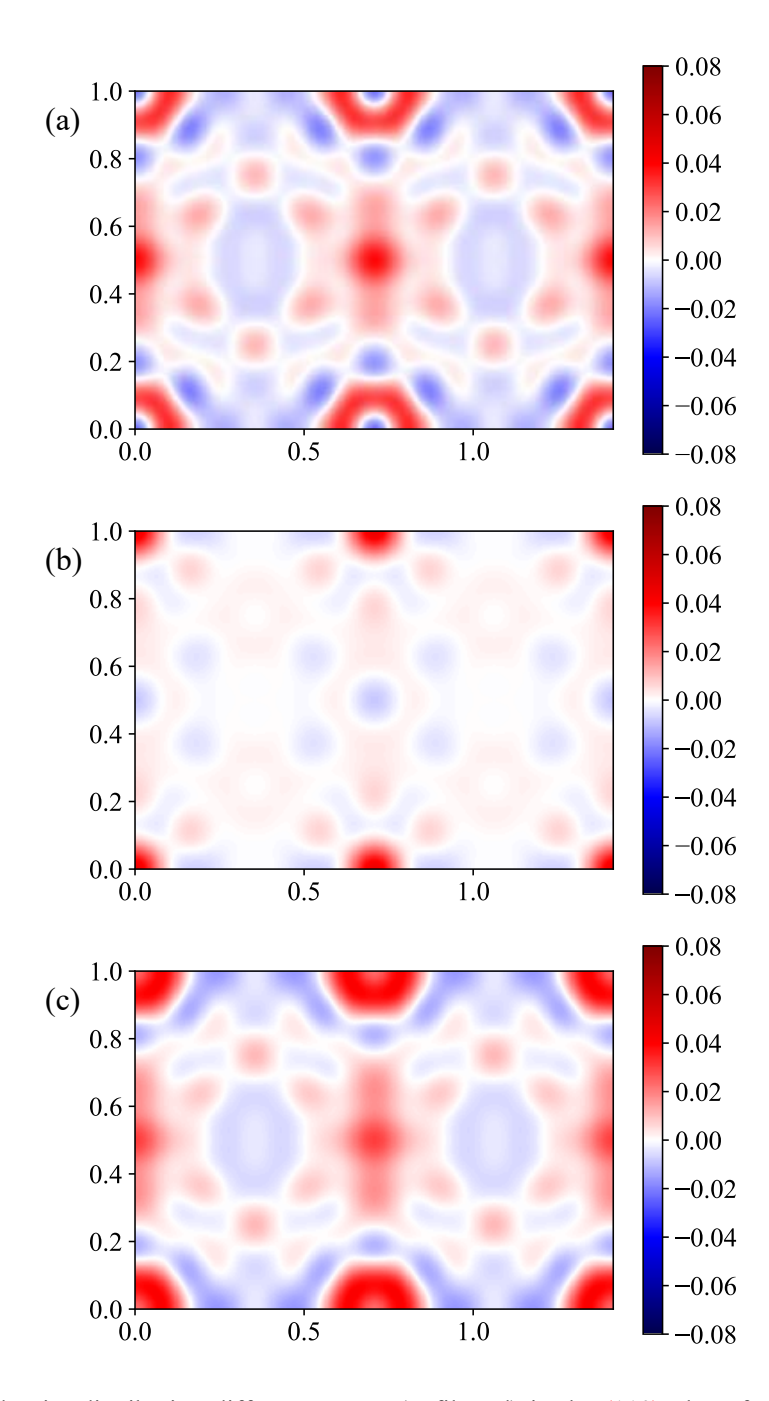


FIG. S8. Electron-density distribution difference maps (unfiltered) in the (110) plane for $(Fe_{0.53}Mg_{0.47})O$ at room temperature for (a) end-transition (56 GPa) minus minimum compression (18 GPa), (b) maximum (74 GPa) minus end-transition compression (56 GPa), and (c) maximum (74 GPa) minus minimum compression (18 GPa). The vertical edges are the same as the edges in Fig. S7. Note that values in the diagonal cation lobes of (a) are -0.0196, slightly larger than the vertical cation lobes, -0.0164, which are the same as the vertical cation lobes in Fig. S7(a).

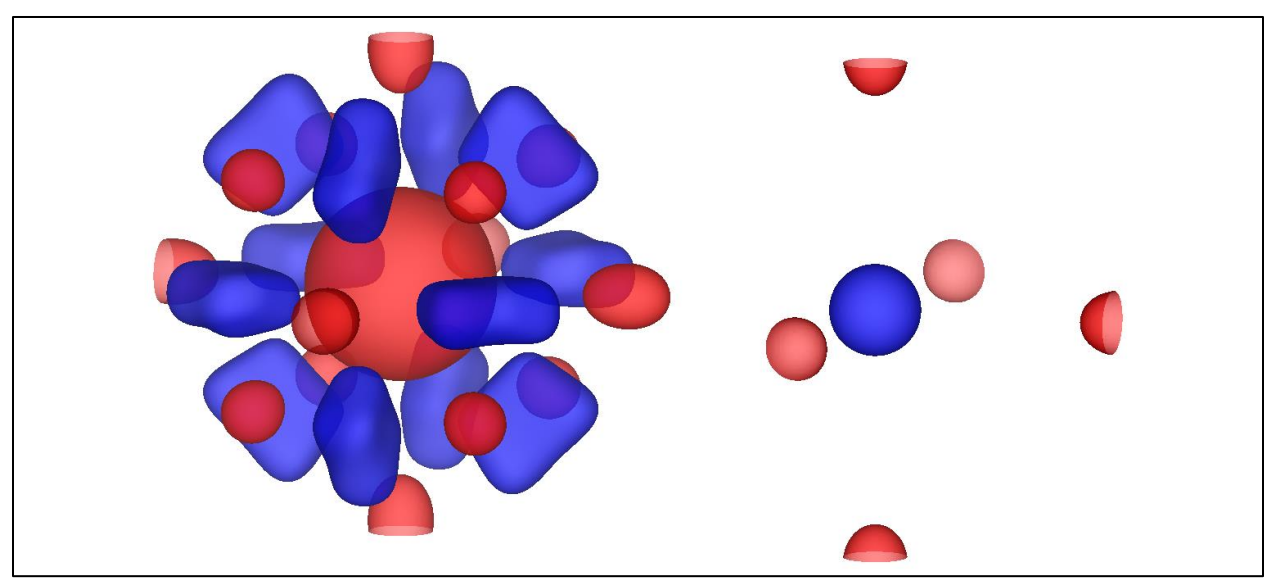


FIG. S9. Electron-density distribution difference maps of the cation (left) and oxygen (right) sites as three-dimensional isosurfaces (plotted with VESTA [50]) for (Fe_{0.53}Mg_{0.47})O at room temperature for maximum (74 GPa) minus end-transition compression (56 GPa) to show the change attributed to pressure-induced increase in covalency around the cation site. Isosurface levels are shown at \pm 0.0046, as normalized to the 18 GPa data in the same manner as with the two-dimensional maps, with positive values in red, and negative values in blue. Note that different length scales are used for Fig. 4(a) and this figure. Electron density changes around the cation site show increases in the directions of both first- and second-nearest oxygen neighbors (<100> and <111> directions, respectively), and decreases in the direction of nearest cation neighbors (<110> directions).

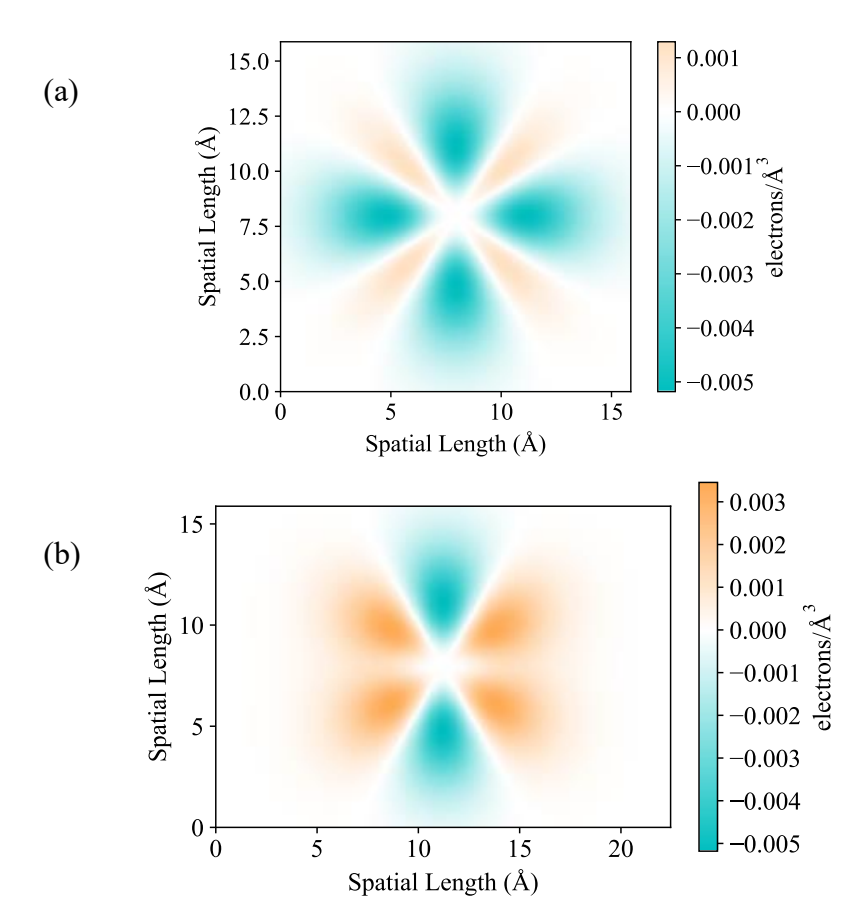


FIG. S10. Slices of hydrogenic 3d orbitals in the (100) (a) and (110) (b) planes, distinguishing the $d_{x^2-y^2}$ and d_{z^2} (teal) from the d_{xy} , d_{xz} and d_{yz} (orange) orbitals, which make up the e_g and t_{2g} orbitals respectively.

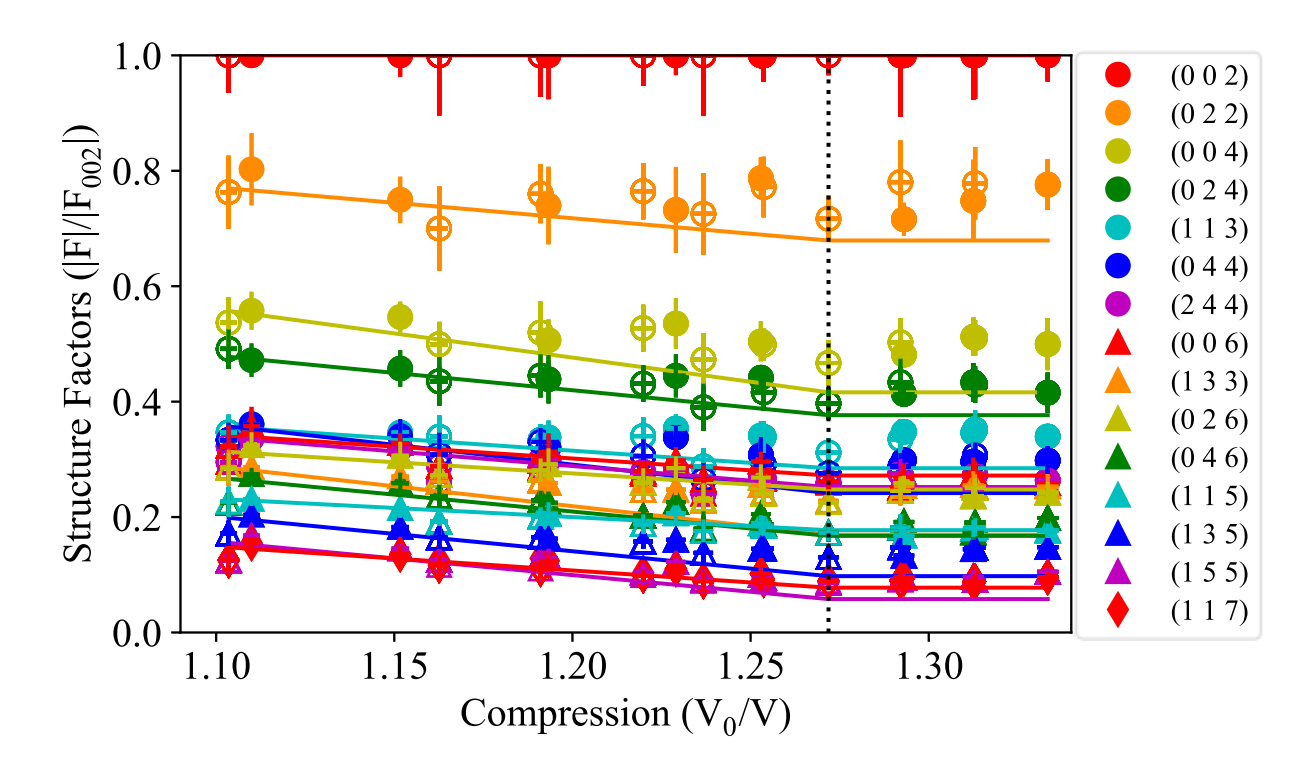


FIG. S11. Fitted relative structure factors vs. compression for (Fe_{0.53}Mg_{0.47})O after correction due to change in covalency. The change in covalency is inferred from the slope for compressions exceeding 1.27 in Fig. 1; it is then removed from each trend, with the assumption that the covalency starts to increase at the minimum-compression point.

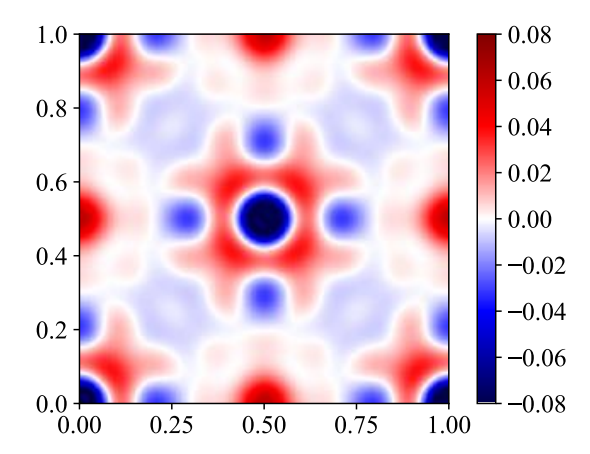


FIG. S12. Electron-density distribution difference map (unfiltered) in the (100) plane across the high- to low-spin transition in (Fe_{0.53}Mg_{0.47})O, corrected for pressure-induced covalency changes (the lowest peak intensities, to -0.141 at the cation center, are saturated on the present color scale). The pattern exhibits an imprint of the cubic unit cell due to spatial aliasing caused by the limited number of independent structure factors available for our analysis (i.e., maximum observed *hkl*; see Fig. 1). Fig. 3 is obtained from the map shown here by applying the Butterworth filter described in Fig. S6.

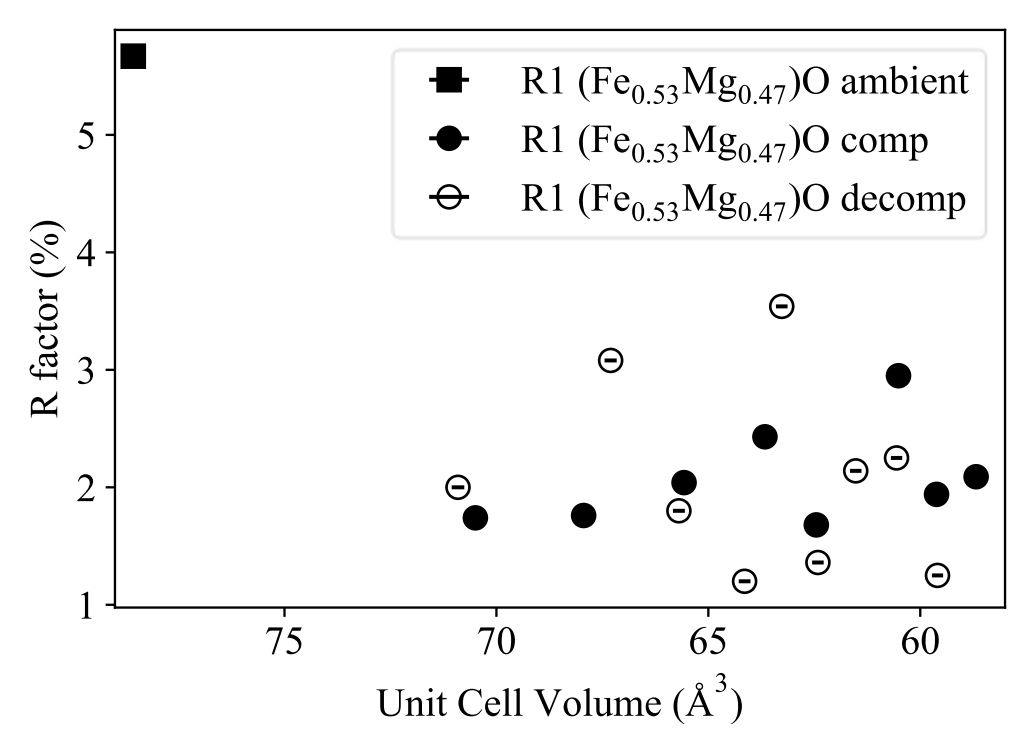


FIG. S13. R factors for (Fe_{0.53}Mg_{0.47})O from SHELX. SHELX R factors indicate good quality (2 ± 1%) for all but our ambient crystal measurement (P0, measured on thin plastic outside the diamond cell). However, the SHELX-refined structure factors were not used in our data analysis.

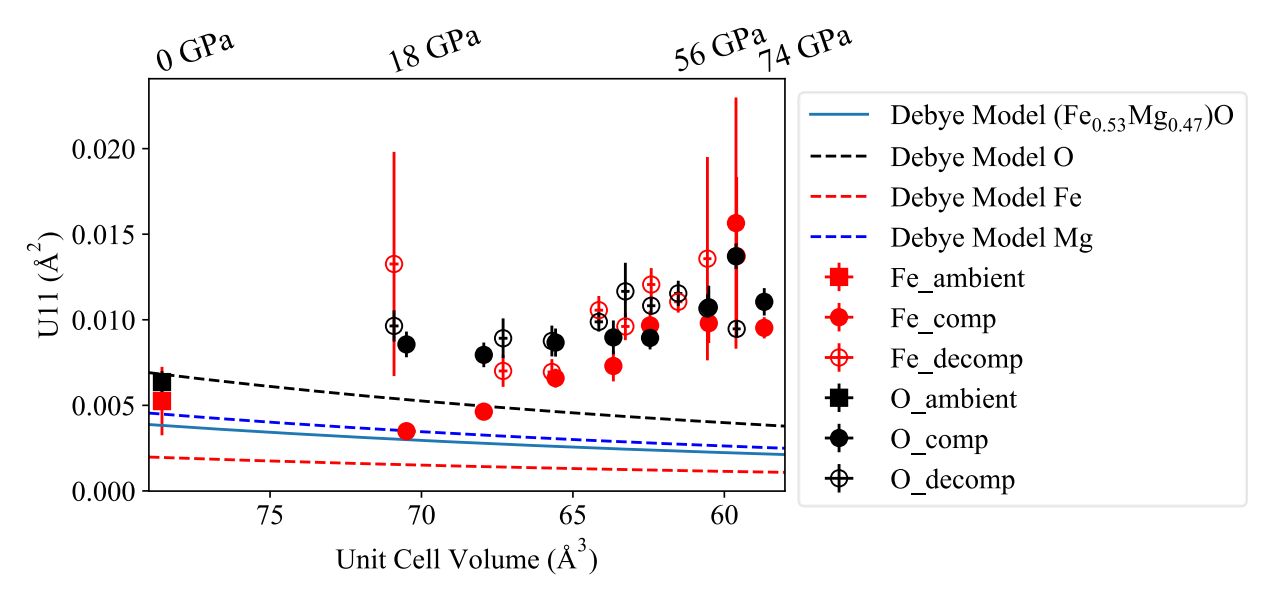


FIG. S14. One-dimensional thermal parameters *U11* determined from SHELX (*red* and *black symbols*) increase with compression, whereas our Debye-Grüneisen model (*lines*) shows a gradual decrease with compression. We include our ambient measurement *P0* for Fe and O, showing fair agreement with predicted *U11* values. The *U11* model for (Fe_{0.53}Mg_{0.47})O is based on a linear combination of the constituent molar masses of its chemical elements. Modeled crystal properties were taken from Table 1 of Ref. [41]. The Mg SHELX values are omitted due to being inconsistent with the Fe values.

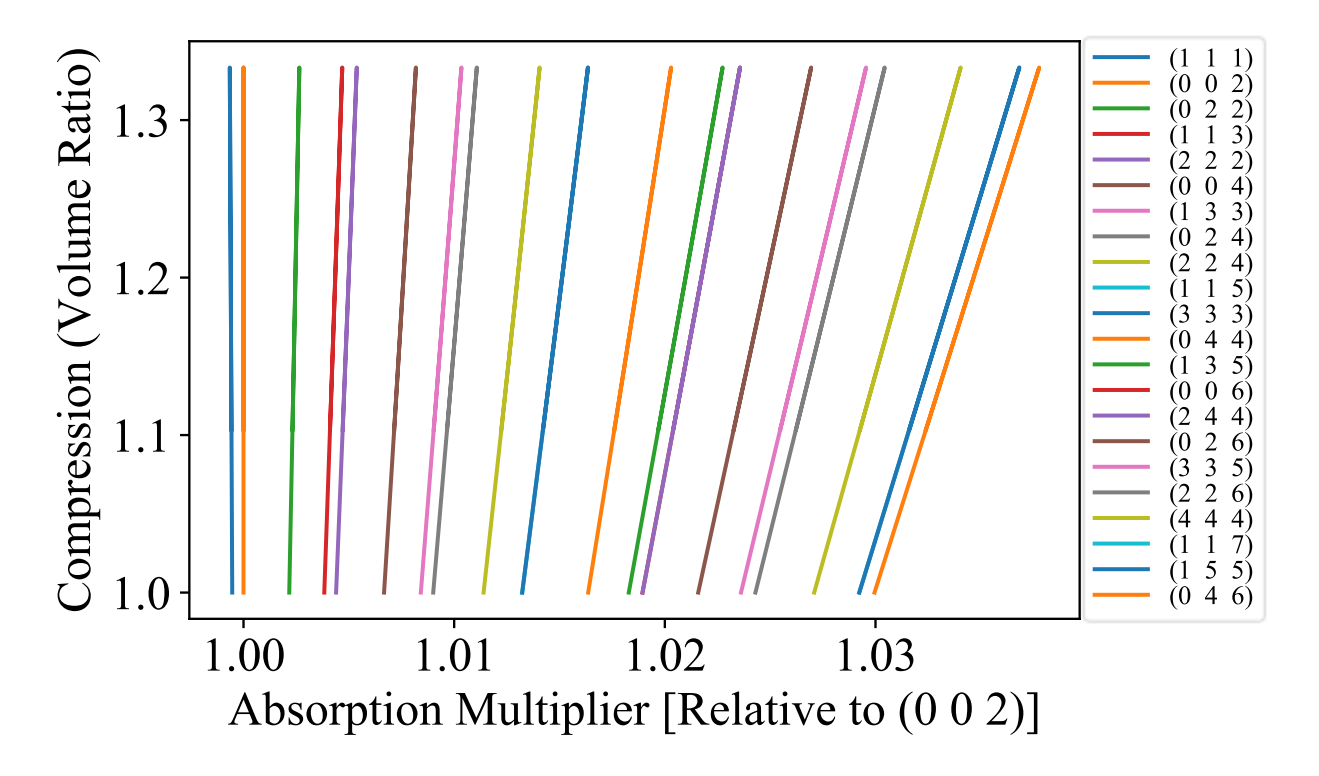


FIG. S15. Projections of increase in relative absorption [with respect to the (0 0 2) reflection] with compression for rock-salt structure reflections. As compression pushes reflections to higher angles, their path lengths through the diamond anvil increase, increasing x-ray absorption from the diamonds. We assume a diamond-anvil thickness of 2.5 mm and an absorption coefficient of 0.08 per mm [51]. The effect on absorption relative to (0 0 2) that we calculate is negligible, so it was not applied as a correction to the data.

TABLE SII. Output from XDS XSCALE.LP files. Data quality from combined data sets at each resolution shell. Datasets are labeled by 'P' number; 'MW50' refers to (Fe_{0.53}Mg_{0.47})O and 'MW15' refers to (Fe_{0.15}Mg_{0.85})O.

MW50 Dataset name: P0
THE DATA COLLECTION STATISTICS REPORTED BELOW ASSUMES: SPACE_GROUP_NUMBER= 225 UNIT_CELL_CONSTANTS= 4.28 4.28 90.000 90.000 90.000 SUBSET OF INTENSITY DATA WITH SIGNAL/NOISE >= -3.0 AS FUNCTION OF RESOLUTION RESOLUTION NUMBER OF REFLECTIONS COMPLETENESS R-FACTOR R-FACTOR COMPARED I/SIGMA R-meas CC(1/2) Anomal SigAno Nano LIMIT OBSERVED UNIQUE POSSIBLE OF DATA observed expected 100.0% 9.9% 27.81 10.5% 0.0 0 0.000 2.20 7.6% 0 1.10 38 4 100.0% 7.1% 7.3% 38 29.74 7.6% 99.3 0 0.000 8 100.0% 10.5% 7.6% 8 27.75 11.2% 0.0 0.000 1.00 1 1 0 0.90 28 2 100.0% 46 2% 8.4% 28 27 57 49.2% 0.0 Ω 0.000 0 0.80 43 3 100.0% 7.7% 8.1% 43 35.15 8.0% 100.0* 0 0.000 0 70 4 100.0% 9.1% 70 35.32 9.4% 99.1* 0.000 0 4 Ο 12 50.0% 9.0% 9.2% 126 37.17 9.2% 99.9* 0 0.000 0.50 126 6 0 373 total 25 31 80.6% 11.0% 7.9% 373 33.12 11.6% 99.6* 0 0.000 0 MW50 Dataset name: P02
THE DATA COLLECTION STATISTICS REPORTED BELOW ASSUMES: SPACE_GROUP_NUMBER= 4.13 90.000 90.000 90.000 UNIT_CELL_CONSTANTS= 4.13 SUBSET OF INTENSITY DATA WITH SIGNAL/NOISE >= -3.0 AS FUNCTION OF RESOLUTION RESOLUTION NUMBER OF REFLECTIONS COMPLETENESS R-FACTOR R-FACTOR COMPARED I/SIGMA CC(1/2) Anomal SigAno Nano LIMIT OBSERVED UNIQUE POSSIBLE OF DATA observed expected Corr 0 0 0 2.20 0.0% -99.9% -99.9% 0.00 -99.9% 0.0 0 0.000 1.10 24 3 4 75.0% 7.9% 1.5% 2.4 130.81 8.6% 100.0* 0 0.000 1.00 100.0% 9.2% 1.4% 95.36 10.6% 0.0 0.000 0 0.90 22 2 100.0% 9.8% 1.6% 22 150.23 10.3% 0.0 0 0.000 0 0.0% -99.9% -99.98 0.00 -99.9% Ο 18 66.7% 11.8% 18 119.93 12.8% 0 0.000 0.70 1.8% 0.0 0 12.7% 0.60 34 6 66.7% 11.8% 1.8% 34 112.62 98.4 0 0.000 25 3 11 27.3% 9.0% 2.2% 25 90.98 0.50 9.6% 99.8* 0 0.000 total 127 15 29 51.7% 9.1% 1.6% 127 116.77 9.8% 99.9* 0 0.000 THE DATA COLLECTION STATISTICS REPORTED BELOW ASSUMES: SPACE_GROUP_NUMBER= $\;$ 225 UNIT_CELL_CONSTANTS= 4.08 4.08 4.08 90.000 90.000 90.000 SUBSET OF INTENSITY DATA WITH SIGNAL/NOISE >= -3.0 AS FUNCTION OF RESOLUTION RESOLUTION NUMBER OF REFLECTIONS COMPLETENESS R-FACTOR R-FACTOR COMPARED I/SIGMA R-meas CC(1/2) Anomal SigAno Nano LIMIT OBSERVED UNIOUE POSSIBLE OF DATA observed expected Corr 2 20 Ω Λ 0.0% -99 9% -99 9% Ο 0 00 -99 9% 0 0 Ω 0 000 1.10 24 75.0% 6.6% 1.5% 133.71 7.2% 99.6 0.000 0 100.0% 7.3% 96.05 0.000 0 0.90 21 100.0% 10.8% 1.6% 21 147.61 11.3% 0.0 0.000 0 0 -99.9% -99.9% -99.9% 0.0 0 0.80 0.0% 0.00 0.000 0.70 19 2 3 66.7% 11.8% 1.8% 19 123.75 12.6% 0.0 0 0.000 0 60 33 4 6 66 7% 10 9% 1 8% 33 108 89 11 7% 98 9* Ω 0 000 0.50 24 3 8 37 5% 13 0% 2 5% 24 79.07 14.1% 100 0* Ω 0.000 total 125 15 26 57.7% 8.4% 1.6% 125 114.18 9.0% 99.8* 0.000

0

MW50 Dataset name: P04

THE DATA COLLECTION STATISTICS REPORTED BELOW ASSUMES: SPACE GROUP NUMBER= 225

UNIT_CELL_CONSTANTS= 4.03 4.03 90.000 90.000 90.000 4.03

CHECKE OF IMPENCIAL DATA MITH CICNAL MOTER >- _3 0 AC PRINCIPLON OF DESCRIPTION

:	SUBSET OF I RESOLUTION ano		OF REFL		COMPLETENES			COMPARED	I/SIGMA	R-meas	CC(1/2)	Anomal	SigAno
IN	LIMIT	OBSERVED	UNIQUE	POSSIBLE	OF DATA	observed	expected					Corr	
0	2.20	0	0	1	0.0%	-99.9%	-99.9%	0	0.00	-99.9%	0.0	0	0.000
0	1.10	22	3	4	75.0%	12.0%	1.5%	22	127.30	13.3%	99.8*	0	0.000
0	1.00	4	1	1	100.0%	8.1%	1.4%	4	95.40	9.3%	0.0	0	0.000
0	0.90	18	2	2	100.0%	11.1%	1.6%	18	136.02	11.7%	0.0	0	0.000
0	0.80	0	0	1	0.0%	-99.9%	-99.9%	0	0.00	-99.9%	0.0	0	0.000
0	0.70	18	2	3	66.7%	9.4%	1.9%	18	117.35	10.0%	0.0	0	0.000
0	0.60	29	4	6	66.7%	13.8%	1.9%	29	97.14	15.1%	99.4*	0	0.000
0	0.50	22	3	8	37.5%	13.1%	2.7%	22	70.05	14.2%	99.8*	0	0.000
0	total	113	15	26	57.7%	11.6%	1.6%	113	105.52	12.8%	99.8*	0	0.000

MW50 Dataset name: P05

THE DATA COLLECTION STATISTICS REPORTED BELOW ASSUMES:
SPACE GROUP NUMBER= 225
UNIT_CELL_CONSTANTS= 3.99 3.99 3.99 90.00 3.99 90.000 90.000 90.000

SUBSET OF INTENSITY DATA WITH SIGNAL/NOISE >= -3.0 AS FUNCTION OF RESOLUTION RESOLUTION NUMBER OF REFLECTIONS COMPLETENESS R-FACTOR R-FACTOR COMPARED I/SIGMA R-meas CC(1/2) Anomal SigAno Nano LIMIT OBSERVED UNIQUE POSSIBLE OF DATA observed expected Corr -99.9% 2.20 0.0% -99.9% 0 0.00 -99.9% 0.0 0.000 0 25 4 75.0% 9.1% 1.5% 25 135.08 100.0 0.000 1.10 9.8% 0.90 12 2 2 100.0% 13.7% 1.6% 12 107.00 15.5% 0.0 0

0 0.000 0 2 12 1 50.0% 12.3% 1.6% 12 162.96 12.9% 0.0 0 0.000 0.80 0.70 17 2 3 66.7% 13 3% 1 8% 17 112.57 14 4% 0 0 Ω 0.000 0.60 30 4 6 66.7% 11 6% 1.9% 30 95.64 12.5% 97 1 Ω 0.000 0 21 3 7 42.9% 11.9% 2.9% 21 63.00 13.0% 100.0* 0 0.000 0 total 117 25 60.0% 10.5% 117 105.26 11.3% 99.8* 0.000 0

MW50 Dataset name: P06

THE DATA COLLECTION STATISTICS REPORTED BELOW ASSUMES: SPACE GROUP NUMBER= 225
UNIT_CELL_CONSTANTS= 3.97 3.97 3.97 90.00

3.97 90.000 90.000 90.000

SUBSET OF INTENSITY DATA WITH SIGNAL/NOISE >= -3.0 AS FUNCTION OF RESOLUTION RESOLUTION NUMBER OF REFLECTIONS COMPLETENESS R-FACTOR R-FACTOR COMPARED I/SIGMA R-meas CC(1/2) Anomal SigAno Nano LIMIT OBSERVED UNIQUE POSSIBLE OF DATA observed expected Corr -99.9% 2.20 0.0% -99.9% 0 0.00 -99.9% 0.0 0.000 Ο 1.10 22 3 4 75.0% 7.0% 1.5% 22 128.01 7.6% 99.8 0.000 0 0.90 2 2 100.0% 11.7% 1.5% 11 105.03 13.3% 0.0 0.000 11 0 2 7.8% 0.80 11 1 50.0% 1.6% 11 157.05 8.1% 0.0 0 0.000 0 0.70 17 2 3 66.7% 13.9% 1.9% 17 110.15 15.0% 0.0 0 0.000 0 0.60 30 5 80.0% 13.2% 2.0% 30 93.31 14.3% 99.9* 0 0.000 0 21 8 37.5% 14.8% 21 56.99 16.2% 99.7* 0.000 0

MW50 Dataset name: P07

total

0

THE DATA COLLECTION STATISTICS REPORTED BELOW ASSUMES:
SPACE GROUP NUMBER= 225
UNIT_CELL_CONSTANTS= 3.93 3.93 3.93 90.00

15

112

3.93 90.000 90.000 90.000

25

SUBSET OF INTENSITY DATA WITH SIGNAL/NOISE >= -3.0 AS FUNCTION OF RESOLUTION

60.0%

NUMBER OF REFLECTIONS COMPLETENESS R-FACTOR R-FACTOR COMPARED I/SIGMA R-meas CC(1/2) Anomal SigAno Nano

8.6%

1.6%

112 101.04

9.3%

99.8*

0.000

	LIMIT	OBSERVED	UNIQUE	POSSIBLE	OF DATA	observed	expected					Corr	
0	2.20	0	0	1	0.0%	-99.9%	-99.9%	0	0.00	-99.9%	0.0	0	0.000
0	1.10	11	3	4	75.0%	4.3%	1.3%	11	91.17	4.9%	99.6	0	0.000
	0.90	6	2	2	100.0%	4.6%	1.3%	6	77.56	5.9%	0.0	0	0.000
0	0.80	6	1	2	50.0%	7.6%	1.5%	6	115.72	8.3%	0.0	0	0.000
	0.70	6	1	2	50.0%	18.0%	2.0%	6	91.68	19.8%	0.0	0	0.000
0	0.60	19	5	5	100.0%	11.9%	1.8%	18	69.86	14.2%	98.3	0	0.000
	0.50	10	3	9	33.3%	7.5%	2.7%	10	40.42	9.1%	100.0*	0	0.000
-	total	58	15	25	60.0%	5.9%	1.4%	57	73.77	6.9%	99.8*	0	0.000
0													
0 0 0	0.50	10	3	9	33.3%	7.5%	2.7%	10	40.42	9.1%	100.0*	0	0.0

THE DATA COLLECTION STATISTICS REPORTED BELOW ASSUMES: SPACE_GROUP_NUMBER= $\;225\;$

UNIT_CELL_CONSTANTS= 3 91 3.91 3.91 90.000 90.000 90.000

SUBSET OF INTENSITY DATA WITH SIGNAL/NOISE \geq = -3.0 AS FUNCTION OF RESOLUTION RESOLUTION COMPLETENESS R-FACTOR R-FACTOR COMPARED I/SIGMA R-meas CC(1/2) Anomal NUMBER OF REFLECTIONS SigAno Nano T.TMTT OBSERVED UNIQUE POSSIBLE OF DATA observed expected Corr 2.20 0 0 0.0% -99.9% -99.9% 0 0.00 -99.9% 0.0 0 0.000 0 1.10 20 3 4 75.0% 9.7% 1.4% 20 121.44 10.9% 100.0* 0 0.000 0 0.90 100.0% 10.7% 1.4% 95.38 12.4% 0.000 Ο 0.80 19 100.0% 10.7% 1.6% 19 140.23 11.3% 0.0 0 0.000 0 10 3 33.3% 14.1% 2.2% 10 107.39 14.8% 0.000 0.70 1 0.0 0 0 5 0.60 33 5 100.0% 11.9% 1.9% 33 91.21 13.0% 96.3 0 0.000 0

20.5%

10.5%

3.5%

1.6%

22

108

53.58

97.62

22.4%

11.6%

99.5

100.0*

0

0

0.000

0.000

MW50 Dataset name: P09b

0.50

total

0

0

THE DATA COLLECTION STATISTICS REPORTED BELOW ASSUMES: SPACE GROUP NUMBER= 225

3

15

22

108

UNIT_CELL_CONSTANTS= 3.89 3.89 3.89 90.000 90.000 90.000

9

2.5

33.3%

60.0%

SUBSET OF INTENSITY DATA WITH SIGNAL/NOISE >= -3.0 AS FUNCTION OF RESOLUTION RESOLUTION COMPLETENESS R-FACTOR R-FACTOR COMPARED I/SIGMA R-meas CC(1/2) Anomal NUMBER OF REFLECTIONS SigAno Nano LIMIT OBSERVED UNIQUE POSSIBLE OF DATA observed expected Corr 2.20 0 0 0.0% -99.9% -99.9% 0.00 -99.9% 0.0 0 0.000 0 1.10 34 4 75.0% 8.6% 1.5% 160.80 99.4 0 0.000 0 100.0% 10.2% 0.000 0.90 1.6% 134.31 10.9% 0.0 0 0 2 10.7% 28 100.0% 1.7% 28 167.32 11.0% 0.0 0 0.000 0.80 0 23 3 33.3% 9.8% 2.2% 23 168.24 10.0% 0.0 0 0.000 0.70 1 0 60 50 5 5 100 0% 11 3% 2 0% 50 113 33 12 0% 96 7 Ω 0 000 0 0.50 31 3 9 33.3% 13.3% 3.3% 31 68 94 14.1% 99.9* Ω 0.000 0 total 174 15 25 60.0% 9.4% 1.6% 174 126.20 9.9% 99.7* 0 0.000 0

MW50 Dataset name: P10

THE DATA COLLECTION STATISTICS REPORTED BELOW ASSUMES: SPACE_GROUP_NUMBER= 225

UNIT_CELL_CONSTANTS= 3.90 3.90 3.90 90.000 90.000 90.000

SUBSET OF INTENSITY DATA WITH SIGNAL/NOISE >= -3.0 AS FUNCTION OF RESOLUTION RESOLUTION NUMBER OF REFLECTIONS COMPLETENESS R-FACTOR R-FACTOR COMPARED I/SIGMA R-meas CC(1/2) Anomal SigAno Nano T.TMTT OBSERVED UNIQUE POSSIBLE OF DATA observed expected Corr 2.20 0 0 0.0% -99.9% -99.9% 0.00 -99.9% 0.0 0 0.000 0 1.10 34 4 75.0% 8.9% 1.5% 158.98 9.5% 99.9* 0.000 0 0.90 9 100.0% 7.4% 1.6% 9 138.63 7.8% 0.0 0.000 1 1 0 0 28 2 2 100.0% 9.4% 1.7% 28 162.58 9.8% 0 0.000 0.80 0.0 0

0	0.70	24	1	3	33.3%	11.6%	2.4%	24	160.81	11.8%	0.0	0	0.000
0	0.60	49	5	5	100.0%	8.3%	2.1%	49	104.65	8.9%	98.3*	0	0.000
0	0.50	35	3	9	33.3%	12.4%	4.4%	35	55.01	13.0%	100.0*	0	0.000
٥	total	179	15	25	60.0%	9.0%	1.7%	179	119.32	9.4%	99.9*	0	0.000

MW50 Dataset name: P11
THE DATA COLLECTION STATISTICS REPORTED BELOW ASSUMES:
SPACE_GROUP_NUMBER= 225
UNIT_CELL_CONSTANTS= 3.92 3.92 3.92 90.000 90.000 90.000

R	ESOLUTION		ATA WITH		COMPLETENES			JTION COMPARED	I/SIGMA	R-meas	CC(1/2)	Anomal	SigAno
Na	no LIMIT	OBSERVED	UNIQUE	POSSIBLE	OF DATA	observed	expected					Corr	
0	2.20	0	0	1	0.0%	-99.9%	-99.9%	0	0.00	-99.9%	0.0	0	0.000
0	1.10	35	3	4	75.0%	12.2%	1.5%	35	159.79	12.9%	99.8*	0	0.000
0	0.90	18	2	2	100.0%	9.6%	1.6%	18	130.18	10.2%	0.0	0	0.000
0	0.80	16	1	2	50.0%	9.9%	1.7%	16	183.59	10.2%	0.0	0	0.000
0	0.70	25	1	2	50.0%	12.5%	2.4%	25	167.64	12.7%	0.0	0	0.000
0	0.60	52	5	5	100.0%	9.3%	2.2%	52	105.51	9.8%	96.2	0	0.000
0	0.50	36	3	9	33.3%	14.6%	4.2%	36	57.87	15.3%	99.7*	0	0.000
0	total	182	15	25	60.0%	11.4%	1.7%	182	119.48	12.1%	99.8*	0	0.000

MW50 Dataset name: P12
THE DATA COLLECTION STATISTICS REPORTED BELOW ASSUMES:
SPACE_GROUP_NUMBER= 225
UNIT_CELL_CONSTANTS= 3.95 3.95 3.95 90.000 90.000 90.000

	ESOLUTION		ATA WITH OF REFL		COMPLETENESS		OF RESOLU R-FACTOR		I/SIGMA	R-meas	CC(1/2)	Anomal	SigAno
1101	LIMIT	OBSERVED	UNIQUE	POSSIBLE	OF DATA	observed	expected					Corr	
0	2.20	0	0	1	0.0%	-99.9%	-99.9%	0	0.00	-99.9%	0.0	0	0.000
0	1.10	32	3	4	75.0%	7.2%	1.5%	32	154.88	7.6%	99.9*	0	0.000
0	0.90	17	2	2	100.0%	14.1%	1.6%	17	126.07	15.0%	0.0	0	0.000
0	0.80	16	1	2	50.0%	12.0%	1.7%	16	184.50	12.4%	0.0	0	0.000
0	0.70	25	1	2	50.0%	12.9%	2.3%	25	171.30	13.2%	0.0	0	0.000
0	0.60	51	5	6	83.3%	13.4%	2.1%	51	104.49	14.3%	90.5	0	0.000
	0.50	36	3	8	37.5%	14.4%	4.0%	36	63.31	15.1%	99.9*	0	0.000
0	total	177	15	25	60.0%	9.2%	1.7%	177	119.00	9.7%	99.9*	0	0.000
0													

MW50 Dataset name: P13
THE DATA COLLECTION STATISTICS REPORTED BELOW ASSUMES:
SPACE_GROUP_NUMBER= 225
UNIT_CELL_CONSTANTS= 3.96 3.96 3.96 90.000 90.000 90.000

R	ESOLUTION		ATA WITH		COMPLETENES			JTION COMPARED	I/SIGMA	R-meas	CC(1/2)	Anomal	SigAno
Na	no LIMIT	OBSERVED	UNIQUE	POSSIBLE	OF DATA	observed	expected					Corr	
0	2.20	0	0	1	0.0%	-99.9%	-99.9%	0	0.00	-99.9%	0.0	0	0.000
0	1.10	32	3	4	75.0%	7.9%	1.5%	32	155.06	8.3%	99.8*	0	0.000
0	0.90	18	2	2	100.0%	10.3%	1.7%	18	130.85	11.0%	0.0	0	0.000
0	0.80	17	1	2	50.0%	10.1%	1.7%	17	191.01	10.4%	0.0	0	0.000
0	0.70	32	2	3	66.7%	9.6%	2.1%	32	141.73	9.9%	0.0	0	0.000
0	0.60	43	4	5	80.0%	12.2%	2.2%	43	106.78	12.8%	97.5	0	0.000
0	0.50	37	3	8	37.5%	11.7%	3.8%	37	67.98	12.2%	100.0*	0	0.000
0	total	179	15	25	60.0%	8.9%	1.7%	179	122.16	9.3%	99.9*	0	0.000

MW50 Dataset name: P14

THE DATA COLLECTION STATISTICS REPORTED BELOW ASSUMES:

SPACE_GROUP_NUMBER= 225

UNIT_CELL_CONSTANTS= 3.98 3.98 3.98 90.000 90.000 90.000

SUBSET OF INTENSITY DATA WITH SIGNAL/NOISE >= -3.0 AS FUNCTION OF RESOLUTION COMPLETENESS R-FACTOR R-FACTOR COMPARED I/SIGMA R-meas CC(1/2) Anomal RESOLUTION NUMBER OF REFLECTIONS SigAno LIMIT OBSERVED UNIQUE POSSIBLE OF DATA observed expected Corr 2 20 Ω Λ 0.0% -99 9% -99 9% Ο 0 00 -99 9% 0 0 Ω 0 000 0 1.10 28 3 75.0% 10.0% 1.5% 28 140.64 10.8% 99.7 0 0.000 0 14 2 100.0% 12.5% 1.7% 107.10 13.7% 0.000 0.90 0.0 0 0.80 10 50.0% 13.1% 1.7% 10 139.95 13.8% 0.0 0.000 0 0.70 27 3 66.7% 14.3% 2.3% 27 115.66 15.0% 0.0 0 0.000 0

15.8%

28.5%

11 5%

2.5%

4.9%

1.7%

39

37

155

91.35

53.13

102.14

16.8%

30.0%

12.3%

97.4

99.9*

99 8*

0

0

Λ

0.000

0.000

0.000

MW50 Dataset name: P15

0.60

0.50

total

0

0

THE DATA COLLECTION STATISTICS REPORTED BELOW ASSUMES: SPACE GROUP NUMBER= 225

4

3

15

39

37

155

UNIT_CELL_CONSTANTS= 4.00 4.00 4.00 90.000 90.000 90.000

6

7

25

66.7%

42.9%

60.0%

SUBSET OF INTENSITY DATA WITH SIGNAL/NOISE \geq = -3.0 AS FUNCTION OF RESOLUTION COMPLETENESS R-FACTOR R-FACTOR COMPARED I/SIGMA R-meas CC(1/2) Anomal RESOLUTION NUMBER OF REFLECTIONS SigAno Nano T.TMTT OBSERVED UNIQUE POSSIBLE OF DATA observed expected Corr 2.20 0 Λ 0.0% -99.9% -99.9% 0 0.00 -99.9% 0.0 0 0.000 0 1.10 31 4 75.0% 8.0% 1.5% 31 150.85 8.5% 99.9* 0 0.000 0 131.72 1.00 100.0% 9.7% 1.6% 10.4% 0.0 0 0.000 0 100.0% 10.4% 1.9% 116.50 11.1% 0 0.000 0.90 0.0 0 0.80 16 1 2 50.0% 11.5% 1.7% 16 180.77 11.8% 0.0 0 0.000 0 31 2 3 66.7% 12.9% 0 0.70 2.2% 31 129.66 13.6% 0.0 0.000 0.60 44 4 6 66.7% 13 3% 2 3% 44 102.91 14 0% 97 6 Ω 0 000 0 0.50 37 3 8 37.5% 15.0% 4.2% 37 61.76 15.8% 100 0* Ω 0.000 0

9.4%

1.7%

176

115.85

9.9%

99.8*

0

0.000

0.000

MW50 Dataset name: P16

THE DATA COLLECTION STATISTICS REPORTED BELOW ASSUMES: SPACE GROUP NUMBER= 225

15

176

UNIT_CELL_CONSTANTS= 4.03 4.03 90.000 90.000 90.000

26

57.7%

SUBSET OF INTENSITY DATA WITH SIGNAL/NOISE \geq = -3.0 AS FUNCTION OF RESOLUTION RESOLUTION NUMBER OF REFLECTIONS COMPLETENESS R-FACTOR R-FACTOR COMPARED I/SIGMA R-meas CC(1/2) Anomal SigAno Nano LIMIT OBSERVED UNIQUE POSSIBLE OF DATA observed expected 0 0 -99.9% 0.0% 0.00 0.0 0 0.000 Ο 1.10 34 75.0% 10.3% 1.5% 34 156.99 11.0% 99.2 0 0.000 Ο 1.00 100.0% 13.1% 1.6% 131.54 14.0% 0.0 0 0.000 0 2.7 2 2 11.8% 1.7% 27 157.71 0.90 100.0% 12.2% 0.0 0 0.000 0.80 0 0 1 0.0% -99.9% -99.9% 0 0.00 -99.9% 0.0 0 0.000 0 0.70 31 2 3 66.7% 11.2% 2.1% 31 138.98 11.7% 0.0 0 0.000 0 0.60 47 6 66.7% 8.6% 2.2% 47 112.74 9.1% 98.3 0 0.000 0 37 37.5% 12.5% 3.5% 72.24 13.0% 100.0* 0.000

MW50 Dataset name: P17b

total

THE DATA COLLECTION STATISTICS REPORTED BELOW ASSUMES:

15

SPACE_GROUP_NUMBER= 225 UNIT CELL CONSTANTS=

184

4.07 4.07 4.07 90.000 90.000 90.000

26

57.7%

SUBSET OF INTENSITY DATA WITH SIGNAL/NOISE >= -3.0 AS FUNCTION OF RESOLUTION NUMBER OF REFLECTIONS COMPLETENESS R-FACTOR R-FACTOR COMPARED I/SIGMA R-meas CC(1/2) Anomal SigAno

10.7%

1.7%

184

124.24

11.3%

99.6*

Nano

0

0

	LIMIT	OBSERVED	UNIQUE	POSSIBLE	OF DATA	observed	expected					Corr	
0	2.20	0	0	1	0.0%	-99.9%	-99.9%	0	0.00	-99.9%	0.0	0	0.000
0	1.10	29	3	4	75.0%	10.8%	1.5%	29	144.11	11.5%	100.0*	0	0.000
0	1.00	7	1	1	100.0%	6.0%	1.6%	7	123.56	6.5%	0.0	0	0.000
0	0.90	29	2	2	100.0%	9.6%	1.7%	29	160.42	9.9%	0.0	0	0.000
0	0.80	0	0	1	0.0%	-99.9%	-99.9%	0	0.00	-99.9%	0.0	0	0.000
0	0.70	27	2	3	66.7%	16.3%	2.2%	27	124.94	17.1%	0.0	0	0.000
0	0.60	45	4	6	66.7%	14.7%	2.2%	45	106.48	15.5%	86.9	0	0.000
0	0.50	32	3	8	37.5%	11.3%	3.6%	32	64.95	11.9%	99.3	0	0.000
0	total	169	15	26	57.7%	10.9%	1.7%	169	116.49	11.6%	100.0*	0	0.000

MW50 Dataset name: P18
THE DATA COLLECTION STATISTICS REPORTED BELOW ASSUMES:
SPACE_GROUP_NUMBER= 225
UNIT_CELL_CONSTANTS= 4.14 4.14 4.14 90.000 90.000 90.000

	ESOLUTION		ATA WITH		OISE >= -3.0 COMPLETENES		OF RESOLU		I/SIGMA	R-meas	CC(1/2)	Anomal	SigAno
IVGI	LIMIT	OBSERVED	UNIQUE	POSSIBLE	OF DATA	observed	expected					Corr	
	2.20	0	0	1	0.0%	-99.9%	-99.9%	0	0.00	-99.9%	0.0	0	0.000
0	1.10	34	3	4	75.0%	11.3%	1.6%	34	156.61	11.9%	99.5	0	0.000
0	1.00	8	1	1	100.0%	11.1%	1.6%	8	131.20	11.8%	0.0	0	0.000
0	0.90	25	2	2	100.0%	11.7%	1.8%	25	145.99	12.1%	0.0	0	0.000
0	0.80	0	0	1	0.0%	-99.9%	-99.9%	0	0.00	-99.9%	0.0	0	0.000
0	0.70	51	3	4	75.0%	14.8%	2.5%	51	121.22	15.3%	99.9*	0	0.000
0	0.60	26	3	5	60.0%	14.1%	2.1%	26	101.02	15.1%	-5.0	0	0.000
0	0.50	33	3	11	27.3%	17.8%	4.0%	33	61.32	18.7%	99.9*	0	0.000
0	total	177	15	29	51.7%	11.9%	1.8%	177	116.24	12.6%	99.6*	0	0.000

MW15 Dataset name: P01

THE DATA COLLECTION STATISTICS REPORTED BELOW ASSUMES:

SPACE_GROUP_NUMBER= 225 UNIT_CELL_CONSTANTS= 4.22 4.22 90.000 90.000 90.000

SUBSET OF INTENSITY DATA WITH SIGNAL/NOISE >= -3.0 AS FUNCTION OF RESOLUTION NUMBER OF REFLECTIONS COMPLETENESS R-FACTOR R-FACTOR COMPARED I/SIGMA R-meas CC(1/2) Anomal SigAno Nano LIMIT OBSERVED UNIQUE POSSIBLE OF DATA observed expected 0 0.0% -99.9% 0 -99.9% 0.000 2.20 -99.9% 0.00 0.0 0 0 19 1.10 3 4 75.0% 10.0% 1.4% 19 106.84 10.9% 99.9* 0 0.000 0 100.0% 13.7% 79.50 1.00 3 1 1 1.4% 3 16.8% 0.0 0 0.000 17 0.90 2 2 100.0% 14.0% 1.7% 17 116.64 14.9% 0.0 0 0.000 0 0.80 19 2 3 66.7% 17.6% 2.0% 19 93.62 19.3% 0.0 0 0.000 0 100.0% 16.6% 2.2% 18.8% 0.000 0.70 26 4 74.40 0 19 4 75.0% 14.8% 19 75.79 15.8% 99.9* 0.000 Ο

13.0%

1.7%

103

89.70

14.3%

99.4*

99.5*

0

Corr

0.000

0.000

MW15 Dataset name: P02

total

0

THE DATA COLLECTION STATISTICS REPORTED BELOW ASSUMES:

15

SPACE_GROUP_NUMBER= 225

103

UNIT CELL CONSTANTS= 4.14 4.14 90.000 90.000 90.000 4.14

19

78.9%

SUBSET OF INTENSITY DATA WITH SIGNAL/NOISE >= -3.0 AS FUNCTION OF RESOLUTION COMPLETENESS R-FACTOR R-FACTOR COMPARED I/SIGMA NUMBER OF REFLECTIONS R-meas CC(1/2) Anomal SigAno Nano LIMIT OBSERVED UNIQUE POSSIBLE OF DATA Corr observed expected 0 -99.9% 2.20 0 0.0% -99.9% 0 0.00 -99.9% 0.0 0 0.000 0 70.61 1.10 8 3 4 75.0% 10.8% 1.3% 14.1% 0.0 0 0.000 1.00 0 0 1 0.0% -99.9% -99.9% 0 0.00 -99.9% 0.0 0 0.000 0 0.90 12 2 100.0% 8.0% 1.6% 12 102.33 8.6% 0.0 0 0.000 0 0.80 3 1 100.0% 5.7% 1.5% 3 75.71 7.0% 0.0 0 0.000 0 3 66.7% 15.2% 17.2% 0.000 0.70 11 2.3% 11 68.32 0.0 0 20 6 6 100.0% 12.7% 2.1% 19 50.72 15.1% 85.5 0 0.000 0.60 0 77.8% 10.1% 1.7% 52 66.66 12.1%

total

0

14

54

MW15 Dataset name: P03
THE DATA COLLECTION STATISTICS REPORTED BELOW ASSUMES:
SPACE_GROUP_NUMBER= 225
UNIT_CELL_CONSTANTS= 4.05 4.05 4.05 90.00 4.05 90.000 90.000 90.000

18

SUBSET OF INTENSITY DATA WITH SIGNAL/NOISE >= -3.0 AS FUNCTION OF RESOLUTION RESOLUTION NUMBER OF REFLECTIONS COMPLETENESS R-FACTOR R-FACTOR COMPARED I/SIGMA R-meas CC(1/2) Anomal SigAno Nano LIMIT OBSERVED UNIOUE POSSIBLE OF DATA observed expected Corr 0 0 0.0% -99.9% 2.20 -99.9% 0 0.00 -99.9% 0.0 0 0.000 1 10 22 3 4 75 0% 5 6% 1 4% 22 121 02 6.0% 99 6 Ω 0 000 1 00 3 1 1 100.0% 2 9% 1 3% 3 83 82 3 5% 0.0 Ω 0 000 0 0.90 22 2 100.0% 8.3% 1.6% 22 148.39 8.7% 0.0 0 0.000 0 0.80 100.0% 6.6% 124.58 7.1% 0.0 0 0.000 0 0.70 22 66.7% 10.9% 1.9% 22 123.33 11.6% 0.0 0 0.000 0 6 45 6 100.0% 10.4% 1.8% 45 98.40 11.2% 99.0 0 0.000 0.60 0 total 121 15 18 83.3% 7.3% 1.6% 121 113.69 7.9% 99.8* 0 0.000

MW15 Dataset name: P04

LIMIT

THE DATA COLLECTION STATISTICS REPORTED BELOW ASSUMES:

OBSERVED UNIQUE POSSIBLE

SPACE_GROUP_NUMBER= 225 UNIT_CELL_CONSTANTS=

4.01 4.01 4.01 90.000 90.000 90.000

SUBSET OF INTENSITY DATA WITH SIGNAL/NOISE \geq = -3.0 AS FUNCTION OF RESOLUTION R-meas CC(1/2) Anomal SigAno RESOLUTION COMPLETENESS R-FACTOR R-FACTOR COMPARED I/SIGMA NUMBER OF REFLECTIONS Nano

OF DATA observed expected

0	2.20	0	0	1	0.0%	-99.9%	-99.9%	0	0.00	-99.9%	0.0	0	0.000
0	1.10	10	3	4	75.0%	6.3%	1.4%	9	82.21	7.3%	0.0	0	0.000
0	1.00	1	1	1	100.0%	-99.9%	-99.9%	0	0.00	-99.9%	0.0	0	0.000
0	0.90	4	1	1	100.0%	14.5%	1.7%	4	79.43	16.7%	0.0	0	0.000
0	0.80	10	2	2	100.0%	8.6%	1.5%	10	102.58	9.6%	0.0	0	0.000
0	0.70	10	2	3	66.7%	12.2%	1.8%	10	81.06	14.2%	0.0	0	0.000
0	0.60	22	6	6	100.0%	12.1%	1.9%	20	62.16	13.7%	89.6	0	0.000
-	total	57	15	18	83.3%	8.9%	1.6%	53	74.26	10.1%	99.5*	0	0.000

MW15 Dataset name: P05b
THE DATA COLLECTION STATISTICS REPORTED BELOW ASSUMES:
SPACE_GROUP_NUMBER= 225
UNIT_CELL_CONSTANTS= 3.97 3.97 3.97 90.000 3.97 90.000 90.000 90.000

	SUBSET OF I		ATA WITE OF REFI		OISE >= -3.0 A COMPLETENESS				I/SIGMA	R-meas	CC(1/2)	Anomal	SigAno	
1	Nano LIMIT	OBSERVED	UNIQUE	POSSIBLE	OF DATA	observed	expected					Corr		
	2.20	0	0	1	0.0%	-99.9%	-99.9%	0	0.00	-99.9%	0.0	0	0.000	
	0 1.10	13	3	4	75.0%	4.5%	1.4%	13	96.64	5.1%	100.0*	0	0.000	
	0.90	6	2	2	100.0%	5.6%	1.3%	6	72.46	7.5%	0.0	0	0.000	
	0.80	12	2	2	100.0%	5.5%	1.6%	12	112.20	6.1%	0.0	0	0.000	
	0.70	10	2	3	66.7%	8.8%	1.8%	10	78.75	10.1%	0.0	0	0.000	
	0.60	28	5	5	100.0%	9.6%	2.1%	28	68.09	10.9%	96.4	0	0.000	
	0.50	6	1	8	12.5%	17.4%	1.9%	6	93.72	19.0%	0.0	0	0.000	
	0 total	75	15	25	60.0%	6.1%	1.6%	75	83.39	7.0%	99.8*	0	0.000	

MW15 Dataset name: P06
THE DATA COLLECTION STATISTICS REPORTED BELOW ASSUMES: SPACE GROUP NUMBER= 225

UNIT_CELL_CONSTANTS= 3.96 3.96 3.96 90.000 90.000 90.000

	ESOLUTION		ATA WITH		OISE >= -3.0 I			JTION COMPARED	I/SIGMA	R-meas	CC(1/2)	Anomal	SigAno
Nai	LIMIT	OBSERVED	UNIQUE	POSSIBLE	OF DATA	observed	expected					Corr	
0	2.20	0	0	1	0.0%	-99.9%	-99.9%	0	0.00	-99.9%	0.0	0	0.000
0	1.10	27	3	4	75.0%	10.7%	1.5%	27	127.04	11.7%	99.8*	0	0.000
0	0.90	12	2	2	100.0%	8.9%	1.7%	12	96.07	10.0%	0.0	0	0.000
0	0.80	25	2	2	100.0%	13.1%	1.7%	25	153.44	13.7%	0.0	0	0.000
0	0.70	17	1	2	50.0%	18.5%	3.7%	17	105.24	19.0%	0.0	0	0.000
-	0.60	59	6	6	100.0%	13.2%	2.5%	59	86.34	14.1%	96.5*	0	0.000
0	0.50	10	1	8	12.5%	16.1%	2.4%	10	105.79	16.9%	0.0	0	0.000
0	total	150	15	25	60.0%	11.9%	1.8%	150	107.28	12.8%	99.7*	0	0.000

MW15 Dataset name: P07

THE DATA COLLECTION STATISTICS REPORTED BELOW ASSUMES:
SPACE_GROUP_NUMBER= 225
UNIT_CELL_CONSTANTS= 3.94 3.94 3.94 90.00

3.94 3.94 90.000 90.000 90.000

SUBSET OF INTENSITY DATA WITH SIGNAL/NOISE \geq -3.0 AS FUNCTION OF RESOLUTION COMPLETENESS R-FACTOR R-FACTOR COMPARED I/SIGMA R-meas CC(1/2) Anomal SigAno RESOLUTION NUMBER OF REFLECTIONS Nano LIMIT OBSERVED UNIQUE POSSIBLE OF DATA observed expected Corr 0.0% 0 0 2.20 1 -99.9% -99.9% 0 0.00 -99.9% 0.0 0 0.000 0 1.10 27 4 75.0% 11.9% 1.6% 27 119.15 13.1% 99.4 0 0.000 0 0.90 100.0% 13.1% 88.29 0.000 14.8% 0 2 1.9% 24 137.80 14.8% 0.80 24 2 100.0% 14.1% 0.0 0 0.000 0 0.70 17 1 2 50.0% 28.8% 6.7% 17 87.81 29.7% 0.0 0 0.000 0

Color													
State 150 15 25 60.08 13.38 2.28 150 96.48 14.68 99.4* 0 0 0 0 0 0 0 0 0	0.60	58	6	6	100.0%	14.7%	3.6%	58	74.95	15.8%	96.9*	0	0.00
	0.50	11	1	8	12.5%	21.0%	3.6%	11	100.04	22.0%	0.0	0	0.00
BIATA COLLECTION STATISTICS REPORTED BELOW ASSUMES: MARCH GROUD NUMBER 225 3,92 3,92 3,92 90,000 90,000 10,000	total	150	15	25	60.0%	13.5%	2.2%	150	96.48	14.6%	99.4*	0	0.00
SOLUTION NUMBER OF REFLECTIONS COMPLETENESS R-FACTOR COMPARED I/SIGMA R-meas CC(1/2) Anomal Silo LIMIT OBSERVED UNIQUE POSSIBLE OF DATA observed expected 2.20 0 0 1 1 0.0% -99.9% -99.9% 0 0 0.00 -99.9% 0.0 0 0 0 1.10 26 3 4 75.0% 10.7% 1.7% 26 112.73 12.1% 99.9% 0 0 0.80 31 3 3 100.0% 12.2% 2.2% 31 116.67 12.8% 99.4 0 0 0.80 31 3 3 100.0% 12.2% 2.2% 31 116.67 12.8% 99.4 0 0 0.60 53 5 5 100.0% 14.1% 3.8% 53 87.54 15.0% 98.5* 0 0 0.50 16 2 9 22.2% 11.8% 4.2% 16 67.39 12.5% 0.0 0 0 0.50 16 2 9 22.2% 11.8% 4.2% 16 67.39 12.5% 0.0 0 0 0.50 16 2 9 22.2% 11.8% 2.4% 147 95.99 12.8% 99.9* 0 0 0.50 16 2 9 22.2% 11.8% 4.2% 16 67.39 12.5% 0.0 0 0 0.50 16 2 9 3 22.2% 11.8% 4.2% 16 67.39 12.5% 0.0 0 0 0.50 16 2 9 20.0% 11.8% 2.4% 147 95.99 12.8% 99.9* 0 0 0.50 16 2 9 22.2% 11.8% 4.2% 16 67.39 12.5% 0.0 0 0 0.50 16 2 9 22.2% 11.8% 4.2% 16 67.39 12.5% 0.0 0 0 0.50 16 2 9 22.2% 11.8% 4.2% 16 67.39 12.5% 0.0 0 0 0.50 16 2 9 22.2% 10.0% 11.8% 2.4% 147 95.99 12.8% 99.9* 0 0 0.0 0.0 0 0 0 0 0 0 0 0 0 0 0 0 0	E DATA C ACE_GROU	COLLECTION S JP_NUMBER=	TATISTIC 225				0 90.000						
Corr									I/SIGMA	R-meas	CC(1/2)	Anomal	SigA
1.10					OF DATA	observed	expected						-
0.90 4 1 1 1 100.0% 7.1% 1.6% 4 87.93 8.2% 0.0 0 0 0 0 0 0 0 0 0 0 0 0 0 0 0 0 0	2.20	0	0	1	0.0%	-99.9%	-99.9%	0	0.00	-99.9%	0.0	0	0.0
0.80 31 3 3 100.0% 12.2% 2.2% 31 116.67 12.8% 99.4 0 0 0 0 0 0 0 0 17 1 2 2 50.0% 25.2% 7.8% 17 91.27 25.9% 0.0 0 0 0 0 0 0 0 0 0 0 53 5 5 100.0% 14.1% 3.8% 53 87.54 15.0% 98.5* 0 0 0 0 0 0 0 0 0 0 0 0 0 0 0 0 0 0 0	1.10	26	3	4	75.0%	10.7%	1.7%	26	112.73	12.1%	99.9*	0	0.0
0.70	0.90	4	1	1	100.0%	7.1%	1.6%	4	87.93	8.2%	0.0	0	0.0
0.60 53 5 5 100.0% 14.1% 3.8% 53 87.54 15.0% 98.5* 0 0 0.50 16 2 9 22.2% 11.8% 4.2% 16 67.39 12.5% 0.0 0 0 0 total 147 15 25 60.0% 11.8% 2.4% 147 95.99 12.8% 99.9* 0 0 0 total 147 15 25 60.0% 11.8% 2.4% 147 95.99 12.8% 99.9* 0 0 0 0 0 0 0 0 0 0 0 0 0 0 0 0 0 0 0	0.80	31	3	3	100.0%	12.2%	2.2%	31	116.67	12.8%	99.4	0	0.0
0.50	0.70	17	1	2	50.0%	25.2%	7.8%	17	91.27	25.9%	0.0	0	0.0
0.50 16 2 9 22.2% 11.8% 4.2% 16 67.39 12.5% 0.0 0 0 total 147 15 25 60.0% 11.8% 2.4% 147 95.99 12.8% 99.9% 0 0 total 147 15 25 60.0% 11.8% 2.4% 147 95.99 12.8% 99.9% 0 0 0 1	0.60	53	5	5				53				0	0.0
Dataset name: P09c		16	2	9				16		12.5%		0	0.0
Solution Statistics Stati		147	1.5	2.5	60.0%			147				0	0.0
E DATA COLLECTION STATISTICS REPORTED BELOW ASSUMES: ACE GROUP AURIBER = 225 IT_CELL_CONSTANTS = 3.89 3.89 3.89 90.000 90.000 90.000 BSET OF INTENSITY DATA WITH SIGNAL/NOISE >= -3.0 AS FUNCTION OF RESOLUTION SOLUTION NUMBER OF REFLECTIONS COMPLETENESS R-FACTOR R-FACTOR COMPARED I/SIGMA R-meas CC(1/2) Anomal Signal Control of Resolution LIMIT OBSERVED UNIQUE POSSIBLE OF DATA observed expected Corr 2.20 0 0 1 0 0.0% -99.9% -99.9% 0 0.00 -99.9% 0.0 0 0 0 1.10 40 3 4 75.0% 11.4% 1.6% 40 162.79 12.0% 99.9* 0 0 0.80 33 2 2 2 100.0% 10.2% 1.8% 33 156.42 10.5% 0.0 0 0 0 0.80 33 2 2 2 100.0% 10.2% 1.8% 33 156.42 10.5% 0.0 0 0 0 0.70 37 2 3 66.7% 10.1% 2.1% 37 138.10 10.5% 0.0 0 0 0 0.60 79 5 5 100.0% 11.0% 2.4% 79 114.19 11.5% 99.7* 0 0 0.50 26 2 9 22.2% 14.2% 2.8% 26 80.50 14.7% 0.0 0 0 0 total 224 15 25 60.0% 11.3% 1.8% 224 129.77 11.8% 99.9* 0 0 5 Dataset name: P10 E DATA COLLECTION STATISTICS REPORTED BELOW ASSUMES: ACE GROUP AURIBER = 225 IT_CELL_CONSTANTS 3.91 3.91 3.91 90.000 90.000 90.000 BBET OF INTENSITY DATA WITH SIGNAL/NOISE >= -3.0 AS FUNCTION OF RESOLUTION SOLUTION NUMBER OF REFLECTIONS COMPLETENESS R-FACTOR R-FACTOR COMPARED I/SIGMA R-meas CC(1/2) Anomal Signal Of Section of The Sectio	00001			20	00.00	11.00	2.10	117	30.33	12.00	33.3	Ü	0.0
2.20 0 0 0 1 0.0% -99.9% -99.9% 0 0.00 -99.9% 0.0 0 0 0 1.10 40 3 4 75.0% 11.4% 1.6% 40 162.79 12.0% 99.9* 0 0 0 0 0 0.90 9 1 1 100.0% 12.9% 1.6% 9 137.22 13.7% 0.0 0 0 0 0 0.80 33 2 2 100.0% 10.2% 1.8% 33 156.42 10.5% 0.0 0 0 0 0.70 37 2 3 66.7% 10.1% 2.1% 37 138.10 10.5% 0.0 0 0 0 0.60 79 5 5 100.0% 11.0% 2.4% 79 114.19 11.5% 99.7* 0 0 0.50 26 2 9 22.2% 14.2% 2.8% 26 80.50 14.7% 0.0 0 0 0 0 0 0 0 0 0 0 0 0 0 0 0 0 0	SOLUTION								I/SIGMA	R-meas	CC(1/2)	Anomal	SigA
1.10							-						
0.90 9 1 1 1 100.0% 12.9% 1.6% 9 137.22 13.7% 0.0 0 0 0 0.80 33 2 2 100.0% 10.2% 1.8% 33 156.42 10.5% 0.0 0 0 0 0.70 37 2 3 66.7% 10.1% 2.1% 37 138.10 10.5% 0.0 0 0 0 0.60 79 5 5 100.0% 11.0% 2.4% 79 114.19 11.5% 99.7* 0 0 0.50 26 2 9 22.2% 14.2% 2.8% 26 80.50 14.7% 0.0 0 0 0 0 0 0 0 0 0 0 0 0 0 0 0 0 0													0.0
0.80 33 2 2 100.0% 10.2% 1.8% 33 156.42 10.5% 0.0 0 0 0 0.70 37 2 3 66.7% 10.1% 2.1% 37 138.10 10.5% 0.0 0 0 0 0.60 79 5 5 100.0% 11.0% 2.4% 79 114.19 11.5% 99.7* 0 0 0.50 26 2 9 22.2% 14.2% 2.8% 26 80.50 14.7% 0.0 0 0 0 0 0 0 0 0 0 0 0 0 0 0 0 0 0													0.0
0.70 37 2 3 66.7% 10.1% 2.1% 37 138.10 10.5% 0.0 0 0 0.60 79 5 5 100.0% 11.0% 2.4% 79 114.19 11.5% 99.7* 0 0 0.50 26 2 9 22.2% 14.2% 2.8% 26 80.50 14.7% 0.0 0 0 total 224 15 25 60.0% 11.3% 1.8% 224 129.77 11.8% 99.9* 0 0 1.5 Dataset name: P10 1.6 DATA COLLECTION STATISTICS REPORTED BELOW ASSUMES: PACE GROUP NUMBER = 225 NIT_CELL_CONSTANTS 3.91 3.91 3.91 90.000 90.000 1.6 DIAGRAPH WITH SIGNAL/NOISE >= -3.0 AS FUNCTION OF RESOLUTION DESCLUTION NUMBER OF REFLECTIONS COMPLETENESS R-FACTOR R-FACTOR COMPARED I/SIGMA R-meas CC(1/2) Anomal Signal Completeness R-FACTOR R-FACTOR COMPARED I/SIGMA R-meas CC(1/2) Anomal Signal Completeness R-FACTOR R-FACTOR COMPARED I/SIGMA R-meas CC(1/2) Anomal Signal Completeness R-FACTOR R-FACTOR COMPARED I/SIGMA R-meas CC(1/2) Anomal Signal Completeness R-FACTOR R-FACTOR COMPARED I/SIGMA R-meas CC(1/2) Anomal Signal Completeness R-FACTOR R-FACTOR COMPARED I/SIGMA R-meas CC(1/2) Anomal Signal Completeness R-FACTOR R-FACTOR COMPARED I/SIGMA R-meas CC(1/2) Anomal Signal Completeness R-FACTOR R-FACTOR COMPARED I/SIGMA R-meas CC(1/2) Anomal Signal Completeness R-FACTOR R-FACTOR COMPARED I/SIGMA R-meas CC(1/2) Anomal Signal Completeness R-FACTOR R-FACTOR COMPARED I/SIGMA R-meas CC(1/2) Anomal Signal Completeness R-FACTOR R-FACTOR COMPARED I/SIGMA R-meas CC(1/2) Anomal Signal Completeness R-FACTOR R-FACTOR COMPARED I/SIGMA R-meas CC(1/2) Anomal Signal Completeness R-FACTOR R-FACTOR COMPARED I/SIGMA R-meas CC(1/2) Anomal Signal Completeness R-FACTOR R-FACTOR COMPARED I/SIGMA R-meas CC(1/2) Anomal Signal Completeness R-FACTOR R-FACTOR COMPARED I/SIGMA R-meas CC(1/2) Anomal Signal Completeness R-FACTOR R-FACTOR COMPARED I/SIGMA R-meas CC(1/2) Anomal Signal Completeness R-FACTOR R-FACTOR COMPARED I/SIGMA R-meas CC(1/2) Anomal Signal Completeness R-FACTOR R-FACTOR COMPARED I/SIGMA R-meas CC(1/2) Anomal Signal R-MACTOR R-FACTOR R													0.0
0.60 79 5 5 100.0% 11.0% 2.4% 79 114.19 11.5% 99.7* 0 0 0.50 26 2 9 22.2% 14.2% 2.8% 26 80.50 14.7% 0.0 0 0 total 224 15 25 60.0% 11.3% 1.8% 224 129.77 11.8% 99.9* 0 0 15 Dataset name: P10 HE DATA COLLECTION STATISTICS REPORTED BELOW ASSUMES: PACE GROUP NUMBER = 225 NIT_CELL_CONSTANTS= 3.91 3.91 3.91 90.000 90.000 90.000 DESET OF INTENSITY DATA WITH SIGNAL/NOISE >= -3.0 AS FUNCTION OF RESOLUTION DESOLUTION NUMBER OF REFLECTIONS COMPLETENESS R-FACTOR R-FACTOR COMPARED I/SIGMA R-meas CC(1/2) Anomal Signal Comparison of the state of	0.80				100.0%	10.2%	1.8%	33	156.42	10.5%	0.0	0	0.0
0.50	0.70	37	2	3	66.7%	10.1%	2.1%	37	138.10	10.5%	0.0	0	0.0
total 224 15 25 60.0% 11.3% 1.8% 224 129.77 11.8% 99.9* 0 0 15 Dataset name: P10 HE DATA COLLECTION STATISTICS REPORTED BELOW ASSUMES: PACE GROUP NUMBER = 225 NIT_CELL_CONSTANTS = 3.91 3.91 3.91 90.000 90.000 90.000 JESET OF INTENSITY DATA WITH SIGNAL/NOISE >= -3.0 AS FUNCTION OF RESOLUTION ESOLUTION NUMBER OF REFLECTIONS COMPLETENESS R-FACTOR R-FACTOR COMPARED I/SIGMA R-meas CC(1/2) Anomal Signal Completeness R-FACTOR R-FACTOR COMPARED I/SIGMA R-meas CC(1/2) Anomal Signal Completeness R-FACTOR R-FACTOR COMPARED I/SIGMA R-meas CC(1/2) Anomal Signal Completeness R-FACTOR R-FACTOR COMPARED I/SIGMA R-meas CC(1/2) Anomal Signal Completeness R-FACTOR R-FACTOR COMPARED I/SIGMA R-meas CC(1/2) Anomal Signal Completeness R-FACTOR R-FACTOR COMPARED I/SIGMA R-meas CC(1/2) Anomal Signal Completeness R-FACTOR R-FACTOR COMPARED I/SIGMA R-meas CC(1/2) Anomal Signal Completeness R-FACTOR R-FACTOR COMPARED I/SIGMA R-meas CC(1/2) Anomal Signal Completeness R-FACTOR R-FACTOR COMPARED I/SIGMA R-meas CC(1/2) Anomal Signal Completeness R-FACTOR R-FACTOR COMPARED I/SIGMA R-meas CC(1/2) Anomal Signal Completeness R-FACTOR R-FACTOR COMPARED I/SIGMA R-meas CC(1/2) Anomal Signal Completeness R-FACTOR R-FACTOR COMPARED I/SIGMA R-meas CC(1/2) Anomal Signal Completeness R-FACTOR R-FACTOR COMPARED I/SIGMA R-meas CC(1/2) Anomal Signal Completeness R-FACTOR R-FACTOR COMPARED I/SIGMA R-meas CC(1/2) Anomal Signal Completeness R-FACTOR R-FACTOR COMPARED I/SIGMA R-meas CC(1/2) Anomal Signal Completeness R-FACTOR R-FACTOR COMPARED I/SIGMA R-meas CC(1/2) Anomal Signal R-MACTOR R-MACTOR R-FACTOR R-	0.60	79	5	5	100.0%	11.0%	2.4%	79	114.19	11.5%	99.7*	0	0.0
L5 Dataset name: P10 HE DATA COLLECTION STATISTICS REPORTED BELOW ASSUMES: PACE_GROUP_NUMBER = 225 NIT_CELL_CONSTANTS = 3.91 3.91 3.91 90.000 90.000 90.000 JESSET OF INTENSITY DATA WITH SIGNAL/NOISE >= -3.0 AS FUNCTION OF RESOLUTION SSOLUTION NUMBER OF REFLECTIONS COMPLETENESS R-FACTOR R-FACTOR COMPARED I/SIGMA R-meas CC(1/2) Anomal Signal LIMIT OBSERVED UNIQUE POSSIBLE OF DATA observed expected Corr 2.20 0 0 0 1 0.0% -99.9% -99.9% 0 0.00 -99.9% 0.0 0 0 1.10 70 3 4 75.0% 9.2% 1.6% 70 208.53 9.5% 99.5 0 0	0.50	26	2	9	22.2%	14.2%	2.8%	26	80.50	14.7%	0.0	0	0.0
HE DATA COLLECTION STATISTICS REPORTED BELOW ASSUMES: PACE GROUP_NUMBER= 225 NIT_CELL_CONSTANTS= 3.91 3.91 3.91 90.000 90.000 90.000 UBSET OF INTENSITY DATA WITH SIGNAL/NOISE >= -3.0 AS FUNCTION OF RESOLUTION ESOLUTION NUMBER OF REFLECTIONS COMPLETENESS R-FACTOR R-FACTOR COMPARED I/SIGMA R-meas CC(1/2) Anomal Signal Control	total	224	15	25	60.0%	11.3%	1.8%	224	129.77	11.8%	99.9*	0	0.0
ESOLUTION NUMBER OF REFLECTIONS COMPLETENESS R-FACTOR R-FACTOR COMPARED I/SIGMA R-meas CC(1/2) Anomal Signal Compared UNIQUE POSSIBLE OF DATA observed expected Corr 2.20 0 0 1 0.0% -99.9% -99.9% 0 0.00 -99.9% 0.0 0 0 1.10 70 3 4 75.0% 9.2% 1.6% 70 208.53 9.5% 99.5 0 0	HE DATA C	COLLECTION S	TATISTIC	S REPORTED	BELOW ASSUME								
LIMIT OBSERVED UNIQUE POSSIBLE OF DATA observed expected				3.91	3.91 90	.000 90.00	0 90.000						
1.10 70 3 4 75.0% 9.2% 1.6% 70 208.53 9.5% 99.5 0 0	IIT_CELL_ JBSET OF SOLUTION	_CONSTANTS= INTENSITY D	3.91 ATA WITH	SIGNAL/NO	ISE >= -3.0 A	AS FUNCTION	OF RESOLU		I/SIGMA	R-meas	CC(1/2)	Anomal	SigA
	IIT_CELL_ UBSET OF SOLUTION	CONSTANTS= INTENSITY D NUMBER	3.91 DATA WITH R OF REFL	SIGNAL/NO	ISE >= -3.0 P	AS FUNCTION S R-FACTOR	OF RESOLU R-FACTOR		I/SIGMA	R-meas	CC(1/2)		SigA
0.90 17 1 1 100.0% 10.4% 1.7% 17 186.81 10.8% 0.0 0 0	NIT_CELL_ UBSET OF CSOLUTION OO LIMIT	CONSTANTS= INTENSITY D NUMBER OBSERVED	3.91 DATA WITH OF REFL UNIQUE	SIGNAL/NOI ECTIONS POSSIBLE	SE >= -3.0 A COMPLETENESS OF DATA	AS FUNCTION S R-FACTOR observed	OF RESOLU R-FACTOR expected	COMPARED				Corr	,
	NIT_CELL_ UBSET OF SOLUTION O LIMIT 2.20	CONSTANTS= INTENSITY E NUMBER OBSERVED 0	3.91 DATA WITH OF REFL UNIQUE 0	SIGNAL/NOI ECTIONS POSSIBLE	ISE >= -3.0 A COMPLETENESS OF DATA 0.0%	AS FUNCTION S R-FACTOR observed -99.9%	OF RESOLU R-FACTOR expected -99.9%	COMPARED 0	0.00	-99.9%	0.0	Corr 0	SigA 0.0 0.0
0.80 58 2 2 100.0% 10.1% 1.9% 58 203.18 10.3% 0.0 0 0	NIT_CELL_ UBSET OF SSOLUTION LIMIT 2.20 1.10	CONSTANTS= INTENSITY D NUMBER OBSERVED 0 70	3.91 DATA WITH OF REFL UNIQUE 0 3	SIGNAL/NOI ECTIONS POSSIBLE 1	ISE >= -3.0 i COMPLETENESS OF DATA 0.0% 75.0%	AS FUNCTION S R-FACTOR observed -99.9% 9.2%	OF RESOLU R-FACTOR expected -99.9% 1.6%	COMPARED 0 70	0.00	-99.9% 9.5%	0.0	Corr 0	0.0

MW15 Dataset name: P11
THE DATA COLLECTION STATISTICS REPORTED BELOW ASSUMES: SPACE_GROUP_NUMBER= 225

2

5

2

3

5

9

66.7%

100.0%

22.2%

60.0%

67

131

38

381

0.70

0.60

0.50

total

0

0

0

0

11.7%

13.5%

14.0%

10.4%

2.2%

2.6%

3.1%

1.9%

67 177.68

131 140.02

38 96.00

381 164.41

11.9%

13.9%

14.3%

10.7%

0.0

99.4*

0.0

99.7*

0

0

0

0.000

0.000

0.000

0.000

UNIT_CELL_CONSTANTS= 3.94 3.94 3.94 90.000 90.000 90.000

0 1.10 84 3 4 75.0% 10.1% 1.6% 84 232.50 10.3% 99.9* 0 0 0 0 0 0 0 0 0 0 0 0 0 0 0 0 0 0 0		10				COMPLETENESS			COMPARED	1/SIGMA	к-meas	CC (1/2)		SigA
0 1.10 84 3 4 75.0% 10.1% 1.6% 84 232.50 10.3% 99.9* 0 0 0 0 0.90 44 2 2 100.0% 11.3% 1.6% 44 180.25 11.6% 0.0 0 0 0 0 0 0.80 73 2 2 100.0% 11.1% 1.8% 73 280.87 11.2% 0.0 0 0 0 0 0 0 0 0 0 0 0 0 0 0 0 0 0								-						
0 0.90	0													0.
0.80 73 2 2 100.0% 11.1% 1.8% 73 260.87 11.2% 0.0 0 0 0 0 0 0.70 52 1 2 50.0% 10.0% 3.3% 52 179.51 10.1% 0.0 0 0 0 0 0.60 177 6 6 6 100.0% 11.7% 2.5% 177 144.07 11.9% 99.5% 0 0 0 0.50 32 1 8 12.5% 12.0% 2.4% 32 187.91 12.1% 0.0 0 0 0 0 total 462 15 25 60.0% 10.7% 1.9% 462 187.44 10.9% 99.9% 0 0 0 0 0 0 0 0 0 0 0 0 0 0 0 0 0 0 0	0	1.10	84	3	4	75.0%	10.1%	1.6%	84	232.50	10.3%	99.9*	0	0.
0.80 73 2 2 100.0% 11.1% 1.8% 73 260.87 11.2% 0.0 0 0 0 0 0 0 0 0 0 0 0 0 0 0 0 0 0)	0.90	44	2	2	100.0%	11.3%	1.8%	44	180.25	11.6%	0.0	0	0.
0.70 52 1 2 50.0% 10.0% 3.3% 52 179.51 10.1% 0.0 0 0 0 0 0 0 0 0		0.80	73	2	2	100.0%	11.1%	1.8%	73	260.87	11.2%	0.0	0	0.
0.60 177 6 6 100.0% 11.7% 2.5% 177 144.07 11.9% 99.5% 0 0 0 0 0 5.50 32 1 8 12.5% 12.0% 2.4% 32 187.91 12.1% 0.0 0 0 0 0 1 0 1 0 1 0 1 0 1 0 1 0 1 0		0.70	52	1	2	50.0%	10.0%	3.3%	52	179.51	10.1%	0.0	0	0.
0.50 32 1 8 12.5% 12.0% 2.4% 32 187.91 12.1% 0.0 0 0 0 0 0 1 1 1 1		0.60	177	6	6	100.0%	11.7%	2.5%	177	144.07	11.9%	99.5*	0	0.
Total 462 15 25 60.0% 10.7% 1.9% 462 187.44 10.9% 99.9* 0 0 0 0 0 0 0 0 0 0 0 0 0 0 0 0 0 0 0		0.50	32	1	8	12.5%	12.0%	2.4%	32	187.91	12.1%	0.0	0	0.
THE DATA COLLECTION STATISTICS REPORTED BELOW ASSUMES: SPACE GROUP NUMBER= 225 UNIT_CELL_CONSTANTS= 3.97 3.97 3.97 90.000 90.000 SUBSET OF INTENSITY DATA WITH SIGNAL/NOISE >= -3.0 AS FUNCTION OF RESOLUTION RESOLUTION NUMBER OF REFLECTIONS COMPLETENESS R-FACTOR COMPARED I/SIGMA R-meas CC(1/2) Anomal Signal CLIMIT OBSERVED UNIQUE POSSIBLE OF DATA observed expected COTY 2.20 0 0 1 0.0% -99.9% -99.9% 0 0.00 -99.9% 0.0 0 0 0 0 0 0 0 0 0 0 0 0 0 0 0 0 0		total	462	15	25	60.0%	10.7%	1.9%	462	187.44	10.9%	99.9*	0	0 .
SPACE GROUP NUMBER - 225 UNIT_CELL_CONSTANTS - 3.97 3.97 3.97 90.000 90.000 SUBSET OF INTENSITY DATA WITH SIGNAL/NOISE >= -3.0 AS FUNCTION OF RESOLUTION RESOLUTION NUMBER OF REFLECTIONS COMPLETENESS R-FACTOR R-FACTOR COMPARED I/SIGMA R-meas CC(1/2) Anomal SIANO LIMIT OBSERVED UNIQUE POSSIBLE OF DATA observed expected	IW.	15 Dataset	name: P12	!										
SUBET OF INTENSITY DATA WITH SIGNAL/NOISE >= -3.0 AS FUNCTION OF RESOLUTION RESOLUTION NUMBER OF REFLECTIONS COMPLETENESS R-FACTOR R-FACTOR COMPARED I/SIGMA R-meas CC(1/2) Anomal SIGNAL TO SIGNAL RESOLUTION LIMIT OBSERVED UNIQUE POSSIBLE OF DATA observed expected C COTT 2.20 0 0 1 0.0% -99.9% -99.9% 0 0.00 -99.9% 0.0 0 0 0 0 0 0 0 0 0 0 0 0 0 0 0 0 0					S REPORTED	BELOW ASSUME	ES:							
RESOLUTION NUMBER OF REFLECTIONS COMPLETENESS R-FACTOR R-FACTOR COMPARED I/SIGMA R-meas CC(1/2) Anomal SI I I I I I I I I I I I I I I I I I I					3.97	3.97 90	.000 90.00	0 90.000						
LIMIT OBSERVED UNIQUE POSSIBLE OF DATA observed expected	RI	ESOLUTION								I/SIGMA	R-meas	CC(1/2)	Anomal	Sig
1.10 13 3 4 75.0% 5.0% 1.4% 13 93.22 5.8% 100.0* 0 0 0 0.90 9 2 2 100.0% 7.9% 1.6% 9 84.33 9.1% 0.0 0 0 0 0 0.80 11 2 2 100.0% 12.7% 1.7% 11 100.32 14.1% 0.0 0 0 0 0 0.70 10 2 3 66.7% 14.0% 2.1% 10 68.52 16.3% 0.0 0 0 0 0 0.60 28 5 5 100.0% 12.7% 2.3% 28 60.10 13.9% 99.2* 0 0 0.50 5 1 8 12.5% 14.4% 2.1% 5 73.73 16.1% 0.0 0 0 0 0 0 0 0 0 0 0 0 0 0 0 0 0 0	·		OBSERVED	UNIQUE	POSSIBLE	OF DATA	observed	expected					Corr	
1.10 13 3 4 75.0% 5.0% 1.4% 13 93.22 5.8% 100.0* 0 0 0.90 9 2 2 100.0% 7.9% 1.6% 9 84.33 9.1% 0.0 0 0 0.80 11 2 2 100.0% 12.7% 1.7% 11 100.32 14.1% 0.0 0 0 0.70 10 2 3 66.7% 14.0% 2.1% 10 68.52 16.3% 0.0 0 0 0.60 28 5 5 100.0% 12.7% 2.3% 28 60.10 13.9% 99.2* 0 0 0.50 5 1 8 12.5% 14.4% 2.1% 5 73.73 16.1% 0.0 0 0 0.50 5 1 8 12.5% 14.4% 2.1% 5 73.73 16.1% 0.0 0 0 0.50 5 1 8 12.5% 14.4% 7.6% 76 77.35 9.4% 99.8* 0 0 0.50 5 1 8 12.5% 14.4% 2.1% 5 73.73 16.1% 0.0 0 0 0.50 5 1 8 12.5% 14.4% 2.1% 5 73.73 16.1% 0.0 0 0 0.50 5 1 8 12.5% 14.4% 2.1% 5 76 77.35 9.4% 99.8* 0 0 0.50 5 1 8 12.5% 14.4% 2.1% 5 76 77.35 9.4% 99.8* 0 0 0.50 5 1 8 12.5% 14.4% 2.1% 5 76 77.35 9.4% 99.8* 0 0 0.50 5 1 8 12.5% 14.4% 2.1% 5 76 77.35 9.4% 99.8* 0 0 0.50 5 1 8 12.5% 14.4% 2.1% 76 77.35 9.4% 99.8* 0 0 0.50 5 1 8 0.0% 8.3% 1.6% 76 77.35 9.4% 99.8* 0 0 0.50 5 1 8 0.0% 8.3% 1.6% 76 77.35 9.4% 99.8* 0 0 0.50 5 1 8 0.0% 8.3% 1.6% 76 77.35 9.4% 99.8* 0 0 0.50 5 1 8 0.0% 8.3% 1.6% 76 77.35 9.4% 99.8* 0 0 0.50 5 1 8 0.0% 8.3% 1.6% 76 77.35 9.4% 99.8* 0 0 0.00 0.00 0.00 0.00 0.00 0.00 0.00		2.20	0	0	1	0.0%	-99.9%	-99.9%	0	0.00	-99.9%	0.0	0	0
0.90 9 2 2 100.0% 7.9% 1.6% 9 84.33 9.1% 0.0 0 0 0 0 0 0 0 0 0 0 0 0 0 0 0 0 0		1.10	13	3	4	75.0%	5.0%	1.4%	13	93.22	5.8%	100.0*	0	0
0.80 11 2 2 100.0% 12.7% 1.7% 11 100.32 14.1% 0.0 0 0 0 0.70 10 2 3 66.7% 14.0% 2.1% 10 68.52 16.3% 0.0 0 0 0 0.60 28 5 5 100.0% 12.7% 2.3% 28 60.10 13.9% 99.2* 0 0 0.50 5 1 8 12.5% 14.4% 2.1% 5 73.73 16.1% 0.0 0 0 0 0 0.50 5 1 8 12.5% 14.4% 2.1% 5 73.73 16.1% 0.0 0 0 0 0 0.50 5 1 8 12.5% 14.4% 2.1% 5 73.73 16.1% 0.0 0 0 0 0 0 0 0 0 0 0 0 0 0 0 0 0 0		0.90	9	2	2	100.0%	7.9%	1.6%	9	84.33	9.1%	0.0	0	0
0.70 10 2 3 66.7% 14.0% 2.1% 10 68.52 16.3% 0.0 0 0 0 0 0.60 28 5 5 100.0% 12.7% 2.3% 28 60.10 13.9% 99.2* 0 0 0 0.50 5 1 8 12.5% 14.4% 2.1% 5 73.73 16.1% 0.0 0 0 0 total 76 15 25 60.0% 8.3% 1.6% 76 77.35 9.4% 99.8* 0 0 0 0 0 0 0 0 0 0 0 0 0 0 0 0 0 0 0		0.80	11	2	2	100.0%	12.7%	1.7%	11	100.32	14.1%	0.0	0	0
0.60		0.70	10	2	3	66.7%	14.0%	2.1%	10	68.52	16.3%	0.0	0	0
0.50 5 1 8 12.5% 14.4% 2.1% 5 73.73 16.1% 0.0 0 0 total 76 15 25 60.0% 8.3% 1.6% 76 77.35 9.4% 99.8* 0 0 W15 Dataset name: P13b THE DATA COLLECTION STATISTICS REPORTED BELOW ASSUMES: SPACE_GROUP_NUMBER = 225 UNIT_CELL_CONSTANTS= 4.01 4.01 4.01 90.000 90.000 SUBSET OF INTENSITY DATA WITH SIGNAL/NOISE >= -3.0 AS FUNCTION OF RESOLUTION RESOLUTION NUMBER OF REFLECTIONS COMPLETENESS R-FACTOR R-FACTOR COMPARED I/SIGMA R-meas CC(1/2) Anomal Si and LIMIT OBSERVED UNIQUE POSSIBLE OF DATA observed expected Corr 2.20 0 0 1 0.0% -99.9% -99.9% 0 0.00 -99.9% 0.0 0 0 0 1.10 29 3 4 75.0% 10.0% 1.5% 29 139.59 10.8% 100.0* 0 0 1.00 7 1 1 1 100.0% 4.4% 1.6% 7 125.77 4.8% 0.0 0 0 0 0 0.90 11 1 1 1 100.0% 5.9% 2.1% 11 121.53 6.1% 0.0 0 0 0 0 0.90 11 1 1 1 100.0% 5.9% 2.1% 11 121.53 6.1% 0.0 0 0 0 0 0.80 25 2 2 100.0% 8.1% 1.7% 25 158.91 8.4% 0.0 0 0 0 0 0.70 24 2 3 66.7% 9.6% 2.2% 24 110.26 10.2% 0.0 0 0 0 0 0.60 64 6 6 100.0% 8.4% 2.1% 64 101.91 8.9% 98.1* 0 0 0 0 0 0 0 0 0 0 0 0 0 0 0 0 0 0 0	1	0.60	28	5	5	100.0%	12.7%	2.3%	28	60.10	13.9%	99.2*	0	0
total 76 15 25 60.0% 8.3% 1.6% 76 77.35 9.4% 99.8* 0 0 WISS Dataset name: P13b THE DATA COLLECTION STATISTICS REPORTED BELOW ASSUMES: SPACE_GROUP_NUMBER= 225 UNIT_CELL_CONSTANTS= 4.01 4.01 4.01 90.000 90.000 90.000 SUBSET OF INTENSITY DATA WITH SIGNAL/NOISE >= -3.0 AS FUNCTION OF RESOLUTION RESOLUTION NUMBER OF REFLECTIONS COMPLETENESS R-FACTOR R-FACTOR COMPARED I/SIGMA R-meas CC(1/2) Anomal Si ANO LIMIT OBSERVED UNIQUE POSSIBLE OF DATA observed expected Corr 2.20 0 0 1 0.0% -99.9% -99.9% 0 0.00 -99.9% 0.0 0 0 1.10 29 3 4 75.0% 10.0% 1.5% 29 139.59 10.8% 100.0* 0 0 1.00 7 1 1 1 100.0% 4.4% 1.6% 7 125.77 4.8% 0.0 0 0 0.90 11 1 1 1 100.0% 5.9% 2.1% 11 121.53 6.1% 0.0 0 0 0.80 25 2 2 100.0% 8.1% 1.7% 25 158.91 8.4% 0.0 0 0 0.70 24 2 3 66.7% 9.6% 2.2% 24 110.26 10.2% 0.0 0 0 0.60 64 6 6 100.0% 8.4% 2.1% 64 101.91 8.9% 98.1* 0 0 total 160 15 18 83.3% 8.8% 1.7% 160 121.06 9.4% 99.9* 0	1													0
W15 Dataset name: P13b THE DATA COLLECTION STATISTICS REPORTED BELOW ASSUMES: SPACE GROUP NUMBER = 225 UNIT_CELL_CONSTANTS = 4.01)	0.00	Ü	_	o o	12.00	-1.10	2.10	_	,0.,0	-00	0.0		
THE DATA COLLECTION STATISTICS REPORTED BELOW ASSUMES: SPACE GROUP NUMBER = 225 UNIT_CELL_CONSTANTS = 4.01 4.01 4.01 90.000 90.000 90.000 SUBSET OF INTENSITY DATA WITH SIGNAL/NOISE >= -3.0 AS FUNCTION OF RESOLUTION RESOLUTION NUMBER OF REFLECTIONS COMPLETENESS R-FACTOR R-FACTOR COMPARED I/SIGMA R-meas CC(1/2) Anomal Silano LIMIT OBSERVED UNIQUE POSSIBLE OF DATA observed expected Corr 2.20 0 0 0 1 0.0% -99.9% -99.9% 0 0.00 -99.9% 0.0 0 0 1.10 29 3 4 75.0% 10.0% 1.5% 29 139.59 10.8% 100.0* 0 0 1.00 7 1 1 1 100.0% 4.4% 1.6% 7 125.77 4.8% 0.0 0 0 0.90 11 1 1 1 100.0% 5.9% 2.1% 11 121.53 6.1% 0.0 0 0 0.80 25 2 2 100.0% 8.1% 1.7% 25 158.91 8.4% 0.0 0 0 0.70 24 2 3 66.7% 9.6% 2.2% 24 110.26 10.2% 0.0 0 0 0.70 24 2 3 66.7% 9.6% 2.2% 24 110.26 10.2% 0.0 0 0 0.60 64 6 6 100.0% 8.4% 2.1% 64 101.91 8.9% 98.1* 0 0 0.60 64 6 6 100.0% 8.4% 2.1% 64 101.91 8.9% 98.1* 0 0 0.60 64 6 6 100.0% 8.4% 2.1% 64 101.91 8.9% 98.1* 0 0		total	76	15	25	60 N&	8 3%	1 6%	76	77 35	9.4%	99 8*	0	Ω
Tano LIMIT OBSERVED UNIQUE POSSIBLE OF DATA observed expected 2.20 0 0 1 0.0% -99.9% -99.9% 0 0.00 -99.9% 0.0 0 0 1.10 29 3 4 75.0% 10.0% 1.5% 29 139.59 10.8% 100.0* 0 0 1.00 7 1 1 1 100.0% 4.4% 1.6% 7 125.77 4.8% 0.0 0 0 0.90 11 1 1 1 100.0% 5.9% 2.1% 11 121.53 6.1% 0.0 0 0 0.80 25 2 2 100.0% 8.1% 1.7% 25 158.91 8.4% 0.0 0 0 0.70 24 2 3 66.7% 9.6% 2.2% 24 110.26 10.2% 0.0 0 0.60 64 6 6 100.0% 8.4% 2.1% 64 101.91 8.9% 98.1* 0 0 total 160 15 18 83.3% 8.8% 1.7% 160 121.06 9.4% 99.9* 0 0	IW.	15 Dataset	name: P13	lb				1.6%	76	77.35	9.4%	99.8*	0	0.
2.20 0 0 1 0.0% -99.9% -99.9% 0 0.00 -99.9% 0.0 0 0 0 1.10 29 3 4 75.0% 10.0% 1.5% 29 139.59 10.8% 100.0* 0 0 1.00 7 1 1 100.0% 4.4% 1.6% 7 125.77 4.8% 0.0 0 0 0 0 0 0 0 0 0 0 0 0 0 0 0 0 0	IW: TI SI Ul	15 Dataset HE DATA CO PACE_GROUI NIT_CELL_C	name: P13 DLLECTION S P_NUMBER= CONSTANTS=	Bb STATISTIC 225 4.01	S REPORTED	BELOW ASSUME 4.01 90	ES: .000 90.00	0 90.000		77.35	9.4%	99.8*	0	0
1.10 29 3 4 75.0% 10.0% 1.5% 29 139.59 10.8% 100.0* 0 0 1.00 7 1 1 100.0% 4.4% 1.6% 7 125.77 4.8% 0.0 0 0 0.90 11 1 1 100.0% 5.9% 2.1% 11 121.53 6.1% 0.0 0 0 0.80 25 2 2 100.0% 8.1% 1.7% 25 158.91 8.4% 0.0 0 0 0.70 24 2 3 66.7% 9.6% 2.2% 24 110.26 10.2% 0.0 0 0 0.60 64 6 6 100.0% 8.4% 2.1% 64 101.91 8.9% 98.1* 0 0 total 160 15 18 83.3% 8.8% 1.7% 160 121.06 9.4% 99.9* 0 0	IW: TH SI UN SI RI	15 Dataset HE DATA CO PACE_GROUI NIT_CELL_C UBSET OF 1 ESOLUTION	name: P13 DLLECTION S P_NUMBER= CONSTANTS= INTENSITY D NUMBER	ETATISTIC 225 4.01 DATA WITH	S REPORTED 4.01 SIGNAL/NOI ECTIONS	BELOW ASSUMM 4.01 90 SE >= -3.0 i COMPLETENES:	ES: .000 90.00 AS FUNCTION S R-FACTOR	0 90.000 OF RESOLU R-FACTOR	JTION				Anomal	
1.00 7 1 1 100.0% 4.4% 1.6% 7 125.77 4.8% 0.0 0 0 0.90 11 1 1 100.0% 5.9% 2.1% 11 121.53 6.1% 0.0 0 0 0.80 25 2 2 100.0% 8.1% 1.7% 25 158.91 8.4% 0.0 0 0 0.70 24 2 3 66.7% 9.6% 2.2% 24 110.26 10.2% 0.0 0 0.60 64 6 6 100.0% 8.4% 2.1% 64 101.91 8.9% 98.1* 0 0 10 total 160 15 18 83.3% 8.8% 1.7% 160 121.06 9.4% 99.9* 0 0	IW: TH SI UN SI RI	15 Dataset HE DATA CO PACE GROUI NIT_CELL_C UBSET OF 1 ESOLUTION TO LIMIT	name: P13 DLECTION S NUMBER= CONSTANTS= ENTENSITY D NUMBER OBSERVED	Eb ETATISTIC 225 4.01 DATA WITH E OF REFL UNIQUE	S REPORTED 4.01 SIGNAL/NOI ECTIONS POSSIBLE	BELOW ASSUMM 4.01 90 SE >= -3.0 2 COMPLETENESS OF DATA	ES: .000 90.00 AS FUNCTION S R-FACTOR observed	0 90.000 OF RESOLU R-FACTOR expected	JTION COMPARED	I/SIGMA	R-meas	CC (1/2)	Anomal Corr	Siç
0.90 11 1 1 100.0% 5.9% 2.1% 11 121.53 6.1% 0.0 0 0 0.80 25 2 2 100.0% 8.1% 1.7% 25 158.91 8.4% 0.0 0 0 0.70 24 2 3 66.7% 9.6% 2.2% 24 110.26 10.2% 0.0 0 0 0.60 64 6 6 100.0% 8.4% 2.1% 64 101.91 8.9% 98.1* 0 0 10 total 160 15 18 83.3% 8.8% 1.7% 160 121.06 9.4% 99.9* 0 0	IW: TH SI UN SI RI RI	15 Dataset HE DATA CO PACE GROUI NIT_CELL_C UBSET OF 1 ESOLUTION TO LIMIT	name: P13 DLECTION S NUMBER= CONSTANTS= ENTENSITY D NUMBER OBSERVED	Eb ETATISTIC 225 4.01 DATA WITH E OF REFL UNIQUE	S REPORTED 4.01 SIGNAL/NOI ECTIONS POSSIBLE	BELOW ASSUMM 4.01 90 SE >= -3.0 2 COMPLETENESS OF DATA	ES: .000 90.00 AS FUNCTION S R-FACTOR observed	0 90.000 OF RESOLU R-FACTOR expected	JTION COMPARED	I/SIGMA	R-meas	CC (1/2)	Anomal Corr	Siç
0.90 11 1 1 100.0% 5.9% 2.1% 11 121.53 6.1% 0.0 0 0 0 0 0 0 0.80 25 2 2 100.0% 8.1% 1.7% 25 158.91 8.4% 0.0 0 0 0 0 0 0 0 0 0 0 0 0 0 0 0 0 0	IW: TH SH UI SI RH	15 Dataset HE DATA CO PACE_GROUI NIT_CELL_C UBSET OF I ESSOLUTION NO LIMIT 2.20	: name: P13 DLLECTION S P_NUMBER= ONSTANTS= UNTENSITY D NUMBER OBSERVED 0	Sb TATISTIC 225 4.01 DATA WITH OF REFL UNIQUE	S REPORTED 4.01 SIGNAL/NOI ECTIONS POSSIBLE 1	BELOW ASSUME 4.01 90. SE >= -3.0 1 COMPLETENESS OF DATA 0.0%	ES: .000 90.00 AS FUNCTION S R-FACTOR observed -99.9%	0 90.000 OF RESOLU R-FACTOR expected -99.9%	JTION COMPARED 0	I/SIGMA	R-meas -99.9%	CC(1/2)	Anomal Corr	Sic 0
0.80 25 2 2 100.0% 8.1% 1.7% 25 158.91 8.4% 0.0 0 0 0 0 0 0 0 0 0 0 0 0 0 0 0 0 0	TH SI UI SI RH Jan	15 Dataset HE DATA CO PACE_GROUI NIT_CELL_C UBSET OF 1 ESOLUTION TO LIMIT 2.20 1.10	: name: P13 DLLECTION S P_NUMBER= CONSTANTS= INTENSITY D NUMBER OBSERVED 0 29	Sb TATISTIC 225 4.01 DATA WITH OF REFL UNIQUE	S REPORTED 4.01 SIGNAL/NOI ECTIONS POSSIBLE 1	### BELOW ASSUMM 4.01 90 SE >= -3.0 1 COMPLETENES: OF DATA 0.0% 75.0%	ES: .000 90.00 AS FUNCTION S R-FACTOR observed -99.9% 10.0%	0 90.000 OF RESOLU R-FACTOR expected -99.9% 1.5%	UTION COMPARED 0 29	I/SIGMA 0.00 139.59	R-meas -99.9% 10.8%	CC (1/2) 0.0 100.0*	Anomal Corr 0	Siç O
0.70 24 2 3 66.7% 9.6% 2.2% 24 110.26 10.2% 0.0 0 0 0 0 0 0 0 0 0 0 0 0 0 0 0 0 0	IW: TH SH UN SH RH	15 Dataset HE DATA CO PACE_GROUP NIT_CELL_C UBSET OF 1 ESOLUTION TO LIMIT 2.20 1.10 1.00	: name: P13 LLECTION S P.NUMBER= CONSTANTS= LINTENSITY D NUMBER OBSERVED 0 29	Db STATISTIC 225 4.01 DATA WITH OF REFL UNIQUE 0 3 1	S REPORTED 4.01 SIGNAL/NOI ECTIONS POSSIBLE 1 4 1	BELOW ASSUME 4.01 90 SE >= -3.0 ; COMPLETENESS OF DATA 0.0% 75.0% 100.0%	ES: .000 90.00 AS FUNCTION B R-FACTOR observed -99.9% 10.0% 4.4%	0 90.000 OF RESOLUTION RESOLUTION PROPERTIES PROPERTIE	UTION COMPARED 0 29 7	I/SIGMA 0.00 139.59 125.77	R-meas -99.9% 10.8% 4.8%	CC(1/2) 0.0 100.0* 0.0	Anomal Corr 0 0	Si@
0.60 64 6 6 100.0% 8.4% 2.1% 64 101.91 8.9% 98.1* 0 0 total 160 15 18 83.3% 8.8% 1.7% 160 121.06 9.4% 99.9* 0 0	TH SI UI SI RI RI ()	15 Dataset HE DATA CO PACE GROUI NIT_CELL_C UBSET OF 1 ESOLUTION CO LIMIT 2.20 1.10 1.00 0.90	: name: P13 DLLECTION S P_NUMBER= CONSTANTS= INTENSITY D NUMBER OBSERVED 0 29 7 11	DESTRUCTION OF REFLUENCE OF REF	S REPORTED 4.01 SIGNAL/NOI ECTIONS POSSIBLE 1 4 1	BELOW ASSUME 4.01 90. SE >= -3.0 1 COMPLETENESS OF DATA 0.0% 75.0% 100.0%	ES: .000 90.00 AS FUNCTION S R-FACTOR observed -99.9% 10.0% 4.4% 5.9%	0 90.000 OF RESOLU R-FACTOR expected -99.9% 1.5% 1.6% 2.1%	OTION COMPARED 0 29 7 11	I/SIGMA 0.00 139.59 125.77 121.53	R-meas -99.9% 10.8% 4.8% 6.1%	CC (1/2) 0.0 100.0* 0.0 0.0	Anomal Corr 0 0	0 0 0
total 160 15 18 83.3% 8.8% 1.7% 160 121.06 9.4% 99.9* 0 0	MW: TH SI UN SI RH Nan	15 Dataset HE DATA CO PACE_GROUI NIT_CELL_C UBSET OF 1 ESCLUTION 10 LIMIT 2.20 1.10 1.00 0.90 0.80	c name: P13 DLLECTION S P_NUMBER= CONSTANTS= INTENSITY D NUMBER OBSERVED 0 29 7 11 25	thatistic 225 4.01 AATA WITH OF REFL UNIQUE 0 3 1 1 2 2	S REPORTED 4.01 SIGNAL/NOI ECTIONS POSSIBLE 1 4 1 1	BELOW ASSUMM 4.01 90 SE >= -3.0 i COMPLETENESS OF DATA 0.0% 75.0% 100.0% 100.0%	2S: .000 90.00 AS FUNCTION S R-FACTOR observed -99.9% 10.0% 4.4% 5.9% 8.1%	0 90.000 OF RESOLU R-FACTOR expected -99.9% 1.5% 1.6% 2.1% 1.7%	OTION COMPARED 0 29 7 11 25	I/SIGMA 0.00 139.59 125.77 121.53 158.91	R-meas -99.9% 10.8% 4.8% 6.1% 8.4%	CC(1/2) 0.0 100.0* 0.0 0.0	Anomal Corr 0 0 0 0 0 0	0 0 0 0
	IWI SI UI SI RH Jan	15 Dataset HE DATA CC PACE GROUI NIT_CELL_C UBSET OF 1 ESOLUTION TO 1.10 1.00 0.90 0.80 0.70	c name: P13 LLECTION S P. NUMBER = CONSTANTS = INTENSITY D NUMBER OBSERVED 0 29 7 11 25 24	A .01 CATA WITH COF REFL UNIQUE 0 3 1 1 2 2	S REPORTED 4.01 SIGNAL/NOI ECTIONS POSSIBLE 1 4 1 2 3	BELOW ASSUME 4.01 90. SE >= -3.0; COMPLETENESS OF DATA 0.0% 75.0% 100.0% 100.0%	25: .000 90.00 AS FUNCTION S R-FACTOR observed -99.9% 10.0% 4.4% 5.9% 8.1% 9.6%	0 90.000 OF RESOLU R-FACTOR expected -99.9% 1.5% 2.1% 1.7% 2.2%	OTION COMPARED 0 29 7 11 25 24	I/SIGMA 0.00 139.59 125.77 121.53 158.91 110.26	R-meas -99.9% 10.8% 4.8% 6.1% 8.4% 10.2%	CC(1/2) 0.0 100.0* 0.0 0.0 0.0 0.0	Anomal Corr 0 0 0	0 0 0 0
	MW: SI UI SI RH Nan	15 Dataset HE DATA CO PACE GROUI NIT_CELL_C UBSET OF 1 ESOLUTION 1.10 1.00 0.90 0.80 0.70 0.60	c name: P13 DLLECTION S P_NUMBER= CONSTANTS= INTENSITY D NUMBER OBSERVED 0 29 7 11 25 24 64	Db DETATISTIC 225 4.01 DATA WITH COF REFL UNIQUE 0 3 1 1 2 2 2 6	S REPORTED 4.01 SIGNAL/NOI ECTIONS POSSIBLE 1 4 1 1 2 3 6	BELOW ASSUME 4.01 90. SE >= -3.0 2 COMPLETENESS OF DATA 0.0% 75.0% 100.0% 100.0% 66.7% 100.0%	ES: .000 90.00 AS FUNCTION S R-FACTOR observed -99.9% 10.0% 4.4% 5.9% 8.1% 9.6% 8.4%	0 90.000 OF RESOLU R-FACTOR expected -99.9% 1.5% 1.6% 2.1% 2.2% 2.1%	OTION COMPARED 0 29 7 11 25 24 64	I/SIGMA 0.00 139.59 125.77 121.53 158.91 110.26 101.91	R-meas -99.9% 10.8% 4.8% 6.1% 8.4% 10.2% 8.9%	CC (1/2) 0.0 100.0* 0.0 0.0 0.0 98.1*	Anomal Corr 0 0 0 0 0 0	0. 0. 0. 0.
0 0.90 11 1 1 100.0% 5.9% 2.1% 11 121.50 0 0.80 25 2 2 100.0% 8.1% 1.7% 25 158.50 0 0.70 24 2 3 66.7% 9.6% 2.2% 24 110.20 0 0.60 64 6 6 100.0% 8.4% 2.1% 64 101.50 0 0.60 1 160 15 18 83.3% 8.8% 1.7% 160 121.00 121	MW:	15 Dataset HE DATA CO	name: P13	b TATISTIC				1.6%	76	77.3	35	35 9.4%	35 9.4% 99.8*	35 9.4% 99.8* 0
0.90 11 1 1 00.0% 5.9% 2.1% 11 121.53 6.1% 0.0 0 0 0.80 25 2 2 100.0% 8.1% 1.7% 25 158.91 8.4% 0.0 0 0 0.70 24 2 3 66.7% 9.6% 2.2% 24 110.26 10.2% 0.0 0 0 0.60 64 6 6 100.0% 8.4% 2.1% 64 101.91 8.9% 98.1* 0	HE PA NI JE S	Dataset Data CC DATA CC DATA CC DATE CELL DESCRIPTION	: name: P13 DLLECTION S P_NUMBER= ONSTANTS= UNTENSITY D NUMBER OBSERVED 0	Sb TATISTIC 225 4.01 DATA WITH OF REFL UNIQUE	S REPORTED 4.01 SIGNAL/NOI ECTIONS POSSIBLE 1	BELOW ASSUME 4.01 90. SE >= -3.0 1 COMPLETENESS OF DATA 0.0%	ES: .000 90.00 AS FUNCTION S R-FACTOR observed -99.9%	0 90.000 OF RESOLU R-FACTOR expected -99.9%	JTION COMPARED 0	I/SIGMA	R-meas -99.9%	CC(1/2)	Anomal Corr	S
0.70 24 2 3 66.7% 9.6% 2.2% 24 110.26 10.2% 0.0 0 0 0 0 0 0 0 0 0 0 0 0 0 0 0 0 0	FE JI JI RE	15 Dataset HE DATA CO PACE_GROUI NIT_CELL_C UBSET OF 1 ESOLUTION TO LIMIT 2.20 1.10	: name: P13 DLLECTION S P_NUMBER= CONSTANTS= INTENSITY D NUMBER OBSERVED 0 29	Sb TATISTIC 225 4.01 DATA WITH OF REFL UNIQUE	S REPORTED 4.01 SIGNAL/NOI ECTIONS POSSIBLE 1	### BELOW ASSUMM 4.01 90 SE >= -3.0 1 COMPLETENES: OF DATA 0.0% 75.0%	ES: .000 90.00 AS FUNCTION S R-FACTOR observed -99.9% 10.0%	0 90.000 OF RESOLU R-FACTOR expected -99.9% 1.5%	UTION COMPARED 0 29	I/SIGMA 0.00 139.59	R-meas -99.9% 10.8%	CC (1/2) 0.0 100.0*	Anomal Corr 0	Si
0.60 64 6 6 100.0% 8.4% 2.1% 64 101.91 8.9% 98.1* 0 0	TI SI UI SI RI	15 Dataset HE DATA CO PACE_GROUP NIT_CELL_C UBSET OF 1 ESOLUTION TO LIMIT 2.20 1.10 1.00	: name: P13 LLECTION S P.NUMBER= CONSTANTS= LINTENSITY D NUMBER OBSERVED 0 29	Db STATISTIC 225 4.01 DATA WITH OF REFL UNIQUE 0 3 1	S REPORTED 4.01 SIGNAL/NOI ECTIONS POSSIBLE 1 4 1	BELOW ASSUME 4.01 90 SE >= -3.0 ; COMPLETENESS OF DATA 0.0% 75.0% 100.0%	ES: .000 90.00 AS FUNCTION B R-FACTOR observed -99.9% 10.0% 4.4%	0 90.000 OF RESOLUTION RESOLUTION PROPERTIES PROPERTIE	UTION COMPARED 0 29 7	I/SIGMA 0.00 139.59 125.77	R-meas -99.9% 10.8% 4.8%	CC(1/2) 0.0 100.0* 0.0	Anomal Corr 0 0	Si 0 0
0.60 64 6 6 100.0% 8.4% 2.1% 64 101.91 8.9% 98.1* 0 0 total 160 15 18 83.3% 8.8% 1.7% 160 121.06 9.4% 99.9* 0 0	W: SI Ul SI RI	15 Dataset HE DATA CO PACE GROUI NIT_CELL_C UBSET OF 1 ESOLUTION CO LIMIT 2.20 1.10 1.00 0.90	: name: P13 DLLECTION S P_NUMBER= CONSTANTS= INTENSITY D NUMBER OBSERVED 0 29 7 11	DESTRUCTION OF REFLUENCE OF REF	S REPORTED 4.01 SIGNAL/NOI ECTIONS POSSIBLE 1 4 1	BELOW ASSUME 4.01 90. SE >= -3.0 1 COMPLETENESS OF DATA 0.0% 75.0% 100.0%	ES: .000 90.00 AS FUNCTION S R-FACTOR observed -99.9% 10.0% 4.4% 5.9%	0 90.000 OF RESOLU R-FACTOR expected -99.9% 1.5% 1.6% 2.1%	OTION COMPARED 0 29 7 11	I/SIGMA 0.00 139.59 125.77 121.53	R-meas -99.9% 10.8% 4.8% 6.1%	CC (1/2) 0.0 100.0* 0.0 0.0	Anomal Corr 0 0	Si 0 0 0 0 0 0
total 160 15 18 83.3% 8.8% 1.7% 160 121.06 9.4% 99.9* 0 0	W: SI Ul SI RI	15 Dataset HE DATA CO PACE_GROUI NIT_CELL_C UBSET OF 1 ESCLUTION 10 LIMIT 2.20 1.10 1.00 0.90 0.80	c name: P13 DLLECTION S P_NUMBER= CONSTANTS= INTENSITY D NUMBER OBSERVED 0 29 7 11 25	thatistic 225 4.01 AATA WITH OF REFL UNIQUE 0 3 1 1 2 2	S REPORTED 4.01 SIGNAL/NOI ECTIONS POSSIBLE 1 4 1 1	BELOW ASSUMM 4.01 90 SE >= -3.0 i COMPLETENESS OF DATA 0.0% 75.0% 100.0% 100.0%	2S: .000 90.00 AS FUNCTION S R-FACTOR observed -99.9% 10.0% 4.4% 5.9% 8.1%	0 90.000 OF RESOLU R-FACTOR expected -99.9% 1.5% 1.6% 2.1% 1.7%	OTION COMPARED 0 29 7 11 25	I/SIGMA 0.00 139.59 125.77 121.53 158.91	R-meas -99.9% 10.8% 4.8% 6.1% 8.4%	CC(1/2) 0.0 100.0* 0.0 0.0	Anomal Corr 0 0 0 0 0 0	Si 0 0 0 0 0 0 0 0
total 160 15 18 83.3% 8.8% 1.7% 160 121.06 9.4% 99.9* 0 0	W: SI UI SI RI ar	15 Dataset HE DATA CO PACE_GROUI NIT_CELL_C UBSET OF 1 ESCLUTION 10 LIMIT 2.20 1.10 1.00 0.90 0.80	c name: P13 DLLECTION S P_NUMBER= CONSTANTS= INTENSITY D NUMBER OBSERVED 0 29 7 11 25	thatistic 225 4.01 AATA WITH OF REFL UNIQUE 0 3 1 1 2 2	S REPORTED 4.01 SIGNAL/NOI ECTIONS POSSIBLE 1 4 1 1	BELOW ASSUMM 4.01 90 SE >= -3.0 i COMPLETENESS OF DATA 0.0% 75.0% 100.0% 100.0%	2S: .000 90.00 AS FUNCTION S R-FACTOR observed -99.9% 10.0% 4.4% 5.9% 8.1%	0 90.000 OF RESOLU R-FACTOR expected -99.9% 1.5% 1.6% 2.1% 1.7%	OTION COMPARED 0 29 7 11 25	I/SIGMA 0.00 139.59 125.77 121.53 158.91	R-meas -99.9% 10.8% 4.8% 6.1% 8.4%	CC(1/2) 0.0 100.0* 0.0 0.0	Anomal Corr 0 0 0 0 0 0	Si 0 0 0 0 0 0 0 0
	W: SI UI SI RI ar	15 Dataset HE DATA CC PACE GROUI NIT_CELL_C UBSET OF 1 ESOLUTION TO 1.10 1.00 0.90 0.80 0.70	c name: P13 LLECTION S P. NUMBER = CONSTANTS = INTENSITY D NUMBER OBSERVED 0 29 7 11 25 24	A .01 CATA WITH COF REFL UNIQUE 0 3 1 1 2 2	S REPORTED 4.01 SIGNAL/NOI ECTIONS POSSIBLE 1 4 1 2 3	BELOW ASSUME 4.01 90. SE >= -3.0; COMPLETENESS OF DATA 0.0% 75.0% 100.0% 100.0%	25: .000 90.00 AS FUNCTION S R-FACTOR observed -99.9% 10.0% 4.4% 5.9% 8.1% 9.6%	0 90.000 OF RESOLU R-FACTOR expected -99.9% 1.5% 2.1% 1.7% 2.2%	OTION COMPARED 0 29 7 11 25 24	I/SIGMA 0.00 139.59 125.77 121.53 158.91 110.26	R-meas -99.9% 10.8% 4.8% 6.1% 8.4% 10.2%	CC(1/2) 0.0 100.0* 0.0 0.0 0.0 0.0	Anomal Corr 0 0 0	0 0 0 0
	IW1 SI UI SI RI	15 Dataset HE DATA CO PACE GROUI NIT_CELL_C UBSET OF 1 ESOLUTION 1.10 1.00 0.90 0.80 0.70 0.60	c name: P13 DLLECTION S P_NUMBER= CONSTANTS= INTENSITY D NUMBER OBSERVED 0 29 7 11 25 24 64	Db DETATISTIC 225 4.01 DATA WITH COF REFL UNIQUE 0 3 1 1 2 2 2 6	S REPORTED 4.01 SIGNAL/NOI ECTIONS POSSIBLE 1 4 1 1 2 3 6	BELOW ASSUME 4.01 90. SE >= -3.0 2 COMPLETENESS OF DATA 0.0% 75.0% 100.0% 100.0% 66.7% 100.0%	ES: .000 90.00 AS FUNCTION S R-FACTOR observed -99.9% 10.0% 4.4% 5.9% 8.1% 9.6% 8.4%	0 90.000 OF RESOLU R-FACTOR expected -99.9% 1.5% 1.6% 2.1% 2.2% 2.1%	OTION COMPARED 0 29 7 11 25 24 64	I/SIGMA 0.00 139.59 125.77 121.53 158.91 110.26 101.91	R-meas -99.9% 10.8% 4.8% 6.1% 8.4% 10.2% 8.9%	CC (1/2) 0.0 100.0* 0.0 0.0 0.0 98.1*	Anomal Corr 0 0 0 0 0 0	Si 0 0 0 0 0 0 0 0 0 0 0 0
	MW: THE SI UIT SI RI RI NAI O O O THE SI	15 Dataset HE DATA CC PACE GROUI NIT_CELL_(UBSET OF 1 ESOLUTION 10 1.10 1.00 0.90 0.80 0.70 0.60 total	Iname: P13 DLLECTION S ENUMBER CONSTANTS= ENTENSITY D NUMBER OBSERVED 0 29 7 11 25 24 64 160 Ename: P14 DLLECTION S NUMBER=	DESTRUCTION OF REFLECTION OF R	S REPORTED 4.01 SIGNAL/NOI ECTIONS POSSIBLE 1 4 1 2 3 6 18	BELOW ASSUME 4.01 90. SE >= -3.0 i COMPLETENESS OF DATA 0.0% 75.0% 100.0% 100.0% 100.0% 83.3% BELOW ASSUME	2S: .000 90.00 AS FUNCTION S R-FACTOR observed -99.9% 10.0% 4.4% 5.9% 8.1% 9.6% 8.4% 8.8%	0 90.000 OF RESOLUR-FACTOR expected -99.9% 1.5% 2.1% 1.7% 2.2% 2.1%	OTION COMPARED 0 29 7 11 25 24 64	I/SIGMA 0.00 139.59 125.77 121.53 158.91 110.26 101.91	R-meas -99.9% 10.8% 4.8% 6.1% 8.4% 10.2% 8.9%	CC (1/2) 0.0 100.0* 0.0 0.0 0.0 98.1*	Anomal Corr 0 0 0 0 0 0	0 0 0 0 0
	MW: SI UI SI RI Nai	15 Dataset HE DATA CO PACE GROUI NIT_CELL_C UBSET OF 1 ESOLUTION 1.00 1.10 1.00 0.90 0.80 0.70 0.60 total 15 Dataset HE DATA CO PACE GROUI NIT_CELL_C	c name: P13 DLLECTION S P_NUMBER= CONSTANTS= INTENSITY D NUMBER OBSERVED 0 29 7 11 25 24 64 160 c name: P14 DLLECTION S P_NUMBER= CONSTANTS=	0b ETATISTIC 225 4.01 PATA WITH OF REFL UNIQUE 0 3 1 1 2 6 15 ETATISTIC 225 4.04	S REPORTED 4.01 SIGNAL/NOI ECTIONS POSSIBLE 1 4 1 1 2 3 6 18 S REPORTED 4.04	BELOW ASSUME 4.01 90. SE >= -3.0 2 COMPLETENESS OF DATA 0.0% 100.0% 100.0% 100.0% 83.3% BELOW ASSUME 4.04 90.	ES: .000 90.00 AS FUNCTION S R-FACTOR observed -99.9% 10.0% 4.4% 5.9% 8.1% 9.6% 8.4% 8.8%	0 90.000 OF RESOLUTION R-FACTOR expected -99.9% 1.5% 1.6% 2.1% 1.7% 2.2% 2.1% 1.7%	OTION COMPARED 0 29 7 11 25 24 64 160	I/SIGMA 0.00 139.59 125.77 121.53 158.91 110.26 101.91	R-meas -99.9% 10.8% 4.8% 6.1% 8.4% 10.2% 8.9%	CC (1/2) 0.0 100.0* 0.0 0.0 0.0 98.1*	Anomal Corr 0 0 0 0 0 0	0. 0. 0. 0.
SUBSET OF INTENSITY DATA WITH SIGNAL/NOISE >= -3.0 AS FUNCTION OF RESOLUTION RESOLUTION NUMBER OF REFLECTIONS COMPLETENESS R-FACTOR R-FACTOR COMPARED I/SIGMA R-meas CC(1/2) Anomal Si Nano	AW: TH SI UN SU RI RI O O O O O O O O O O O O O O O O O	15 Dataset HE DATA CC PACE GROUI NIT_CELL_C UBSET OF 1 ESOLUTION 1.00 1.100 1.00 0.80 0.70 0.60 total 15 Dataset HE DATA CC PACE GROUI NIT_CELL_C UBSET OF 1 ESOLUTION	I name: P13 DLLECTION S PNUMBER= CONSTANTS= INTENSITY D NUMBER OBSERVED 0 29 7 11 25 24 64 160 I name: P14 LLECTION S PNUMBER= CONSTANTS= INTENSITY D NUMBER	DESTRUCTION OF REFLECTION OF R	S REPORTED 4.01 SIGNAL/NOI ECTIONS POSSIBLE 1 4 1 1 2 3 6 18 S REPORTED 4.04 SIGNAL/NOI ECTIONS	BELOW ASSUME 4.01 90. SE >= -3.0 2 COMPLETENESS OF DATA 0.0% 100.0% 100.0% 100.0% 83.3% BELOW ASSUME 4.04 90. SE >= -3.0 2 COMPLETENESS	2S: .000 90.00 AS FUNCTION S R-FACTOR observed -99.9% 10.0% 4.4% 5.9% 8.1% 9.6% 8.4% 8.8%	0 90.000 OF RESOLU R-FACTOR expected -99.9% 1.5% 1.6% 2.1% 1.7% 2.2% 1.7% 0 90.000 OF RESOLU R-FACTOR	UTION COMPARED 0 29 7 11 25 24 64 160	I/SIGMA 0.00 139.59 125.77 121.53 158.91 110.26 101.91 121.06	R-meas -99.9% 10.8% 4.8% 6.1% 8.4% 10.2% 8.9% 9.4%	CC(1/2) 0.0 100.0* 0.0 0.0 0.0 98.1* 99.9*	Anomal Corr 0 0 0 0 0 0 0	0.0.0.0.0.0.0.0.0.0.0.0.0.0.0.0.0.0.0.
SUBSET OF INTENSITY DATA WITH SIGNAL/NOISE >= -3.0 AS FUNCTION OF RESOLUTION	MW: SI UI SI RI Na O O O O O O O O O O O O O O O O O O	15 Dataset HE DATA CC PACE GROUI NIT_CELL_C UBSET OF 1 ESOLUTION 1.00 1.100 1.00 0.80 0.70 0.60 total 15 Dataset HE DATA CC PACE GROUI NIT_CELL_C UBSET OF 1 ESOLUTION	I name: P13 DLLECTION S PNUMBER= CONSTANTS= INTENSITY D NUMBER OBSERVED 0 29 7 11 25 24 64 160 I name: P14 LLECTION S PNUMBER= CONSTANTS= INTENSITY D NUMBER	DESTRUCTION OF REFLECTION OF R	S REPORTED 4.01 SIGNAL/NOI ECTIONS POSSIBLE 1 4 1 1 2 3 6 18 S REPORTED 4.04 SIGNAL/NOI ECTIONS	BELOW ASSUME 4.01 90. SE >= -3.0 2 COMPLETENESS OF DATA 0.0% 100.0% 100.0% 100.0% 83.3% BELOW ASSUME 4.04 90. SE >= -3.0 2 COMPLETENESS	2S: .000 90.00 AS FUNCTION S R-FACTOR observed -99.9% 10.0% 4.4% 5.9% 8.1% 9.6% 8.4% 8.8%	0 90.000 OF RESOLU R-FACTOR expected -99.9% 1.5% 1.6% 2.1% 1.7% 2.2% 1.7% 0 90.000 OF RESOLU R-FACTOR	UTION COMPARED 0 29 7 11 25 24 64 160	I/SIGMA 0.00 139.59 125.77 121.53 158.91 110.26 101.91 121.06	R-meas -99.9% 10.8% 4.8% 6.1% 8.4% 10.2% 8.9% 9.4%	CC(1/2) 0.0 100.0* 0.0 0.0 0.0 98.1* 99.9*	Anomal Corr 0 0 0 0 0 0 0	Sic. 0 0 0 0 0 0 0 0
SUBSET OF INTENSITY DATA WITH SIGNAL/NOISE >= -3.0 AS FUNCTION OF RESOLUTION RESOLUTION NUMBER OF REFLECTIONS COMPLETENESS R-FACTOR R-FACTOR COMPARED I/SIGMA R-meas CC(1/2) Anomal Si Nano LIMIT OBSERVED UNIQUE POSSIBLE OF DATA observed expected Corr 2.20 0 0 0 1 0.0% -99.9% -99.9% 0 0.00 -99.9% 0.0 0 0	TITE OF THE STATE	15 Dataset HE DATA CC PACE_GROUNIT_CELL_C UBSET OF 1 ESCLUTION OL LIMIT 2.20 1.10 1.00 0.80 0.70 0.60 total 15 Dataset HE DATA CC PACE_GROUNIT_CELL_C UBSET OF 1 ESCLUTION OL ESCLUTION OL O	: name: P13 DLLECTION S PNUMBER= ONSTANTS= INTENSITY D NUMBER OBSERVED 0 29 7 11 25 24 64 160 : name: P14 DLLECTION S PNUMBER= CONSTANTS= INTENSITY D NUMBER OBSERVED	DESCRIPTION OF REFLUNIQUE OATA WITHE OF REFLUNIQUE OATA WITHE OF REFLUNIQUE OATA WITHE OF REFLUNIQUE UNIQUE UNIQUE UNIQUE UNIQUE	S REPORTED 4.01 SIGNAL/NOI ECTIONS POSSIBLE 1 4 1 2 3 6 18 S REPORTED 4.04 SIGNAL/NOI ECTIONS POSSIBLE	BELOW ASSUME 4.01 90. SE >= -3.0 2 COMPLETENESS OF DATA 0.0% 100.0% 100.0% 100.0% 83.3% BELOW ASSUME 4.04 90. SE >= -3.0 2 COMPLETENESS OF DATA	ES: .000 90.00 AS FUNCTION S R-FACTOR observed -99.9% 10.0% 4.4% 5.9% 8.1% 9.6% 8.4% 8.8%	0 90.000 OF RESOLU R-FACTOR expected -99.9% 1.5% 1.6% 2.1% 1.7% 2.2% 2.1% 1.7%	OTION COMPARED 0 29 7 11 25 24 64 160 STION COMPARED	I/SIGMA 0.00 139.59 125.77 121.53 158.91 110.26 101.91 121.06	R-meas -99.9% 10.8% 4.8% 6.1% 8.4% 10.2% 8.9% 9.4%	CC (1/2) 0.0 100.0* 0.0 0.0 98.1* 99.9*	Anomal Corr 0 0 0 0 0 0 0 0 Anomal Corr	Sic. 0 0 0 0 0 0 0 0
SUBSET OF INTENSITY DATA WITH SIGNAL/NOISE >= -3.0 AS FUNCTION OF RESOLUTION RESOLUTION NUMBER OF REFLECTIONS COMPLETENESS R-FACTOR R-FACTOR COMPARED I/SIGMA R-meas CC(1/2) Anomal Si Nano LIMIT OBSERVED UNIQUE POSSIBLE OF DATA observed expected Corr 2.20 0 0 1 0.0% -99.9% -99.9% 0 0.00 -99.9% 0.0 0 0	TITE OF THE STATE	15 Dataset HE DATA CO PACE_GROUI NIT_CELL_C UBSET OF 1 SSOLUTION 1.00 1.10 1.00 0.90 0.80 0.70 0.60 total 15 Dataset HE DATA CO PACE_GROUI NIT_CELL_C UBSET OF 1 SSOLUTION 1.00 1.00 1.00 1.00 1.00 1.00 1.00 1.0	: name: P13 DILECTION S NUMBER= CONSTANTS= ENTENSITY D NUMBER OBSERVED 0 29 7 11 25 24 64 160 : name: P14 DILECTION S NUMBER= CONSTANTS= ENTENSITY D NUMBER OBSERVED 0 0 0 0 0 0 0 0 0 0 0 0 0 0 0 0 0 0 0	DESTATISTIC 225 4.01 VATA WITH COF REFL UNIQUE 0 3 1 1 2 2 6 15 STATISTIC 225 4.04 VATA WITH COF REFL UNIQUE 0 0 0 0 0 0 0 0 0 0 0 0 0 0 0 0 0 0 0	S REPORTED 4.01 SIGNAL/NOI ECTIONS POSSIBLE 1 4 1 2 3 6 18 S REPORTED 4.04 SIGNAL/NOI ECTIONS POSSIBLE	BELOW ASSUME 4.01 90. SE >= -3.0 1 COMPLETENESS OF DATA 0.0% 100.0% 100.0% 100.0% 100.0% 83.3% BELOW ASSUME 4.04 90. SE >= -3.0 1 COMPLETENESS OF DATA 0.0%	2S: .000 90.00 AS FUNCTION S R-FACTOR observed -99.9% 10.0% 4.4% 5.9% 8.1% 9.6% 8.4% 8.8%	0 90.000 OF RESOLUR-FACTOR expected -99.9% 1.5% 1.6% 2.1% 1.7% 2.2% 2.1% 1.7% 0 90.000 OF RESOLUR-FACTOR expected -99.9%	OTION COMPARED 0 29 7 11 25 24 64 160 OTION COMPARED	I/SIGMA 0.00 139.59 125.77 121.53 158.91 110.26 101.91 121.06	R-meas -99.9% 10.8% 4.8% 6.1% 8.4% 10.2% 8.9% 9.4%	CC(1/2) 0.0 100.0* 0.0 0.0 0.0 98.1* 99.9*	Anomal Corr 0 0 0 0 0 0 0 0 Anomal Corr	Si 4 0 0 0 0 0 0 0 0 0 0 0 Si 4 0 0 0 0 0 0 0 0 0 0 0 0 0 0 0 0 0 0

0	1.00	9	1	1	100.0%	11.0%	1.6%	9	138.37	11.7%	0.0	0	0.000
0	0.90	37	2	2	100.0%	9.3%	1.9%	37	167.52	9.5%	0.0	0	0.000
0	0.80	12	1	1	100.0%	8.7%	1.9%	12	144.34	9.1%	0.0	0	0.000
0	0.70	38	2	3	66.7%	13.6%	2.6%	38	128.46	14.1%	0.0	0	0.000
0	0.60	92	6	6	100.0%	12.5%	2.7%	92	109.03	12.9%	99.7*	0	0.000
0	total	230	15	18	83.3%	10.8%	1.9%	230	134.51	11.3%	99.9*	0	0.000